

Dissertation

submitted to the

Combined Faculties for the Natural Sciences and for Mathematics

of the Ruperto-Carola University of Heidelberg, Germany

for the degree of

Doctor of Natural Sciences

Presented by

Borhan Uddin, MSc in Molecular Life Sciences

Specialization: Biomedical Research

Born in: Chandpur, Bangladesh

Oral-examination: **2nd of October, 2018**

Linking dephosphorylation to cellular events:
Functional analysis of human CDC14 (hCDC14) phosphatases

Referees

Professor Dr. Elmar Schiebel

Professor Dr. Sylvia Erhardt

Contents

Summary	i
Zusammenfassung (Summary in German)	ii
1 Introduction	1
1.1 An overview of cell cycle	1
1.2 Regulation of Cell cycle	3
1.3 Phosphatases in animal cells	4
1.4 Cdc14 phosphatase in budding yeast.....	5
1.5 Cdc14: a family of conserved phosphatases.....	8
1.6 Functions of hCDC14 proteins	9
1.7 Connection between Cilia and cell cycle.....	10
1.8 Ciliopathies associated with defects in primary cilium signaling	15
1.9 Actin and ciliogenesis	16
1.10 Aim of the thesis.....	18
2 Results.....	19
2.1 Generation of <i>hCDC14</i> knockout cells.....	19
2.1.1 Strategy for the generation of knockout cell lines.....	19
2.1.2 RT-PCR analysis confirming expression of wild type and in-frame exon-skipped <i>hCDC14A/hCDC14B</i> transcripts	22
2.1.3 Exon-skipping phenomenon is independent of genome editing approach.....	23
2.1.4 Minimizing the degree of alteration salvages the exon skipping	26
2.2 Phenotypic analysis of knockout cell lines	28

2.2.1	<i>hCDC14C</i> is not expressed in RPE-1 and HCT 116 cells.....	28
2.2.2	Growth and cell cycle analysis of <i>hCDC14A^{PD}</i> and <i>hCDC14B^{-/-}</i> cells..	29
2.3	<i>hCDC14A</i> regulates cilia length.....	30
2.3.1	<i>hCDC14A^{PD}</i> RPE-1 cells have longer cilia than Wt cells.....	30
2.3.2	<i>hCDC14A</i> localizes to the basal body and the actin cytoskeleton of ciliated cells.....	37
2.3.3	<i>hCDC14A</i> dephosphorylates actin associated proteins during ciliogenesis.....	40
2.3.4	<i>hCDC14A</i> regulates phosphorylation of DBN1.....	44
2.3.5	Phosphoregulation of DBN1 by <i>hCDC14A</i> contributes to cilia length control.....	46
2.3.6	The kinase CDK5 and <i>hCDC14A</i> phosphatase counteract phosphorylation of DBN1 during ciliogenesis.....	47
2.3.7	<i>hCDC14A^{PD}</i> cells show enhanced recycling endosome as well as elevated docking of ciliary vesicles to the basal body.....	49
3	Discussion.....	54
3.1	Genome editing through large insertion leads to the skipping of targeted exon.....	54
3.2	<i>hCDC14A</i> and <i>hCDC14B</i> double knockout cells show no obvious growth defects.....	55
3.3	The phosphatase <i>hCDC14A</i> regulates cilia length.....	55
4	Concluding Remarks.....	60
5	Materials and Methods.....	61
5.1	Cell culture and transfection.....	61
5.2	Generation of ZFN-mediated knockout cells.....	64

5.3	Generation of Cas9-mediated <i>hCDC14A</i> knockout cells	65
5.4	Southern blot hybridization to confirm knockouts	66
5.5	RNA preparation and expression analysis	66
5.6	Generation of RPE-1 stable cell lines	67
5.7	Generation of Cas9-mediated <i>DBN1</i> knockout cells	68
5.8	Immunofluorescence and Microscopy	68
5.9	Immunoblot analysis	70
5.10	Measuring Cilia length and protein intensity within a defined region of interest (ROI)	70
5.11	<i>In Vitro</i> Phosphatase Assay	71
5.12	Electron microscopy (in collaboration with Annett Neuner)	71
5.13	Quantitative phosphoproteome and BioID mass-spectrometry analyses	72
5.14	Flow cytometry	73
5.15	Transformation of <i>E. coli</i>	74
5.16	List of plasmids	74
6	References	75
7	Publications during PhD	89
8	Appendix	90
9	Acknowledgements	106

Summary

Mitotic phosphatases play crucial roles in anaphase regulation and mitotic exit by annulling the kinase-mediated protein phosphorylation. In budding yeast *Saccharomyces cerevisiae*, Cdc14 (cell division cycle 14) phosphatase antagonizes key Cdk1 (cyclin-dependent kinase 1) functions to drive cells out of mitosis. Despite the presence of highly conserved catalytic domains, human CDC14s are dispensable for cell cycle progression. Nevertheless, to decipher the molecular mechanisms of human CDC14s functions, we have investigated the knockout cellular models aided by various imaging and proteomics approaches. Phenotypic analyses of the generated *hCDC14A* knockout in human retinal pigment epithelium (hTERT-RPE1) cells have exhibited the occurrence of longer primary cilia upon serum starvation. The intermediate longer cilia in haploid-insufficient cells, as well as the extended cilia observed upon siRNA-mediated acute depletion of *hCDC14A*, have further confirmed the phenotype. Primary cilia are microtubule-based structures that control various aspects of growth and development through sensing extracellular signals. Defects in this regulation lead to a host of pathological conditions collectively known as ciliopathies. Indirect immunofluorescence and electron microscopy have revealed that the disassembly pathways, as well as the crucial structures like axoneme and basal body, were intact in the elongated cilia. Inducible expression of *hCDC14A* has indicated its presence in the proximal end and subdistal appendage of the basal body. Global phosphoproteome along with proximity-based interaction proteomics approaches under conditions that favor ciliation have identified substrates for hCDC14A. Some of the identified substrates are involved in actin cytoskeleton reorganization with a function in cilia length control. The actin bundling protein drebrin (DBN1) was one of the identified hCDC14A substrates that have recently been reported to be associated with ciliogenesis. We show that the counteracting phospho-regulation of DBN1 at serine residue 142 by the proline directed kinase CDK5 and hCDC14A phosphatase regulates cilia length. However, significantly longer cilia in *hCDC14A* knockout cells than those from *DBN1* knockout cells indicate that there are more substrates for hCDC14A that might be involved in ciliogenesis. The longer cilia phenotype in *hCDC14A* knockout cells could be explained by the enhanced recycling endosomes (transferrin) as well as increased ciliary vesicle docking (smoothened) in the pericentrosomal areas.

Zusammenfassung (Summary in German)

Mitotische Phosphatasen spielen eine entscheidende Rolle bei der Regulierung der Anaphase und dem Austritt aus der Mitose durch die Aufhebung der Kinasevermittelten Proteinphosphorylierung. In der Bäckerhefe *Saccharomyces cerevisiae* wirkt Cdc14 (Cell division cycle 14) den Schlüsselfunktionen von Cdk1 (Cyclin-dependent kinase 1) entgegen, um die Mitose abzuschließen. Trotz hoch konservierter katalytischer Domänen sind humane CDC14 Phosphatasen für die Zellzyklus-Progression nicht essentiell. Um die molekularen Funktionsmechanismen der humanen CDC14 Phosphatasen zu entschlüsseln, haben wir Knockout-Zellmodelle mittels verschiedener bildgebenden und proteomischen Verfahren untersucht. Phänotypische Analysen des erzeugten hCDC14A-Knockouts in humanen retinalen Pigmentepithelzellen (hTERT-RPE1) zeigten das Auftreten längerer primärer Zilien nach Serumentzug. Die intermediär längeren Zilien in haploid-insuffizienten Zellen sowie die längeren Zilien, die nach siRNA-vermittelter akuter Depletion von hCDC14A beobachtet wurden, haben den Phänotyp weiter bestätigt. Primäre Zilien sind Mikrotubuli-basierende Strukturen, die verschiedene Aspekte des Wachstums und der Entwicklung durch Wahrnehmung extrazellulärer Signale kontrollieren. Fehlfunktionen in dieser Regulierung führen zu einer Vielzahl von pathologischen Veränderungen, die als Ziliopathien zusammengefasst werden. Indirekte Immunofluoreszenz und Elektronenmikroskopie haben gezeigt, dass Abbauwege sowie wichtige Strukturen wie das Axonem und der Basalkörper in den verlängerten Zilien intakt sind. Induzierte Expression von hCDC14A wies auf die Präsenz im proximalen Ende und subdistalen Appendix des Basalkörpers hin. Globale Phosphoproteom- und auf Proximität beruhende Proteomik-Analysen unter Bedingungen, die die Ziliation begünstigen, haben Substrate für hCDC14A identifiziert. Einige der identifizierten Substrate sind an der Reorganisation des Aktin-Zytoskeletts beteiligt, einhergehend mit einer Funktion bei der Längenkontrolle von Zilien. Das Aktin-bündelnde Protein Drebrin (DBN1) ist eines der identifizierten hCDC14A-Substrate, das kürzlich in Zusammenhang mit Ziliogenese gebracht wurde. Wir zeigen, dass die entgegengewirkende Phosphoregulierung von DBN1 am Serin-Rest 142 durch die Prolin-gerichtete Kinase CDK5 und der Phosphatase hCDC14A die Zilienlänge reguliert. Signifikant längere Zilien in hCDC14A-Knockout-Zellen als in DBN1-Knockout-Zellen weisen jedoch darauf hin, dass es weitere Substrate für hCDC14A gibt, die an der Ziliogenese beteiligt sein könnten. Der Phänotyp mit längeren Zilien in hCDC14A-Knockout-Zellen könnte durch ein erhöhtes Aufkommen von Recycling-Endosomen (Transferrin) sowie durch ein gesteigertes Andocken ziliarer Vesikel (Smoothened) in den perizentrosomalen Bereichen erklärt werden.

1 Introduction

1.1 An overview of cell cycle

Cells multiply through a precise series of events that are collectively termed as cell cycle (Temin, 1971). Most of the time, cells stay in G1 or GAP1 phase during which they resume biosynthesis to accumulate nutrients and components necessary for DNA synthesis during the next phase termed as S or Synthesis phase. However, if the conditions are not conducive to growth, the cells can be arrested in G1 and enter a special phase of no growth termed as G0 or GAP0 (Pardee, 1974). When the environmental (presence of nutrients and growth factors) and internal (absence of damages) conditions are fulfilled, the cells passage through G1 and accomplish S phase. S phase is followed by another gap phase, GAP2 or G2, which allows cells to check the integrity of cell components as well as newly synthesized genetic material and to duplicate the necessary cell organelles. Chromosome segregation (karyokinesis) and cell division (cytokinesis) occur during M phase. Mitosis is divided into 5 stages: prophase, prometaphase, metaphase, anaphase, and telophase. Condensation of chromatin as well as the breakdown of nuclear envelope occurs during prophase. Condensed sister chromatids congress during prometaphase and align at the equatorial plate of the bipolar spindle in metaphase which is followed by anaphase that ensures proper separation of the sister chromatids to the opposite spindle poles. Cells exit Mitosis through telophase during which reassembly of nuclear envelope and decondensation of chromosomes occur (Baserga, 1968; Hartwell and Weinert, 1989).

The centrosome serves as the key microtubule-organizing center (MTOC) in animal cells. It is composed of a microtubule based structure called centriole embedded into a protein-rich material organized in concentric circles (pericentriolar matrix, PCM) (Conduit et al., 2015; Mardin and Schiebel, 2012). Centrosome biogenesis, as well as maturation, is tightly coupled to cell cycle events and it duplicates once per cell cycle like cellular genetic material (Figure 1.1). In S phase, a daughter centriole is formed perpendicular to pre-existing mother centriole and

remain tightly engaged with each other throughout S, G2 and M phase. During S-G2 phases, the centrosomes mature by accumulating more PCM with concomitant elongation of the linkers connecting them. Eventually, at G2/M transition, the centrosomes separate by the dissolution of linker and migrate towards opposite poles to form bipolar spindle necessary for sister chromatid separation. After mitosis, the mother-daughter disengagement occurs at G1 phase by the establishment of linker between them. The disengaged centrioles duplicate in S phase to initiate the formation of two mature centrosomes at G2/M transition (Agircan et al., 2014; Bettencourt-Dias and Glover, 2007).

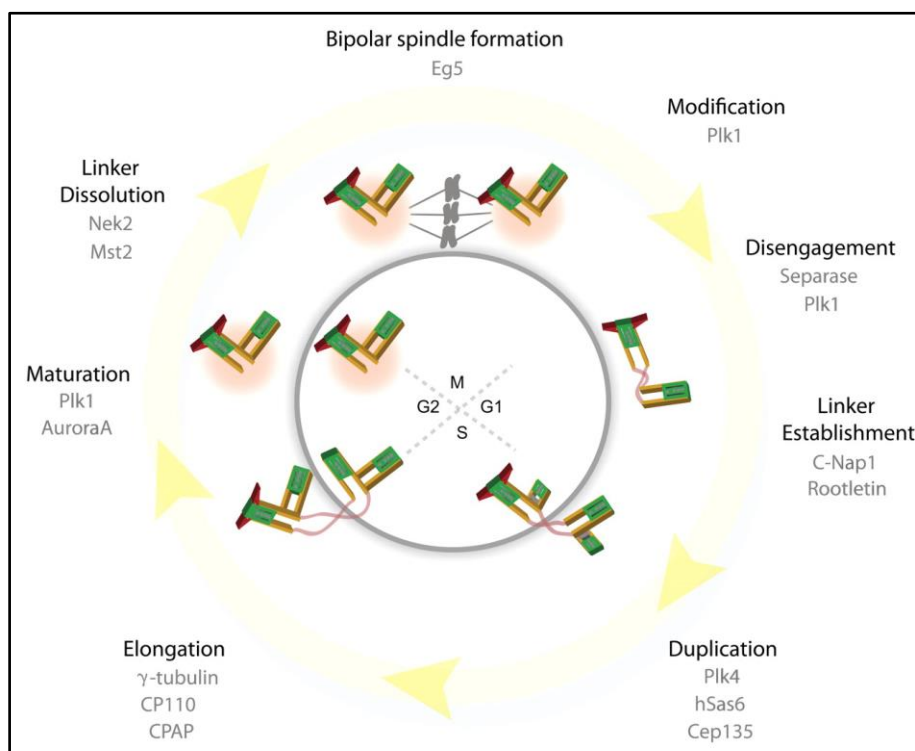


Figure 1.1: The close association between centrosome and cell cycle in animal cells (Adopted from Mardin and Schiebel, 2012).

Centrosomes are the key organelle for bipolar spindle formation in mitosis and, like cellular genetic material, are duplicated once per cell cycle.

1.2 Regulation of Cell cycle

Highly dynamic, yet tightly controlled, protein phosphorylation and dephosphorylation events are important avenues to achieve unidirectional and precise division of cell components. Opposing kinases and phosphatases are the cellular tools to control these processes in a spatial and temporal manner. Cyclin-dependent kinases (Cdks) lie at the heart of cell cycle control system and their activities rise and fall as the cell progresses through the cell cycle (Morgan, 1997). These fluctuations directly correspond to cyclical changes in the phosphorylation of cellular proteins and thereby lead to the initiation and accomplishment of cell-cycle events. Cyclin-dependent kinases (CDKs) are serine/threonine kinases which require cyclin(s) for enzymatic activity. The CDK family in mammals have diverse functions and can be subdivided into three cell-cycle-related subfamilies (Cdk1, Cdk4 and Cdk5) and five transcriptional subfamilies (Cdk7, Cdk8, Cdk9, Cdk11 and Cdk20) (Lim and Kaldis, 2013; Malumbres, 2014). Cdk5 is considered to be an atypical membrane- anchored CDK. It is activated by the non-cyclin proteins Cdk5R1 (p35) or Cdk5R2 (p39) and T-loop phosphorylation is not required (Arif, 2012; Cheung and Ip, 2012). CDK5 is thought to be active in terminally differentiated cells such as neurons because of the expression pattern of p35 and p39. However, apart from its critical role in neurons, Cdk5 take part in other cellular processes ranging from migration to cytoskeletal dynamics (Arif, 2012; Cheung and Ip, 2012; Lim and Kaldis, 2013).

Several molecular mechanisms including post-translational protein modifications and regulated degradation ensure the sequential phase-specific activation/inactivation of Cdks. Thus, it can be convincingly presumed that mitotic phosphatases play pivotal roles in annulling the kinase-mediated protein phosphorylation. However, our current knowledge regarding the regulation as well as substrate-specificity of most of the phosphatases is still in its infancy.

1.3 Phosphatases in animal cells

The kinases and their counteracting phosphatases orchestrate the protein modifications associated with precise cell cycle phases (Barr et al., 2011). Interference with either kinase or phosphatase activity will affect orderly mitotic progression (Heinrich et al., 2002). The phosphatases expressed in human can be divided into two prominent groups depending on the amino acids that they dephosphorylate: (a) protein tyrosine phosphatase (PTP) family and (b) serine/threonine-specific phosphatases (PSTPs) family (Tonks, 2006; Trinkle-Mulcahy and Lamond, 2006). PTP family includes the dual-specificity tyrosine and serine/threonine phosphatases (DUSPs) and, with the exception of Cdc25, PTPs are involved in cellular signal transduction rather than in the regulation of mitosis. The PSTPs can be further classified into two groups that are both dependent on metal ions for catalysis: (a) PPM family of metallo-dependent phosphatases and (b) phospho-protein phosphatases (PPP) family (Kumagai and Dunphy, 1991). PPP family includes the phosphatases PP1, PP2A, PP2B, PP4, PP5, PP6, PP7 and are the key regulators for cell division (Axton et al., 1990; Picard et al., 1989) (Figure 1.2). Treatment of PPP specific inhibitor okadaic acid is sufficient to trigger mitotic changes such as chromatin condensation and organelles rearrangement, indicating the critical opposing role of PPP in mitotic entry (Lucocq et al., 1991; Yamashita et al., 1990). PPP phosphatases function as multimeric holoenzyme complexes consisting of a catalytic subunit and one or more of a number of associated regulatory and scaffolding subunits (Barr et al., 2011).

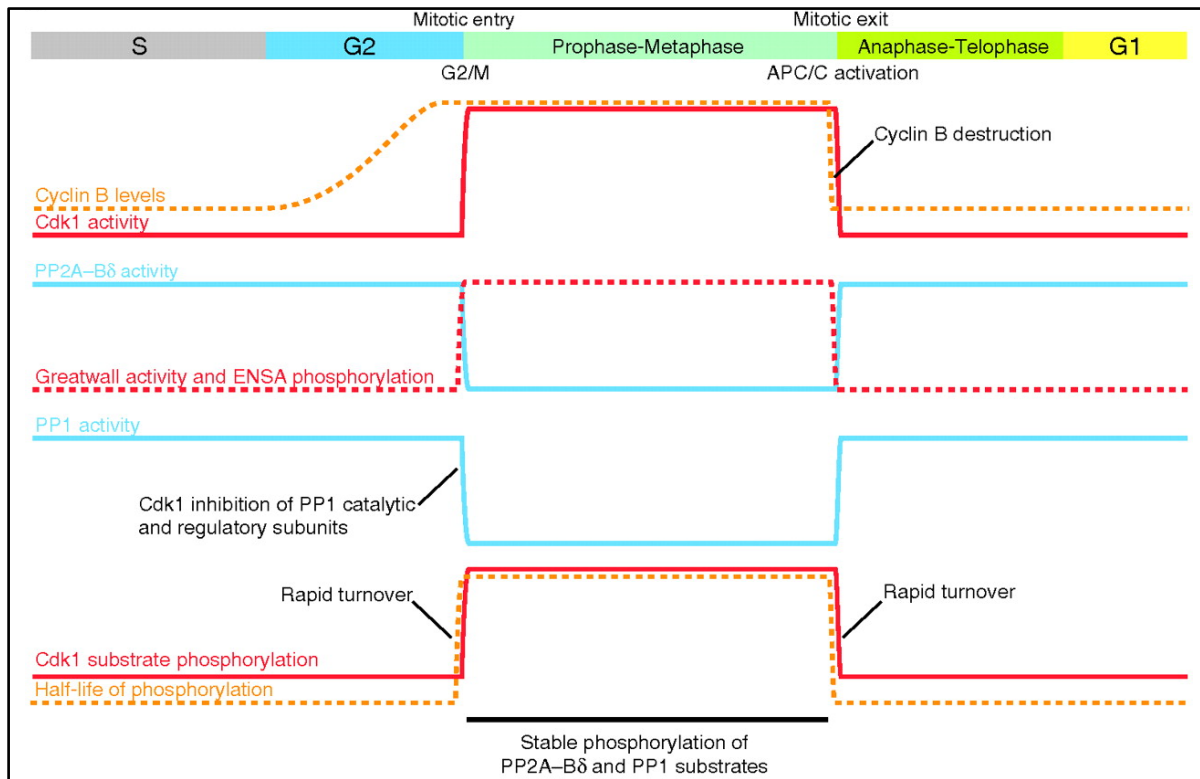


Figure 1.2: Phospho-protein phosphatases (PPP) family are the key regulators of cell cycle progression in animal cells (Adopted from Barr et al., 2011).

Cell cycle dependent rise and fall of key kinase/ phosphatase levels/activity are depicted with respective coloured lines. The balance between kinases and phosphatases determines the cell cycle progression.

1.4 Cdc14 phosphatase in budding yeast

CDC14 (cell division cycle 14) belongs to the dual-specificity phosphatases family and is essential for cell cycle progression in budding yeast *Saccharomyces cerevisiae* (Hartwell et al., 1973). It is the master regulator of cell cycle completion in yeast (Amon, 2008) and mutants of *Cdc14* arrest in late anaphase with duplicated, separated chromosomes and elongated spindles (Pringle and Hartwell, 1981). ScCDC14 is a proline-directed dual specificity phosphatase (serine/threonine) which prefers pSPxK/R sites for substrates (Bremmer et al., 2012; Eissler et al., 2014). CDC14 dephosphorylates and activates Cdh1, which in turn causes the degradation of Clb2 in an APC^{Cdh1} (anaphase-promoting complex) dependent manner. Cdc14 also augments the synthesis of Cdk-Clb2 inhibitor Sic1 through dephosphorylation mediated activation of the transcription factor Swi5. Moreover, Sic1 is stabilized by

CDC14 (Feldman et al., 1997; Jaspersen et al., 1999; Knapp et al., 1996). Thus, ScCDC14 antagonizes the Cdk1 functions to sharpen the metaphase to anaphase transition (Stegmeier and Amon, 2004).

During the whole interphase and up to the anaphase, ScCDC14 is trapped inactive in the nucleolus through the components of RENT (REgulator of Nucleolar silencing and Telophase exit) complex including Net1, Sir2 (a NAD-dependent deacetylase), Tof2, and Fob1 (Shou et al., 1999). Net1, a protein that directly binds to rDNA, is required for the nucleolar localization of ScCdc14 (Huang and Moazed, 2003; Straight et al., 1999). Release from the nucleolus and activation of ScCdc14 occur in two sequential waves: the Fourteen Early Anaphase Release (FEAR) network and the Mitotic Exit Network (MEN) (Amon, 2008; Queralt and Uhlmann, 2008; Wurzenberger and Gerlich, 2011) (Figure 1.3).

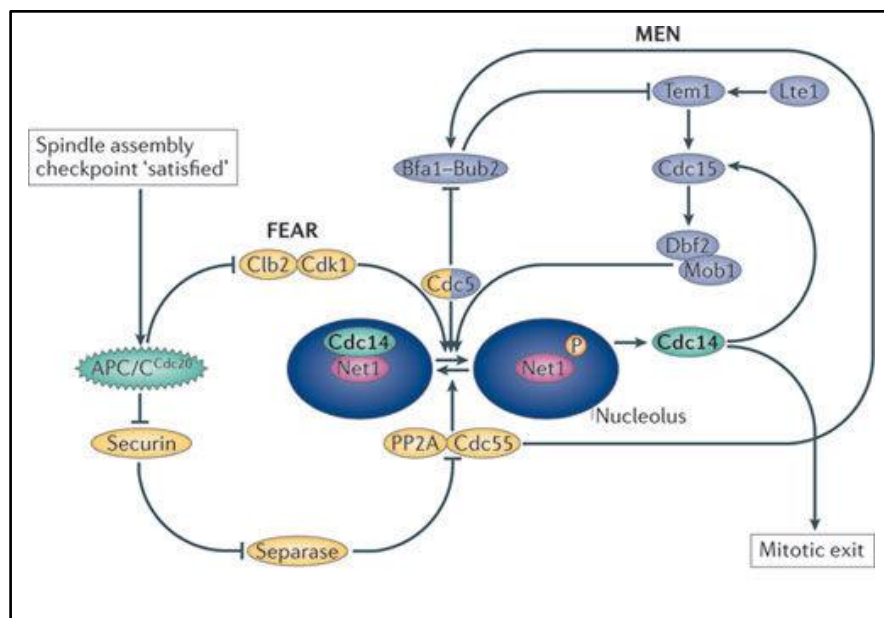


Figure 1.3: The regulatory networks that activate Cdc14 in budding yeast (Adopted from Wurzenberger and Gerlich, 2011).

The Cdc14 early anaphase release (FEAR; yellow) and mitotic exit network (MEN; light blue), regulatory networks activate Cdc14 for budding yeast mitotic exit. FEAR causes the early anaphase partial release whereas MEN leads to the complete release of CDC14 necessary for the completion of mitotic exit (Wurzenberger and Gerlich, 2011).

The FEAR network causes the hyperphosphorylation of Net1 by Cdk1 and Cdc5 (a Polo-like kinase) to cause a partial release of ScCDC14. The APC^{Cdc20} is activated upon spindle assembly checkpoint (SAC) satisfaction and leads to the proteasomal degradation of securin, thereby allowing separase to inactivate PP2A-Cdc55 and inhibit Net1 dephosphorylation. The MEN network ensures the complete CDC14 release by a pathway involving the small GTPase Tem1. The function of Tem1 is regulated by the GTPase-activating protein (GAP) Bfa1-Bub2, and the putative guanine nucleotide exchange factor (GEF) Lte 1 (low temperature essential 1). Tem1 regulates the phosphorylation of Net1 by several downstream MEN kinases, including Cdc15 and the kinase complex Mob1-Dbf2 (Wurzenberger and Gerlich, 2011).

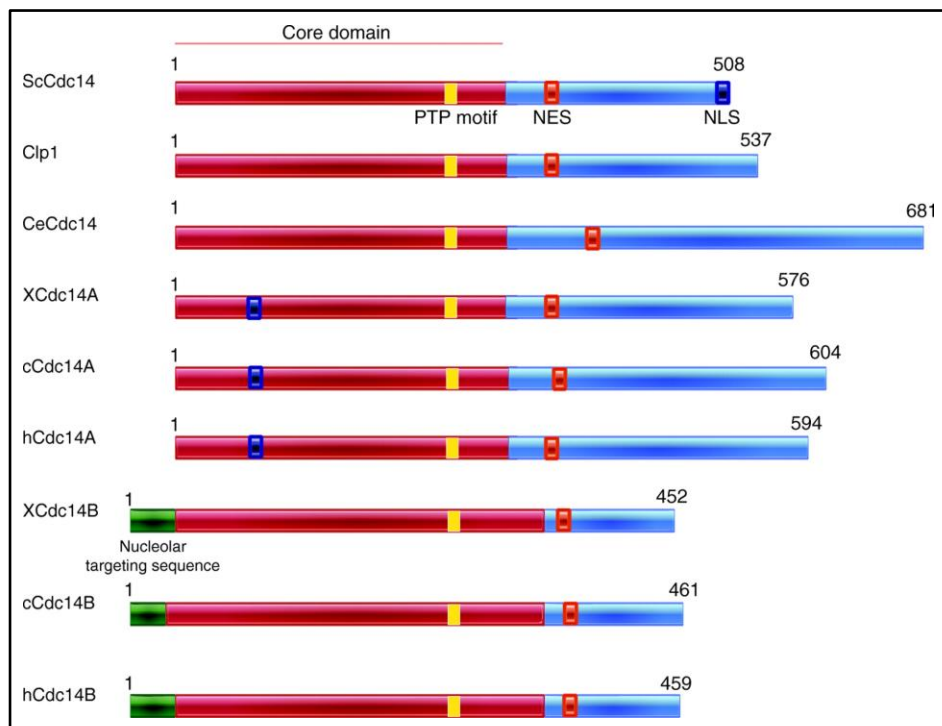


Figure 1.4: Schematic representation of Cdc14 primary structures (Adopted from Mocciaro and Schiebel, 2010).

The N-terminal conserved domains are shown in red and the variable C-terminals are shown in light blue. The nucleolar targeting sequence in green; catalytic motif in yellow; NLS (nuclear localization signal) in dark blue; NES (nuclear export signal) in orange. Here, ScCdc14: Budding yeast Cdc14; Clp1: Fission yeast Cdc14-like

phosphatase (Clp1); CeCdc14: *C. elegans* Cdc14; XCdc14A/B: *Xenopus Laevis* Cdc14A/B; cCdc14A/B: Chicken Cdc14A/B) (Mocciaro and Schiebel, 2010).

1.5 Cdc14: a family of conserved phosphatases

The Cdc14 family of phosphatases is highly conserved in almost all higher eukaryotes including *Saccharomyces cerevisiae*, *Schizosaccharomyces pombe*, *Caenorhabditis elegans*, *Xenopus laevis*, *Gallus gallus* and *Homo Sapiens* (Mocciaro and Schiebel, 2010) (Figure 1.4). *Schizosaccharomyces pombe* and *Caenorhabditis elegans* possess only one gene coding for an ortholog of ScCdc14. The ortholog of ScCDC14 in fission yeast *Saccharomyces pombe* is non-essential and is known as Cdc14-like phosphatase (Clp1) (Trautmann et al., 2001). Although Clp1 and ScCDC14 share 36% sequence identity, the role of Clp1 in cell-cycle control is different than its budding yeast ortholog. Clp1 mainly controls mitotic entry and coordinates cytokinesis with the initiation of the next cell cycle. It is not crucial for mitotic exit (Cueille et al., 2001; Trautmann et al., 2001). Clp1 localization in nucleolus during G1/S phase is similar to that of ScCDC14. However, unlike ScCDC14, Clp1 is released at the G-M transition and is independent of MEN and FEAR pathway activation (Chen et al., 2006). After release, Clp1 associates with kinetochore and functions in collaboration with Aurora B kinase to ensure accurate chromosome segregation (Trautmann et al., 2001). During cytokinesis, Clp1 regulates the septum formation. Nevertheless, it is not essential for either septation or cytokinesis (Clifford et al., 2008; Cueille et al., 2001; Khmelinskii et al., 2009; Simanis, 2003; Trautmann et al., 2001).

Vertebrates such as humans, primates, mice, chickens, and fish were reported to have two genes coding for CDC14 phosphatases, CDC14A and CDC14B, with high degree of sequence homology to ScCDC14 (Clément et al., 2011, 2012; Li et al., 1997; Mocciaro and Schiebel, 2010; Rosso et al., 2008; Wei et al., 2011). A retroduplication event of *CDC14B* gene (from Chromosome 9 to 7) generated a third gene (CDC14C) coding for a member of CDC14 family in hominoids around 18–25 million years ago (Rosso et al., 2008). CDC14C was reported to be transcribed only in brain and testis (Brawand et al., 2011) (Figure 1.5).

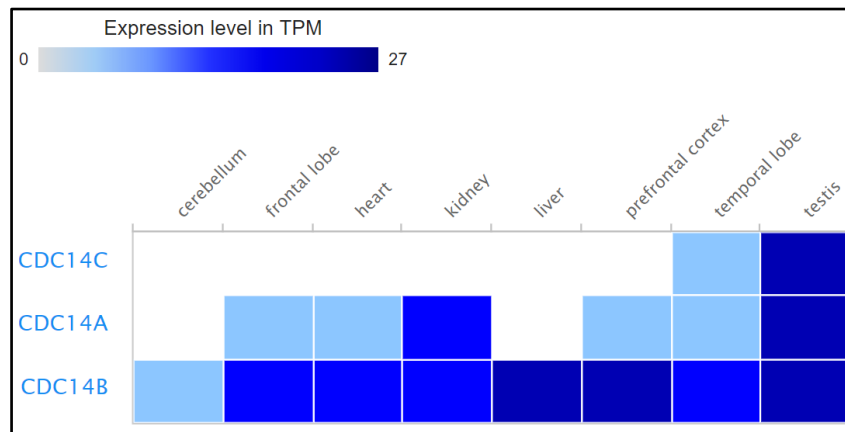


Figure 1.5: Expression of Cdc14 isoforms in different organs of human body.

Degree of expression in TPM (transcript per million) are represented by the intensity of blue colour. The expression data was retrieved from the expression atlas (<https://www.ebi.ac.uk/gxa/home/>). The ‘Mammalian Kaessmann’ data from eight different human tissues are used in the graph (Brawand et al., 2011).

1.6 Functions of hCDC14 proteins

Human cells encode three paralogs of *hCDC14*, namely *hCDC14A*, *hCDC14B* and *hCDC14C* (Li et al., 2000; Rosso et al., 2008). In spite of the high conservations between the catalytic domain of all CDC14 phosphatases (Gray et al., 2003) and the complementation of *ScCDC14* by *hCDC14B* (Cho et al., 2005), human CDC14s have so far been reported to be involved in functions that are more diverse than that of budding yeast (Mocciaro and Schiebel, 2010). *hCDC14A* was proposed to exert its function at centrosome duplication (Mailand et al., 2000) and actin cytoskeleton regulation (Chen et al., 2017, 2016) while *hCDC14B* was implicated in mitotic progression (Tumurbaatar et al., 2011), DNA damage checkpoint activation and DNA repair (Bassermann et al., 2008; Lin et al., 2015). Nevertheless, *hCDC14B* depleted human cells display normal mitotic exit and cytokinesis (Berdougo et al., 2008). Moreover, the viability of *hCDC14A* or *hCDC14B* single knockout (KO) vertebrate cells (Mocciaro et al., 2010) indicates the possible functional redundancy of vertebrate phosphatases. It is noteworthy that most of the previously reported functions of *hCDC14A/B* were deduced upon siRNA depletion (often without a

rescue experiment) or strong over-expression that causes toxic effects. The extent of depletion, as well as the functional redundancy of the phosphatases, was not taken into consideration partly because of the inability of available antibodies to recognize endogenous hCDC14A and hCDC14B proteins (Guillamot et al., 2011; Mocciaro et al., 2010; Ovejero et al., 2012).

CDC14 proteins display a conserved localization to the microtubule organizing centre such as the spindle pole body (SPB) in yeast and the human centrosome (Mailand et al., 2002; Pereira et al., 2002). CDC14 is also associated with the basal body during ciliogenesis (Ah-Fong and Judelson, 2011; Clément et al., 2012). Recently, an autosomal recessive nonsense mutation in *hCDC14A* has been reported to cause severe to profound deafness due to defective transient kinocilia of developing cochlear hair cells and the persistent kinocilia of vestibular hair cells in the organ of Corti (Delmaghani et al., 2016; Imtiaz et al., 2018). Furthermore, shorter cilia have been reported in zebrafish upon *cdc14a* or *cdc14b* depletion with morpholinos (Clément et al., 2011, 2012). However, it is still an open question whether CDC14A regulates primary cilia in human cells and how CDC14A promotes ciliogenesis on a molecular level.

1.7 Connection between Cilia and cell cycle

Cilia and flagella are microtubule-based membranous cell protrusions involved in motility and sensation. They are evolutionarily-conserved structures that differ from each other based on their length as well as number per cell. Vertebrate cilia are conventionally classified into motile cilia and sensory primary cilia (Takeda and Narita, 2012). Motile cilia and flagella are considered as highly comparable organelles due to their 9+2 axonemal configuration (a central pair of singlet microtubules surrounded by nine doublet microtubules) and intraflagellar transport (IFT) machinery (Satir and Christensen, 2007; Satir et al., 2008). Primary cilia are generally non-motile organelle with a 9+0 axonemal configuration and are involved in sensing and integrating external signals. Most cells (not all) have the capacity to form cilia whereas most cancer cells (not all) lack cilia (Keeling et al., 2016).

Assembly of primary cilia is tightly coordinated with the cell cycle phases. Generally, cilia assemble when cells become quiescent (G₀) or differentiate. The primary cilia are disassembled through the signaling cascade that stimulates cells to re-enter the cell cycle. Upon the completion of mitosis, centrosomes become competent again to initiate primary cilia formation either in G₀ or in early G₁ phase (Figure 1.6) (Sánchez and Dynlacht, 2016). The structure of primary cilia can be divided into ciliary skeleton and ciliary membrane (Figure 1.7) (Hoerner and Stearns, 2013). The ciliary skeleton is composed of a basal body with nine microtubule triplets and an axoneme extension with nine microtubule doublets (Gluenz et al., 2010). The transition between microtubule triplet to doublet is termed as transition zone and is marked by Y-shaped bridges extending from microtubule doublets to the ciliary membrane (Aubusson-Fleury et al., 2012; Gluenz et al., 2010). Thus, the transition fibers serve as anchors for the basal body to the ciliary membrane. Ciliary rootlets provide a second level of anchorage by interconnecting the mother centriole (basal body) and daughter centriole (Broekhuis et al., 2014) with the nucleus (Figure 1.7).

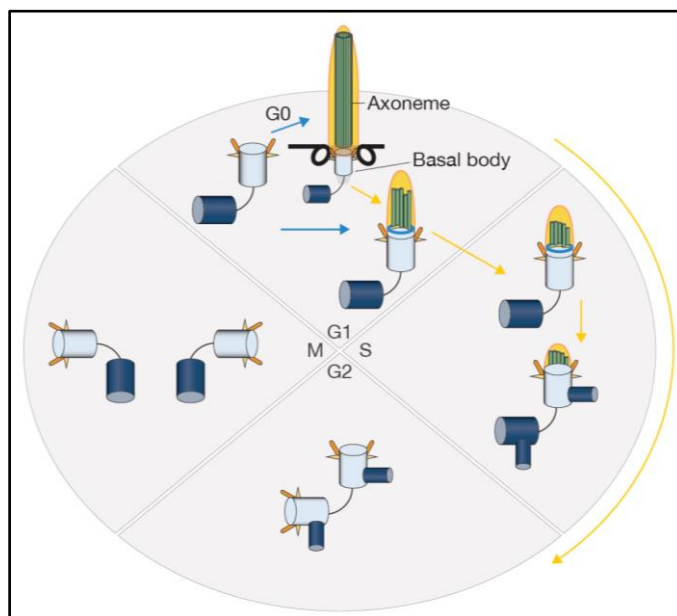


Figure 1.6: Linkage between cilium and cell cycle (Adopted from Sánchez and Dynlacht, 2016).

Primary cilia assemble specifically in G₀ or early G₁ phase. Only the mother centriole with proteinaceous appendages can initiate ciliogenesis (assembly of cilia). Generally,

the cilia assembling role and the microtubule organizing spindle assembling role of centrosomes are mutually exclusive. So, the cilium assembled in G₀ or early G₁ phase must be disassembled to allow cells entering S phase and assemble spindles in M-phase (Sánchez and Dynlacht, 2016).

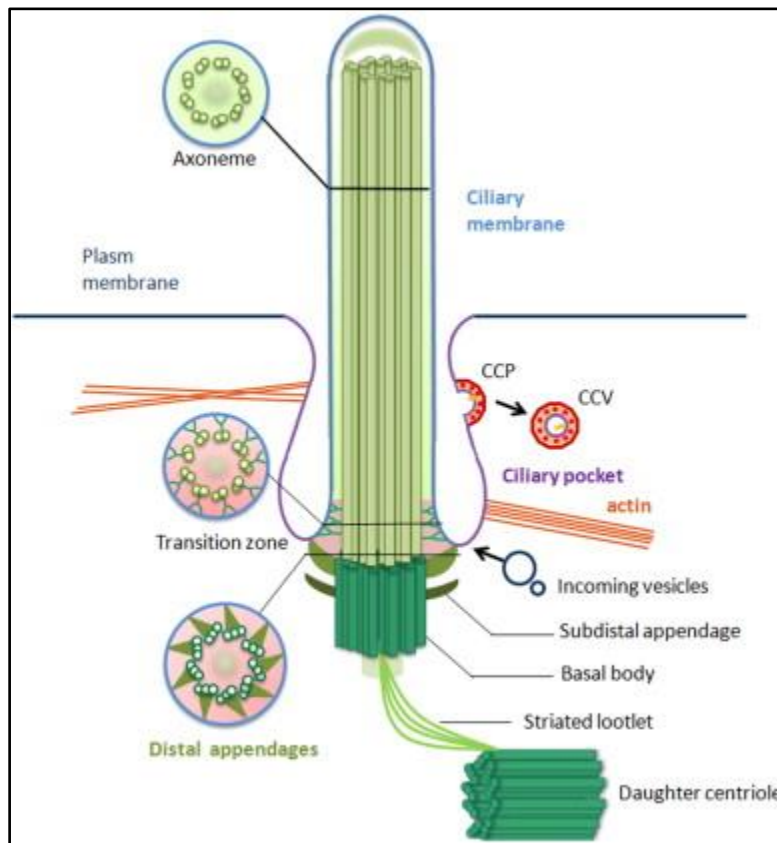


Figure 1.7: Structure of primary cilia (Adopted from Ke and Yang, 2014).

Primary cilia are microtubule-based structures surrounded by ciliary membranes. Mother centriole, termed as basal body, primes ciliogenesis by the extension of microtubule structure. The transition zone is marked with Y-shaped bridges and positioned between basal body with microtubule triplets and axoneme with microtubule doublets. The basal body is connected to the daughter centriole through ciliary rootlet (Ke and Yang, 2014).

Ciliogenesis is a complex process that involves precise spatial as well as temporal regulation of several intertwined cellular events like cell cycle progression, vesicular docking, and ciliary extension (Avasthi and Marshall, 2012). Assembly of primary cilium initiates through the conversion of mother centriole to basal body (Figure 1.8). Upon exit from the cell cycle, a guanine nucleotide exchange factor (GEF) called Rabin 8 is recruited to the pericentriolar recycling endosome and gets

activated by Rab11. Activated Rabin 8, in turn, activates Rab8a vesicles for their recruitment and docking to the distal appendages (distal appendage vesicles, DAV). Smaller distal appendage vesicles undergo EHD1-mediated fusion to form larger ciliary vesicles (CV). Further axoneme growth and microtubule extension depend on the acquisition of positive regulators (TTBK2, MARK4, IFT) as well as the removal of negative regulators (CP110, Trichoplein). Subsequently, the ciliary gate termed as transition zone (TZ) is assembled, and various IFT proteins help transport proteins through this gate (Sánchez and Dynlacht, 2016).

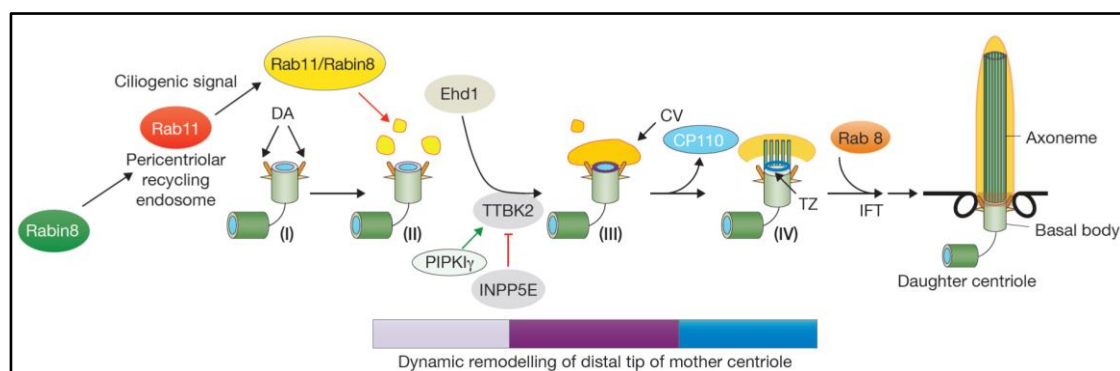


Figure 1.8: Critical events in primary cilia assembly process (Adopted from Sánchez and Dynlacht, 2016).

A series of highly orchestrated events causes the initiation and elongation of cilia termed as ciliogenesis or cilia assembly. The ciliogenesis process can be divided into four sequential events: (I) Conversion of mother centriole to basal body through acquisition of distal appendage; (II) formation of distal appendages vesicles (DAV) through docking of Rab8a vesicles (Yellow); (III) Ehd1-mediated fusion of DAV to form larger ciliary vesicles (CV); (IV) removal of negative regulators and concomitant acquisition of positive regulators ensuring axoneme growth and microtubule extension (Sánchez and Dynlacht, 2016).

Cilium disassembly is triggered when the cell is committed to re-enter the cell cycle through stimulation by serum growth factors (Figure 1.9). In G1 phase, the concerted actions of two kinesin motor proteins (Kif2a and Kif24) and destabilization of acetylated tubulins are critical for cilia disassembly. The kinesins cause the inhibition of axoneme extension whereas tubulin de-acetylation leads to the disassembly of microtubule cytoskeleton (Sánchez and Dynlacht, 2016). Activation of

Aurora A kinase (AurA) by several different ways leads to phosphorylation mediated activation of histone deacetylase 6 (HDAC6) and tubulin de-acetylation (Plotnikova et al., 2012). HDAC6 was also reported to deacetylate cortactin and thereby enhancing actin polymerization by augmenting interaction between cortactin and filamentous actin (Ran et al., 2015). Thus, HDAC6 promotes cilium disassembly through stimulating actin polymerization. Trichoplein and Pitchfork (Pifo) are two additional molecules that lead to activation of AurA and cilium disassembly (Inoko et al., 2012; Kinzel et al., 2010; Sánchez and Dynlacht, 2016).

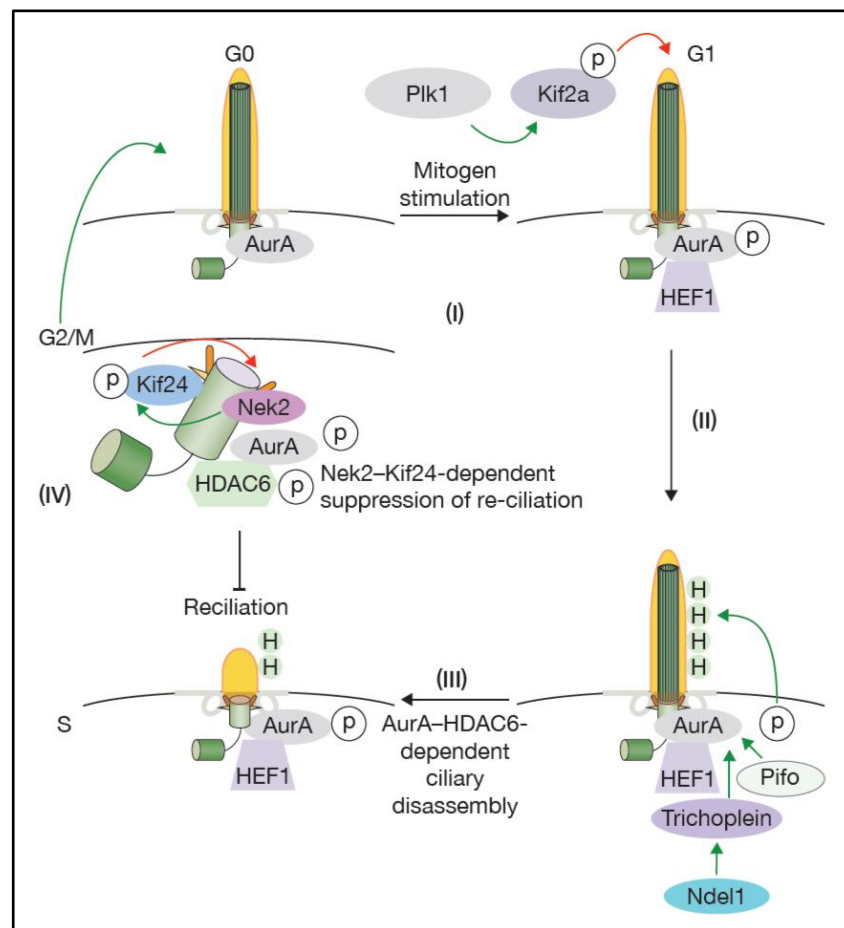


Figure 1.9: Critical events mediating cilium disassembly (Adopted from Sánchez and Dynlacht, 2016).

Upon mitogen stimulation, Plk1-mediated phosphorylation of Kif2a causes destabilization of acetylated tubulins in the ciliary axoneme. Activation of AurA through several signalling inputs activates HDAC6 and causes tubulin destabilization by deacetylation. A second depolymerizing kinesin is activated at a later time by Nek2 and thereby prevent reciliation throughout S/G2/M phases (Sánchez and Dynlacht, 2016).

1.8 Ciliopathies associated with defects in primary cilium signaling

The roles of cilia in integrating a plethora of signalling pathways critical to vertebrate development and differentiation have placed this organelle in the frontier of current research (Ishikawa and Marshall, 2017). Loss or malfunction of cilia affects a wide range of human organ systems and causes diseases that have been termed as ciliopathies (Fry et al., 2014; Reiter and Leroux, 2017). Generally, the ciliopathies can be characterized as monogenic recessive disorders and the disease outcome is the combination of defective cilia structure and associated altered ciliary signalling (Figure 1.10).

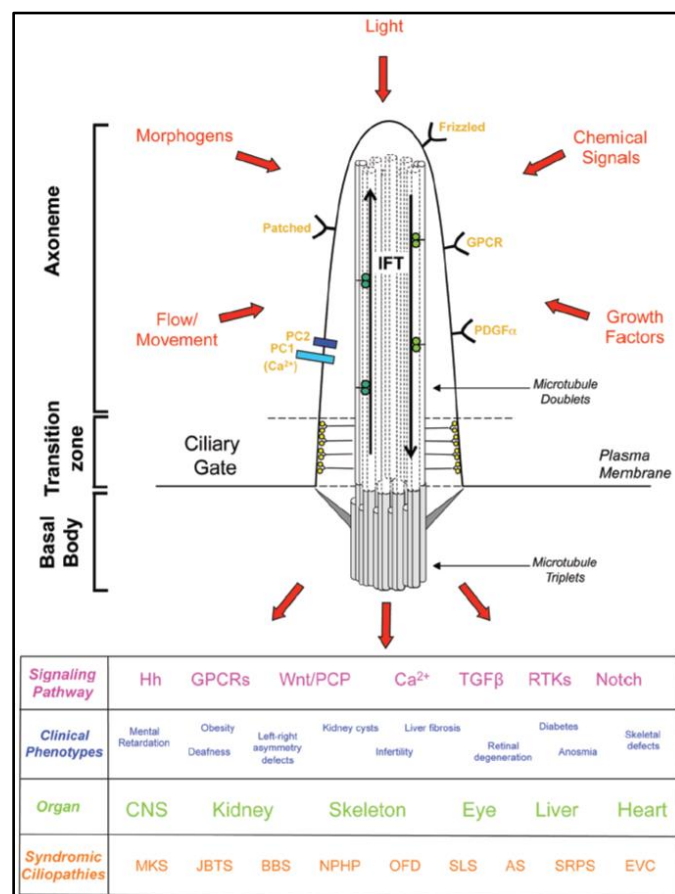


Figure 1.10: A schematic overview of the primary cilium signaling and associated ciliopathies (Adopted from Fry et al., 2014).

Cilia are receptor-enriched cell protrusions and several signalling pathways are regulated through cilia. Defective ciliary signalling affects almost all major organs and leads to ciliopathies such as MKS (Meckel-Gruber Syndrome); JBTS (Joubert Syndrome); BBS (Bardet-Biedl Syndrome); NPHP (nephronophthisis); OFD (Oral-

Facial-Digital Syndrome); SLS (Senior-Løken Syndrome); AS (Alstrom Syndrome); SRPS (Short Rib-Polydactyly Syndrome); EVS (Ellis-van Creveld Syndrome) (Fry et al., 2014).

1.9 Actin and ciliogenesis

The actin cytoskeleton has been described to have significant regulatory input in ciliogenesis (Figure 1.11) (Malicki et al., 2017). In general, actin polymerization inhibits ciliogenesis whereas actin-severing factors, such as cofilin and gelsolin-family proteins, boost cilia formation. The addition of low concentrations of the F-actin depolymerizing drug cytochalasin D promotes cilia elongation partly by regulating vesicle trafficking and inhibiting cilia disassembly factors (Kim et al., 2010, 2015). In addition, actin and the actin regulator drebrin (DBN1) mediate the release of vesicles, so-called ectosomes, from the tip of cilia (Nager et al., 2017). Recently, it was suggested that a branched, Arp2/3 organized actin network surrounds the centrosome and promotes transport of preciliary vesicles to the basal body via the action of the myosin-Va motor protein (Wu et al., 2018). Furthermore, CDK10/CycM protein kinase was proposed to negatively regulate ciliogenesis by inducing actin polymerization (Guen et al., 2016, 2018).

The modulation of cilia function by actin cytoskeleton raises the question about regulators of the actin cytoskeleton, in particular kinases and phosphatases that control properties of cilia. In this respect, it is interesting that the proline directed phosphatase hCDC14A is associated with the actin cytoskeleton where it regulates cell migration and cell adhesion and in addition has functions in ciliogenesis (Chen et al., 2017, 2016; Clément et al., 2012; Delmaghani et al., 2016; Imtiaz et al., 2018). However, the molecular mechanism(s) governing the regulation of ciliogenesis by CDC14A remains elusive.

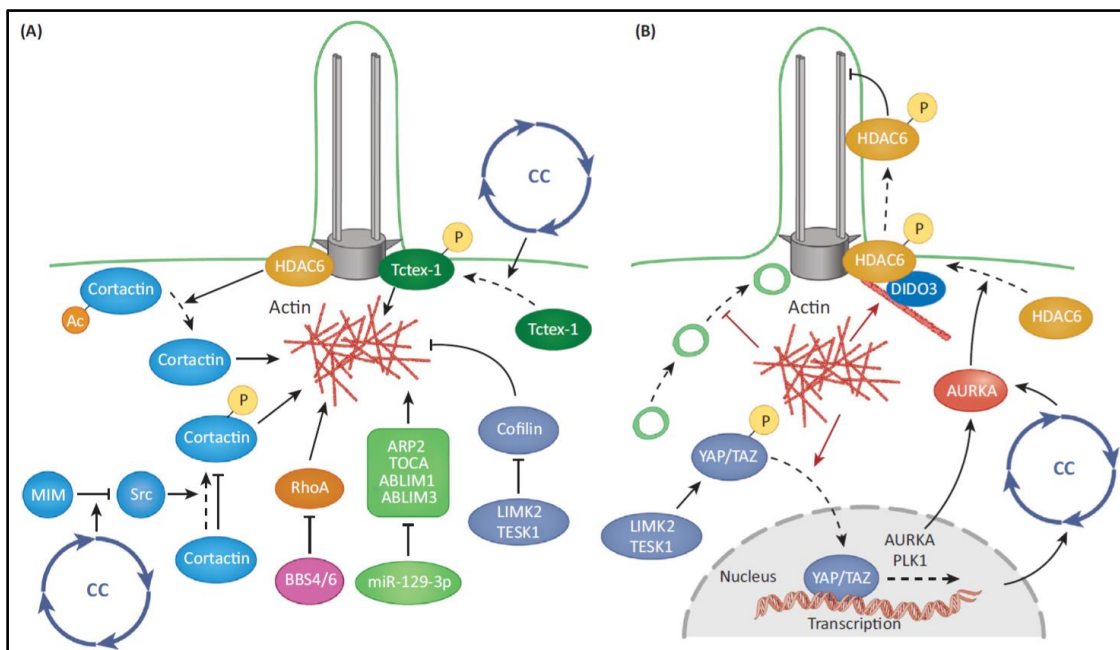


Figure 1.11: Regulation of ciliogenesis by actin cytoskeleton (Adopted from Malicki et al., 2017).

(A) Several pathways regulate periciliary actin cytoskeleton. Posttranslational protein modifications such as deacetylation and phosphorylation of the actin regulator cortactin lead to actin polymerization and cilia disassembly. Cell cycle dependent signalling is also tightly linked to actin cytoskeleton remodelling that has an impact on ciliogenesis. (B) Actin affects ciliogenesis through multiple distinct mechanisms such as vesicle trafficking to the cilia base as well as localization of the ciliogenesis regulators to basal body (Malicki et al., 2017).

1.10 Aim of the thesis

The focus of this study was to decipher the molecular mechanisms of human CDC14s functions by analysing knockout cellular models along with various protein tagging approaches. I have utilized zinc-finger nuclease (ZFN)-catalyzed double strand break followed by homologous recombination-mediated incorporation of premature stop codon and selection marker to target CDC14A (hCDC14A) and CDC14B (hCDC14B) loci in telomerase immortalized human retinal pigment epithelium (hTERT-RPE1) and HCT116 cells. Phenotypic analyses of the generated knockout (KO) cells were conducted to assign molecular functions to these proteins. RPE1 cells lacking hCDC14A functions displayed elongated cilia upon serum starvation. Global phosphoproteome, as well as proximity-based interaction proteomics approaches, were employed to identify substrates and thereby decode the molecular mechanism(s) of longer cilia in hCDC14A KO cells.

2 Results

The following results and figures are parts of an already published article (Uddin et al., 2015) and a manuscript in preparation (Borhan Uddin, Patrick Partscht, Nan-Peng Chen, Annett Neuner, Manuel Weiß, Robert Hardt, Aliakbar Jafar Pour, Bernd Heßling, Thomas Ruppert, Holger Lorenz, Gislene Pereira and Elmar Schiebel; **The phosphatase hCDC14A and CDK5 kinase regulate cilia length through phosphoregulation of the actin-binding protein drebrin**). I have adopted the results from these manuscripts with subtle modifications.

2.1 Generation of *hCDC14* knockout cells

2.1.1 Strategy for the generation of knockout cell lines

Zinc finger nucleases (ZFN) specifically designed to target *hCDC14A* or *hCDC14B* loci were used to generate human cell lines devoid of these two phosphatase activities (CompoZr™ ZFNs, Sigma Advanced Genetic Engineering Labs) (Chen et al., 2016; Uddin et al., 2015). *hCDC14A* and/or *hCDC14B* knockout cell lines were made using two human cell lines with stable genotype (hTERT-RPE-1 and HCT 116). Double strand break-induced homologous recombination strategy was employed to incorporate premature stop codon and selection markers (neomycin or puromycin) into the targeted exons of *hCDC14A* (9th exon) and *hCDC14B* (4th exon) (Figure 2.1). Southern blot analysis has confirmed the successful biallelic targeting of the *hCDC14A* and *hCDC14B* loci by NeoR or PuroR cassettes (Figure 2.2).

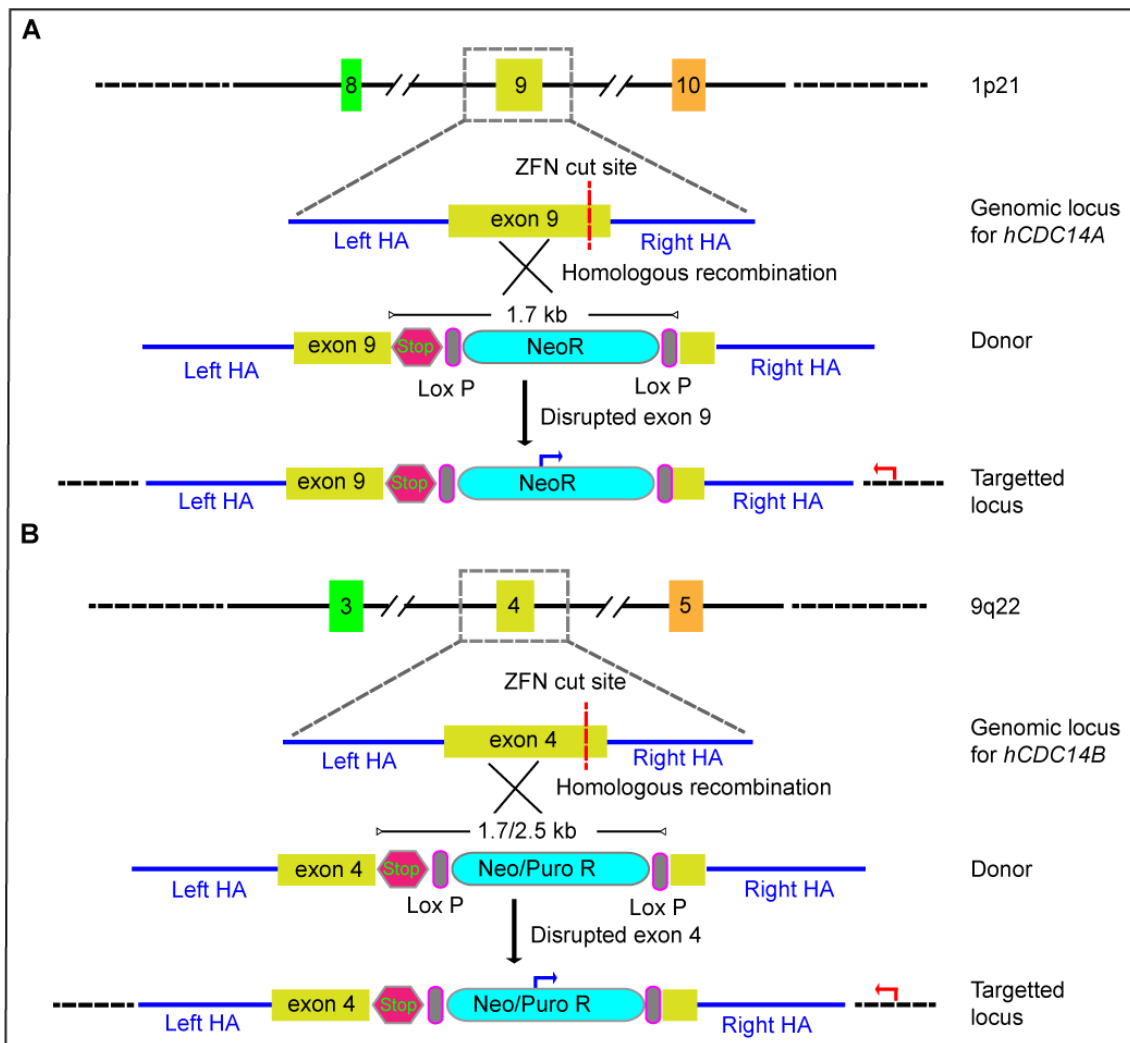


Figure 2.1: Strategy for ZFN-mediated generation of knockout cell lines (Adopted from Uddin et al., 2015).

(A) Exon 9 of *hCDC14A* was targeted by zinc finger nuclease (ZFN). A donor template containing two homologous arms (HA), stop codon and neomycin selection cassette was used for their homologous recombination mediated insertion within the double strand break (DSB) site. Junction PCR with forward primer (blue arrow) in NeoR cassette and reverse primer (red arrow) in the genome outside homology arm confirmed successful targeting and insertion of the selection marker.

(B) Exon 4 was targeted to knockout *hCDC14B* gene. Like donor template for *hCDC14A*, neomycin selection cassette was used to generate *hCDC14B* single knockout. Puromycin cassette was used when *hCDC14B* was knocked out on top of *hCDC14A*^{-/-} cells (neomycin). Forward (blue) and reverse (red) primers used for the junction PCR are shown in the figure.

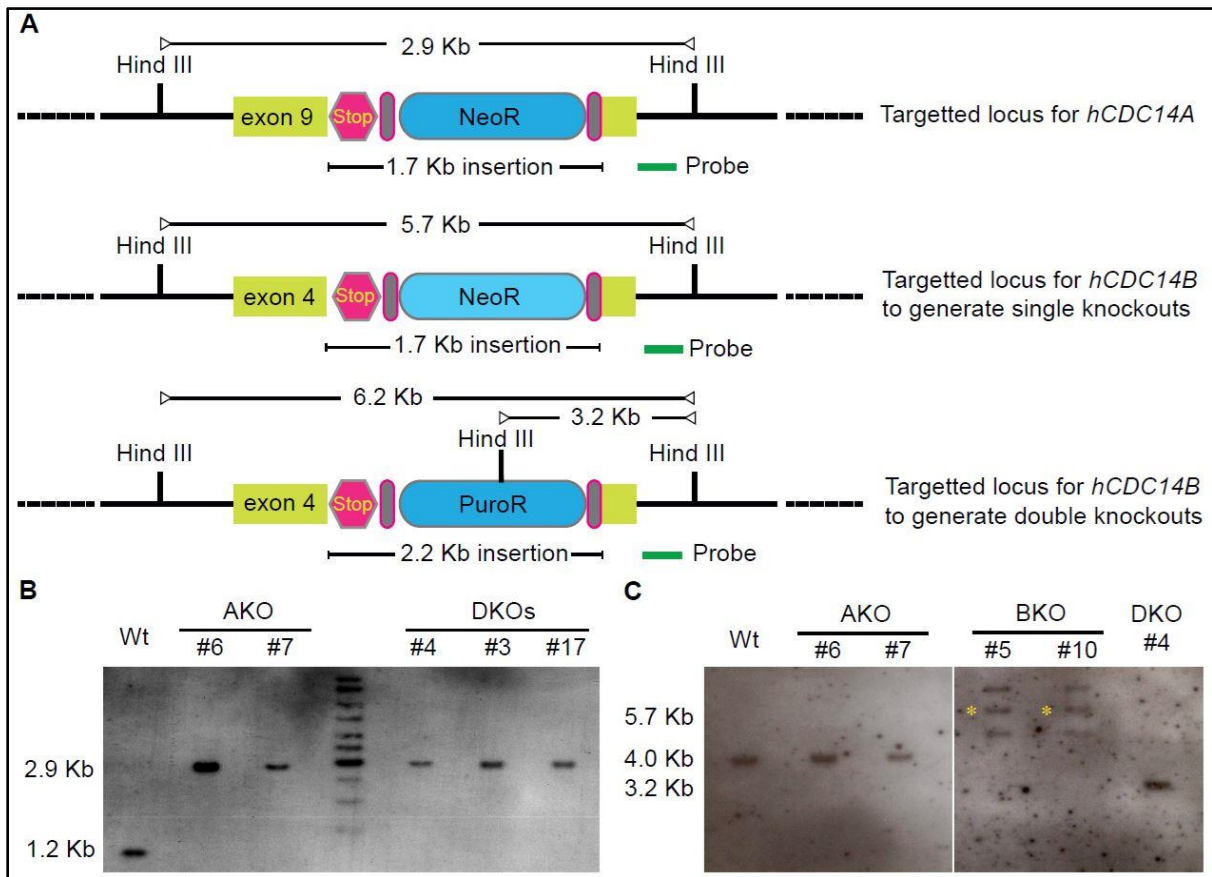


Figure 2.2: Southern blot hybridization to confirm biallelic targeting of *hCDC14A* and *hCDC14B* loci in RPE-1 cells (Adopted from Uddin et al., 2015).

(A) Map for *hCDC14A* and *hCDC14B* genomic locus targeted by zinc finger nuclease (ZFN). The probes for Southern blot hybridization were designed in the right homologous arms (shown as green bar). In case of *hCDC14A*, digestion by Hind III would result in a 2.9 kb fragment for knockout cells instead of wild-type 1.2 kb band. For knocking out *hCDC14B*, neomycin or puromycin inserted donor templates were used. Puromycin construct (with an extra Hind III site) was used when *hCDC14B* knocking out was carried out on top of *hCDC14A*^{-/-} cells (NeoR) (double knockout). On the other hand, neomycin construct was used during generation of single *hCDC14B* knockout. (B) Southern blot hybridization to confirm *hCDC14A* knockout (AKO) with a *hCDC14A* specific probe. The expected *hCDC14A* band sizes were observed for wild type (Wt, 1.2 kb), *hCDC14A* single (AKO) and *hCDC14A hCDC14B* double knockouts (DKO) (2.9 kb). (C) Southern blot hybridization to confirm *hCDC14B* knockout (BKO) with a *hCDC14B* specific probe. The DKO (see A, PuroR) and Wt cells have shown anticipated band sizes of 3.2 kb and 4.0 kb, respectively. For single *hCDC14B* knockouts (BKO), two extra bands above and below the expected band size of 5.7 kb (asterisks) was persistently observed in different clones. Nevertheless, absence of wild type bands (4.0 kb) in these knockouts confirmed the successful targeting of both alleles.

2.1.2 RT-PCR analysis confirming expression of wild type and in-frame exon-skipped *hCDC14A/hCDC14B* transcripts

Sequencing of the *hCDC14A* and *hCDC14B* RT-PCR (reverse transcriptase polymerase chain reaction) products from wild type and selection marker knockins verified the presence of exon-skipped mature mRNA in the targeted *hCDC14A* and *hCDC14B* clones (Figure 2.3). The reading frames remain intact as the skipped exons in both the cases (9th exon for *hCDC14A* and 4th exon for *hCDC14B*) contained nucleotide numbers that could be divided by three. Hence, we assume the presence of truncated hCDC14A and hCDC14B proteins. The 9th exon of *hCDC14A* includes the active site cysteine and aspartate residues necessary for phosphatase activity (Bremmer et al., 2012; Gray et al., 2003; Hall et al., 2008), suggesting the inactivation of hCDC14A phosphatase from these cell lines (we termed these cells as *hCDC14A^{PD}*). Conversely, the catalytically important residues for hCDC14B are located in 9th exon, downstream to the targeted exon (Gray et al., 2003). Thus, in case of *hCDC14B*, the gene interference strategy most likely creates a small truncation of 31 amino acids in the hCDC14B protein that might not affect phosphatase activity.

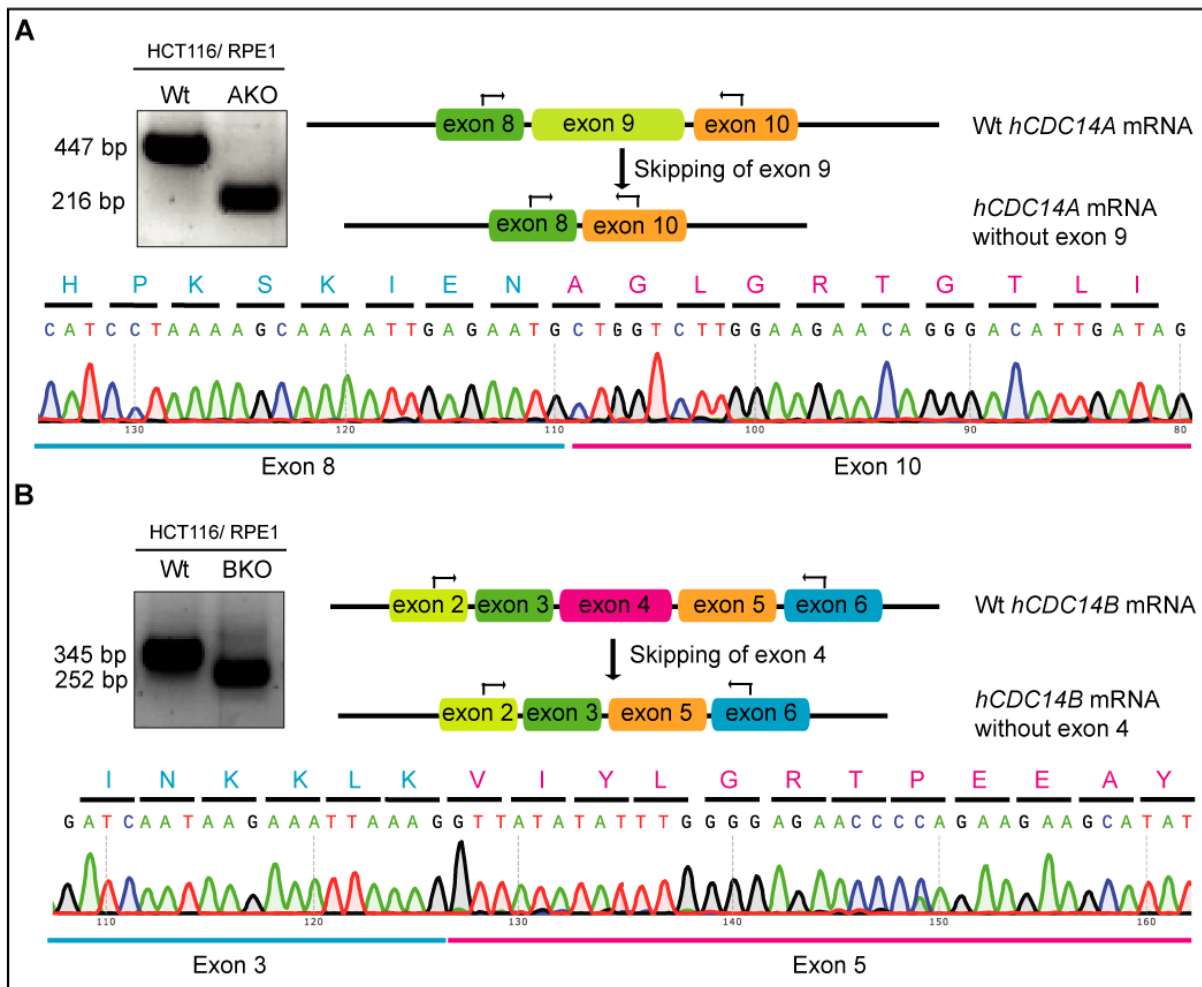


Figure 2.3: RT-PCR analysis to confirm expression of wild type and exon-skipped transcripts (Adopted from Uddin et al., 2015).

Gel images for RT-PCR products of *hCDC14A* (A) and *hCDC14B* (B) transcripts from wild type (Wt) and knockout cells (KO). Maps show the locations of primers (black arrows) used for PCR reaction. The generated DNA bands were gel purified and sequenced. Sequences of alternating exon junctions are shown in the respective lower panels (exon 8 to 10 in case of *hCDC14A* and exon 3 to 5 for *hCDC14B*). In-frame exon skipping can be deduced from the amino acid sequences written above the codons.

2.1.3 Exon-skipping phenomenon is independent of genome editing approach

Our ZFN-mediated genome editing of *hCDC14A* and *hCDC14B* has clearly indicated the skipping of targeted exon from the final transcript. As a faster and more affordable alternative to ZFN, there is a recent surge in use of CRISPR-Cas9 system for genome editing. We have taken the advantage of CRISPR-Cas9 system to target *hCDC14A* locus with the same donor construct and guide RNA that targets the same

genomic *hCDC14A* DNA sequence as the ZFN. As the lengthy custom design of the ZFN was avoided, CRISPR-Cas9 strategy was clearly faster and more than 50-fold cost-efficient than the ZFN approach. As anticipated, we observed exon skipping in HCT 116 and RPE-1 cells in which *hCDC14A* was targeted by CRISPR-Cas9 (Figure 2.4 and Figure 2.5). This further implies that the skipping event is associated with the degree of exon alteration not merely a random outcome of genome editing approach.

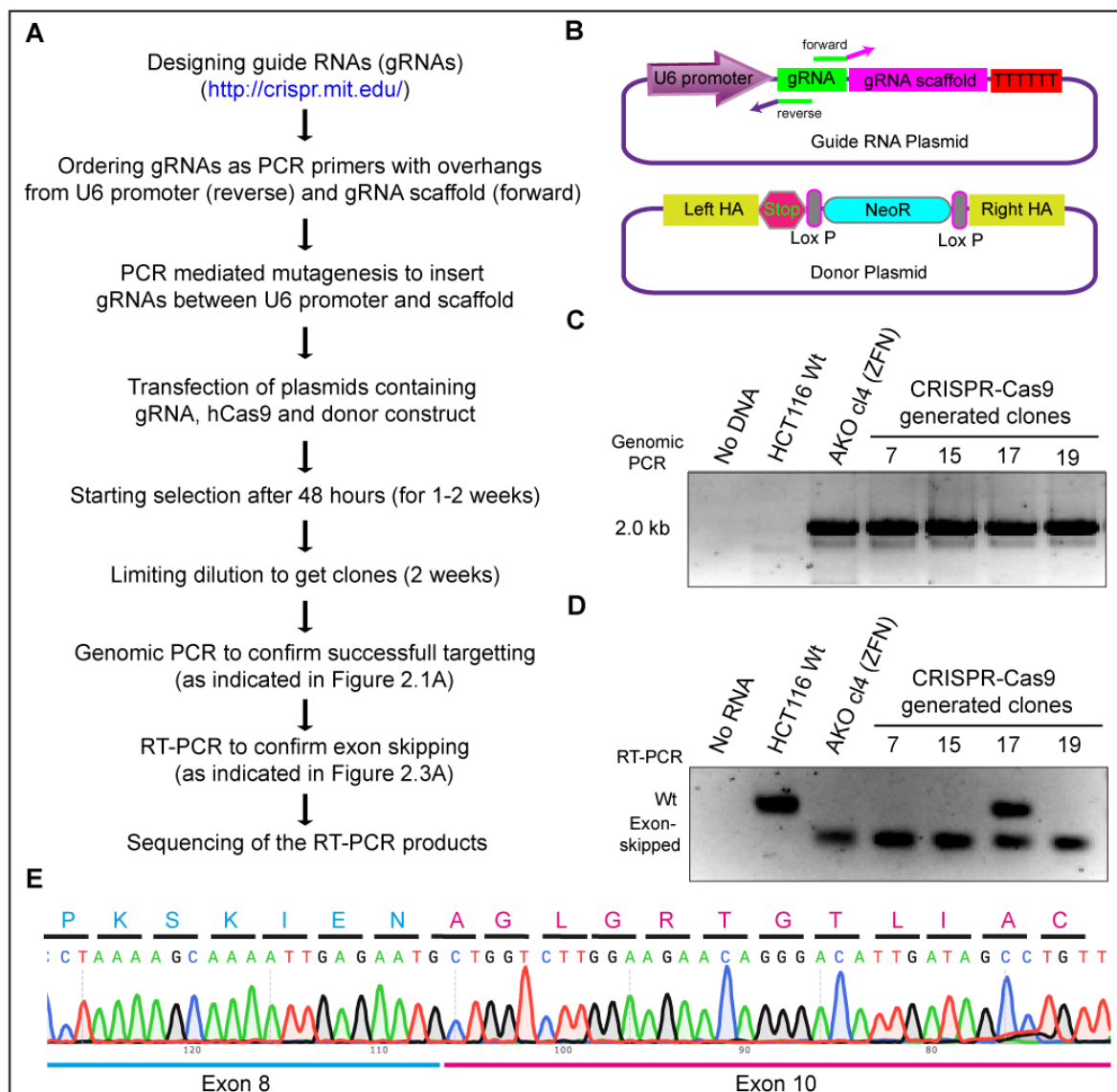


Figure 2.4: Strategy for Cas9-mediated generation of *hCDC14A* knockout HCT 116 cells (Adopted from Uddin et al., 2015).

(A, B) Workflow for CRISPR-Cas9 mediated insertion of NeoR into exon 9 of *hCDC14A*. Guide RNAs (gRNAs) targeting the exon 9 of *hCDC14A* gene were

designed using the web tool (<http://crispr.mit.edu/> (Hsu et al., 2013)). ‘Church gRNA insert’ containing the U6 promoter and gRNA scaffold (Mali et al., 2013) was first synthesized as gBlock and cloned into pJet. The intended gRNAs were then inserted through PCR mutagenesis using primers indicated by arrows (top of B). The same donor construct (bottom of B) as in case of ZFN-mediated genome editing was used to target the locus. (C) Junction PCR (as in Figure 2.1 A) with forward primer in NeoR cassette and reverse primer in the genome outside homology arms confirmed successful targeting and insertion of the selection marker. (D) RT-PCR of purified mRNA from Wt and different CRISPR-Cas9 targeted *hCDC14A*-KO clonal cells. Primers were as in Figure 2.3 A. Presence of both wild type and exon-skipped RNA indicated the targeting of single allele in clone 17. The other NeoR clones 7, 15, and 19 contained bi-allelic targeting of the *hCDC14A* gene. (E) The generated DNA bands of the RT-PCR were gel purified and sequenced. Sequences of alternating exon junctions of *hCDC14A* are shown and in-frame exon skipping can be deduced from the amino acid sequences written above the codons.

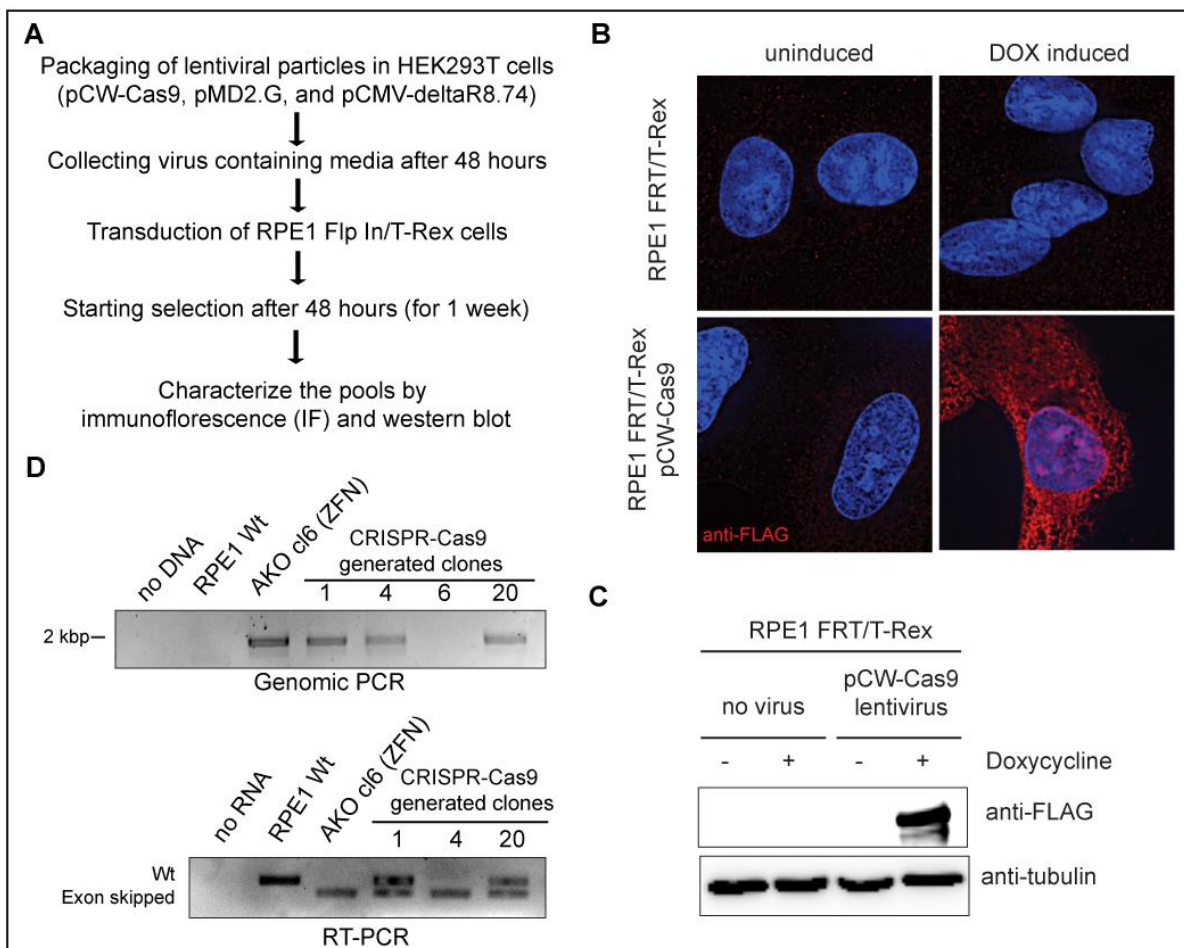


Figure 2.5: Strategy for Cas9-mediated generation of *hCDC14A* knockout RPE-1 cells (Adopted from Uddin et al., 2015).

(A) Workflow for the construction of RPE-1 *hCDC14A*-KO cell line. pCW-Cas9 plasmid containing doxycycline (Dox) inducible spCas9 was lentivirally integrated into RPE-1 FRT/T-Rex cells. (B, C) Successful expression and nuclear localization of

Cas9 was confirmed by indirect-immunofluorescence (B) and immunoblotting (C). (D) Junction PCR with forward primer in NeoR cassette and reverse primer in the genome outside homology arm (as in Figure 2.1) confirmed successful targeting and insertion of the selection marker. Exon skipping was confirmed by RT-PCR (primers as in Figure 2.3). Presence of both wild type and exon-skipped RNA indicated the targeting of single allele in clones 1 and 20.

2.1.4 Minimizing the degree of alteration salvages the exon skipping

As a cause of exon skipping, we hypothesized that large insertion-mediated alteration of the targeted exon affects the pre-mRNA structure (Valentine, 1998). Hence, to avoid large-scale genome editing, we have taken two experimental strategies. First, genomic loci were targeted by the same ZFNs but with error-prone NHEJ, to have random smaller insertions or deletions (Figure 2.6 A). Secondly, the selection markers flanked by loxP sites were removed by Cre-recombinase to generate loci with 45 base pair insertions including stop codons immediately followed by the single loxP site (Figure 2.6 B). In both the cases, sequencing of genomic loci indicated the expected abruptions. Similarly, sequencing of the RT-PCR products confirmed the likewise modifications within the targeted exons without their skipping from the mature transcript (Figure 2.6 A, B). Semi-quantitative RT-PCR using GAPDH as a control (Carbery et al., 2010) indicated that the exon-skipped *hCDC14B* mRNA level was less than half of the wild-type mRNA (Figure 2.6 C). Such decrease in mRNA level might be due to transcriptional control (altered synthesis) and/or post-transcriptional regulation (altered stability) of disrupted cellular transcripts. Because of the lack of anti-hCDC14B antibodies that detect the endogenous proteins (Guillamot et al., 2011; Mocciaro et al., 2010; Ovejero et al., 2012), we were unable to confirm this mRNA decrease at the protein levels. Thus, by ZFN and CRISPR-Cas9 strategies we were able to generate *hCDC14A^{PD}* and/or *hCDC14B^{-/-}* RPE-1 and HCT 116 cells.

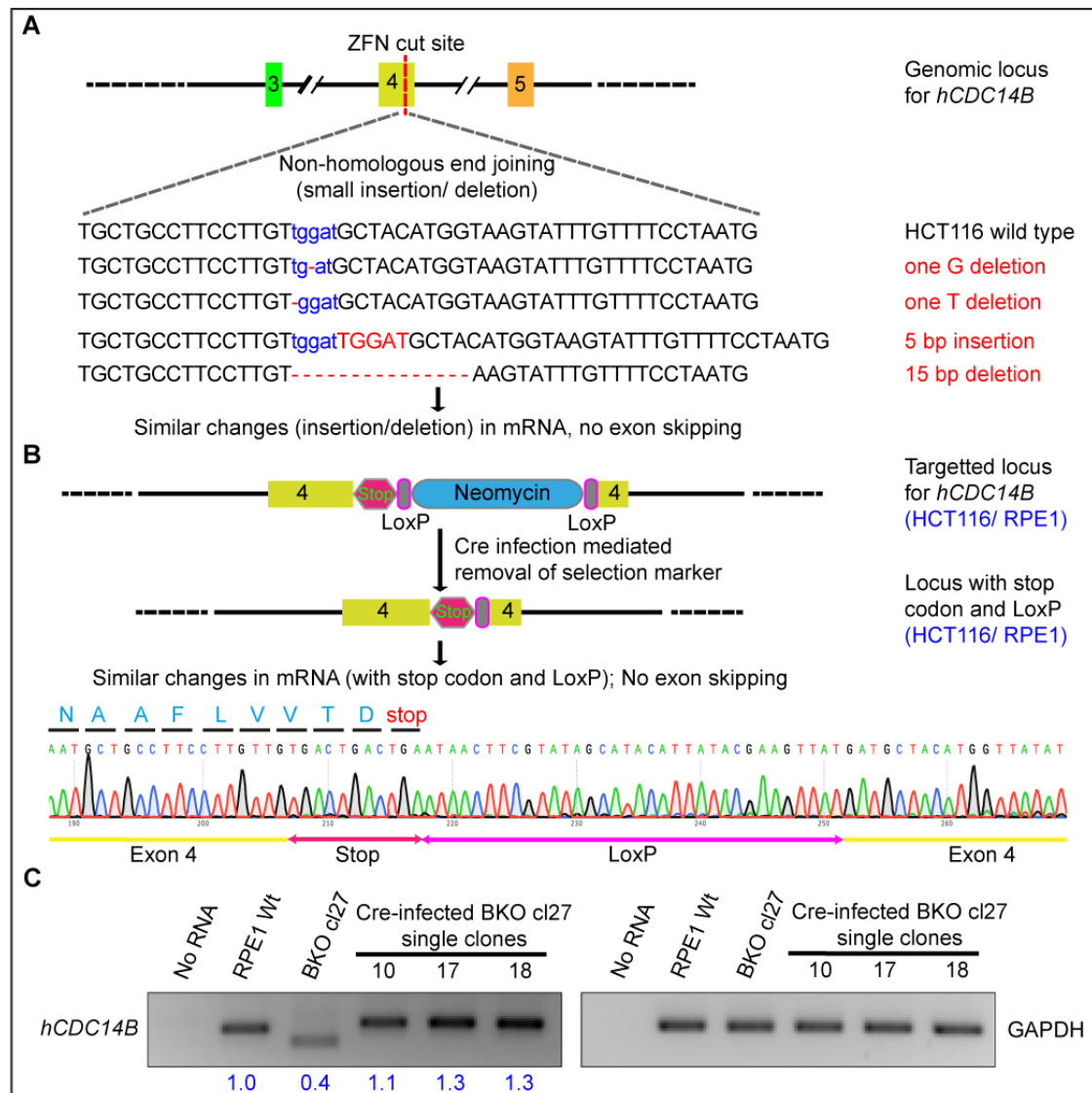


Figure 2.6: Exon skipping can be abolished by minimizing the degree of alteration (Adopted from Uddin et al., 2015).

(A) Exon 4 of *hCDC14B* was targeted by ZFN to introduce double strand break (DSB) and error-prone NHEJ for random insertion and deletion. In some of the targeted loci, small alterations in the exon (one to fifteen bases) were observed. ZFN cutting sites are written in blue font and base deletions or insertions are marked by red font colour. Sequencing of the RT-PCR products confirmed identical base pair changes without exon skipping (sequence not shown). (B) The selection cassette flanked by loxP sites was removed by Cre-recombinase from HCT 116 and RPE-1 *hCDC14B*-KO cells. RT-PCR analysis confirmed the presence of stop codon (11 bp) followed by one loxP site (34 bp) within the targeted exon in both the cell lines. (C) Semi-quantitative RT-PCR indicated that the exon-skipped mRNA level of RPE-1 cells is less than half of the wild-type mRNA. 40 ng of total RNA was used and the input RNA level was confirmed by *GAPDH* amplification as mentioned by Carbery et al. (2010). The experiment was performed three times with similar outcome. One representative

experiment is shown. The numbers below the agarose gel summarizes the relative abundance of the mRNA from three different experiments.

2.2 Phenotypic analysis of knockout cell lines

2.2.1 *hCDC14C* is not expressed in RPE-1 and HCT 116 cells

We have constructed RPE-1 and HCT 116 cells double deleted for *hCDC14A* and *hCDC14B* (*hCDC14A^{PD} hCDC14B^{-/-}*). The puromycin or neomycin marker in exon 4 of *hCDC14B* was removed by Cre recombination to prevent exon skipping. The question remained whether RPE-1 *hCDC14A^{PD} hCDC14B^{-/-}* cells expressed *hCDC14C*. *hCDC14C* is a retrogene that is nearly identical to the cDNA of *hCDC14B* (Rosso et al., 2008). However, *hCDC14C* is different from *hCDC14B* at several nucleotide positions (Figure 2.7, red asterisks). Analysis of the *hCDC14B* and *hCDC14C* mRNA in RPE-1 Wt and RPE-1 *hCDC14A^{PD}* and/or *hCDC14B^{-/-}* cells by RT-PCR and sequencing (mRNA was treated with DNaseI to remove chromosomal DNA) only identified bases characteristic for *hCDC14B* but not for *hCDC14C* (Figure 2.7, middle). Without DNaseI treatment, we detected the mixed-read containing *hCDC14C* signature derived from the chromosomal DNA and the *hCDC14B* signature from the cDNA (Figure 2.7, top). In genomic DNA only the *hCDC14C* fragment was amplified by PCR (Figure 2.7, bottom; retrogene, no introns) because of the large intron size in *hCDC14B*. Identical results were obtained with HCT 116 Wt and HCT 116 *hCDC14A^{PD}* and/or *hCDC14B^{-/-}* cells. Thus, *hCDC14C* is not expressed in RPE-1 Wt, RPE-1 *hCDC14A^{PD}* and/or *hCDC14B^{-/-}*, HCT 116 Wt, HCT 116 *hCDC14A^{PD}* and/or *hCDC14B^{-/-}* cells.

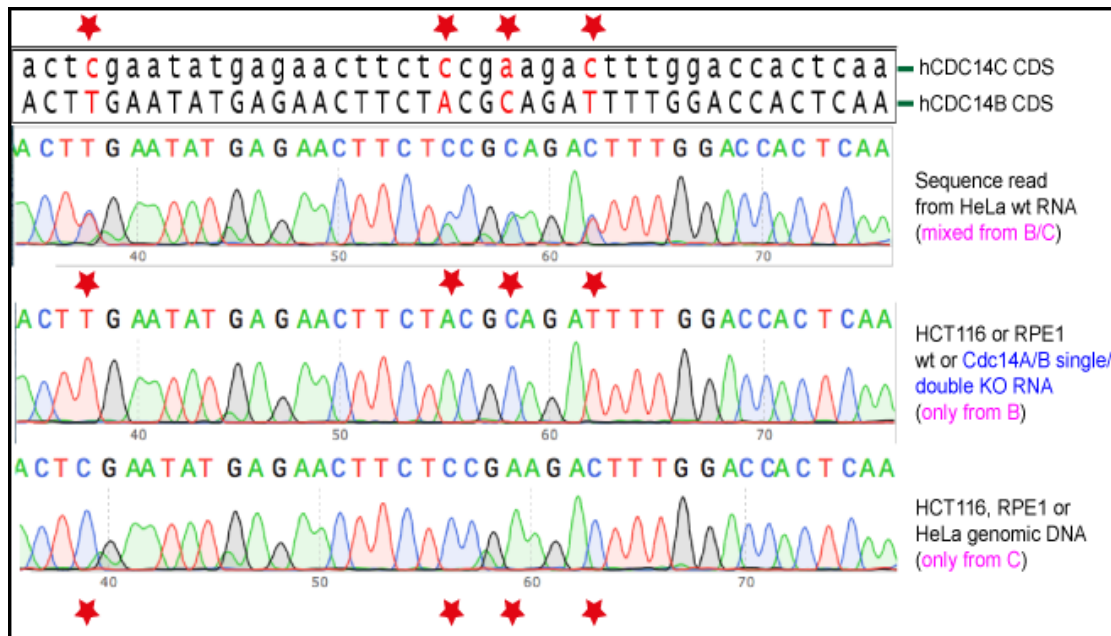


Figure 2.7: *hCDC14C* is not expressed in RPE-1 and HCT 116 cells.

Expression of *hCDC14C* in various cell lines was tested by RT-PCR and sequence analysis. The red stars mark the bases that are different between *hCDC14B* and *hCDC14C*. Upper lane: mix of chromosomal DNA and cDNA from DNase I untreated RNA. Middle: sequence analysis of the RT-PCR product from RPE-1 *hCDC14A^{PD}* and *hCDC14B^{-/-}* (BAKO3) cells showed expression of only *hCDC14B* but not *hCDC14C*. Identical results were obtained for RPE-1 Wt cells. Bottom: PCR analysis of genomic DNA from RPE-1 cells identified only the chromosomal *hCDC14C* signature.

2.2.2 Growth and cell cycle analysis of *hCDC14A^{PD}* and *hCDC14B^{-/-}* cells

MTT assay was used for an indirect measurement of cell growth. It is a colorimetric assay for evaluating cell metabolic activity, which in turn reflects the total number of cells. The MTT assay did not indicate an altered metabolic activity of RPE-1 Wt, *hCDC14A^{PD}* and/or *hCDC14B^{-/-}* cells (Figure 2.8 A, B). Secondly, analysis of the cell cycle profile using FACS analysis showed no significant difference in the cell cycle phases between Wt, single, and double *hCDC14A/B* mutant cell lines (Figure 2.8 C). So, it can be convincingly stated that *hCDC14A/hCDC14B* are not essential for the cell cycle progression of RPE-1 and HCT 116 cells.

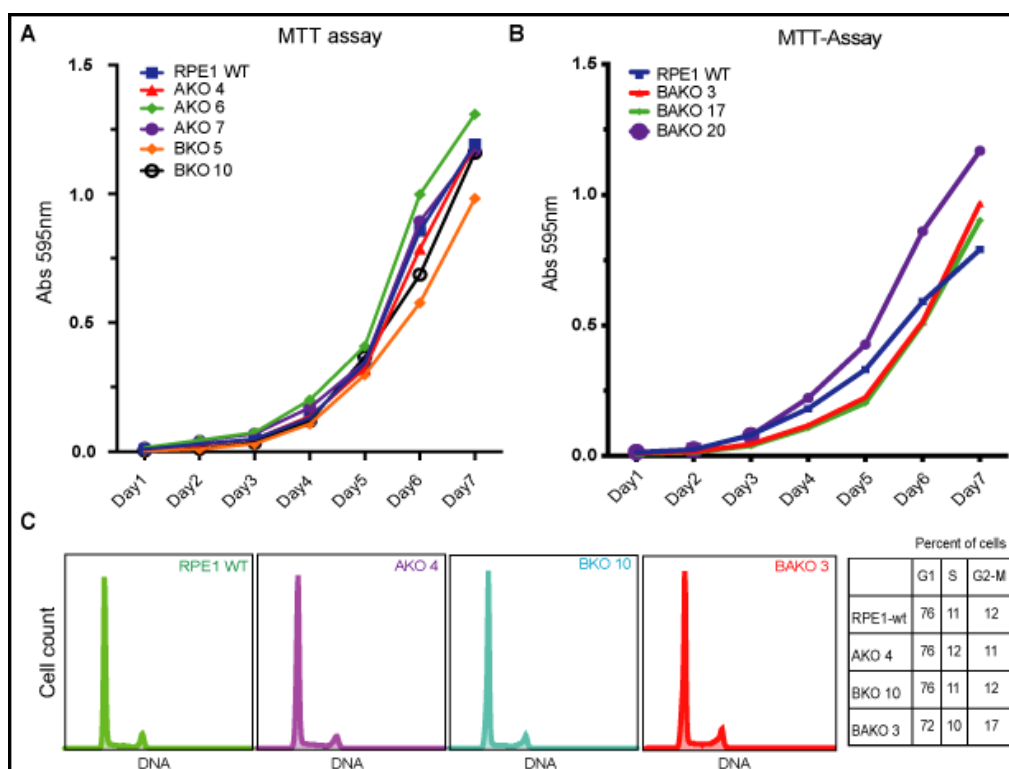


Figure 2.8: Analysis of *hCDC14A*^{PD} and/or *hCDC14B*^{-/-} cell lines.

(A, B) Growth analysis of RPE-1 Wt, *hCDC14A*^{PD} (AKO4, 6 and 7), *hCDC14B*^{-/-} (BKO5 and 10) and *hCDC14A*^{PD} *hCDC14B*^{-/-} (BAKO3, 17 and 20) cell lines using the MTT assay (colorimetric assay for measuring cells' metabolic activity). The small growth differences seen in B) were statistically insignificant. (C) Investigation of the distribution of cell cycle phases of RPE-1 Wt, AKO4, BKO10, and BAKO3 cell lines by FACS (propidium iodide) analysis.

2.3 *hCDC14A* regulates cilia length

2.3.1 *hCDC14A*^{PD} RPE-1 cells have longer cilia than Wt cells

hCDC14A is a conserved phosphatase with suggested but unclear role in ciliogenesis (Ah-Fong and Judelson, 2011; Clément et al., 2012; Delmaghani et al., 2016). To understand the function of *hCDC14A* in cilia formation, we analysed serum starved RPE-1 *hCDC14A*^{PD} cells for cilia formation in comparison to Wt cells. *hCDC14A*^{PD} cells formed cilia as efficient as Wt cells independent of the cells' confluency (Figure 2.9 A, B). However, cilia of *hCDC14A*^{PD} cells were longer in comparison to those of Wt cells (Figure 2.9 A, C). siRNA mediated depletion of *hCDC14A* also caused the formation of elongated cilia (Figure 2.9 D).

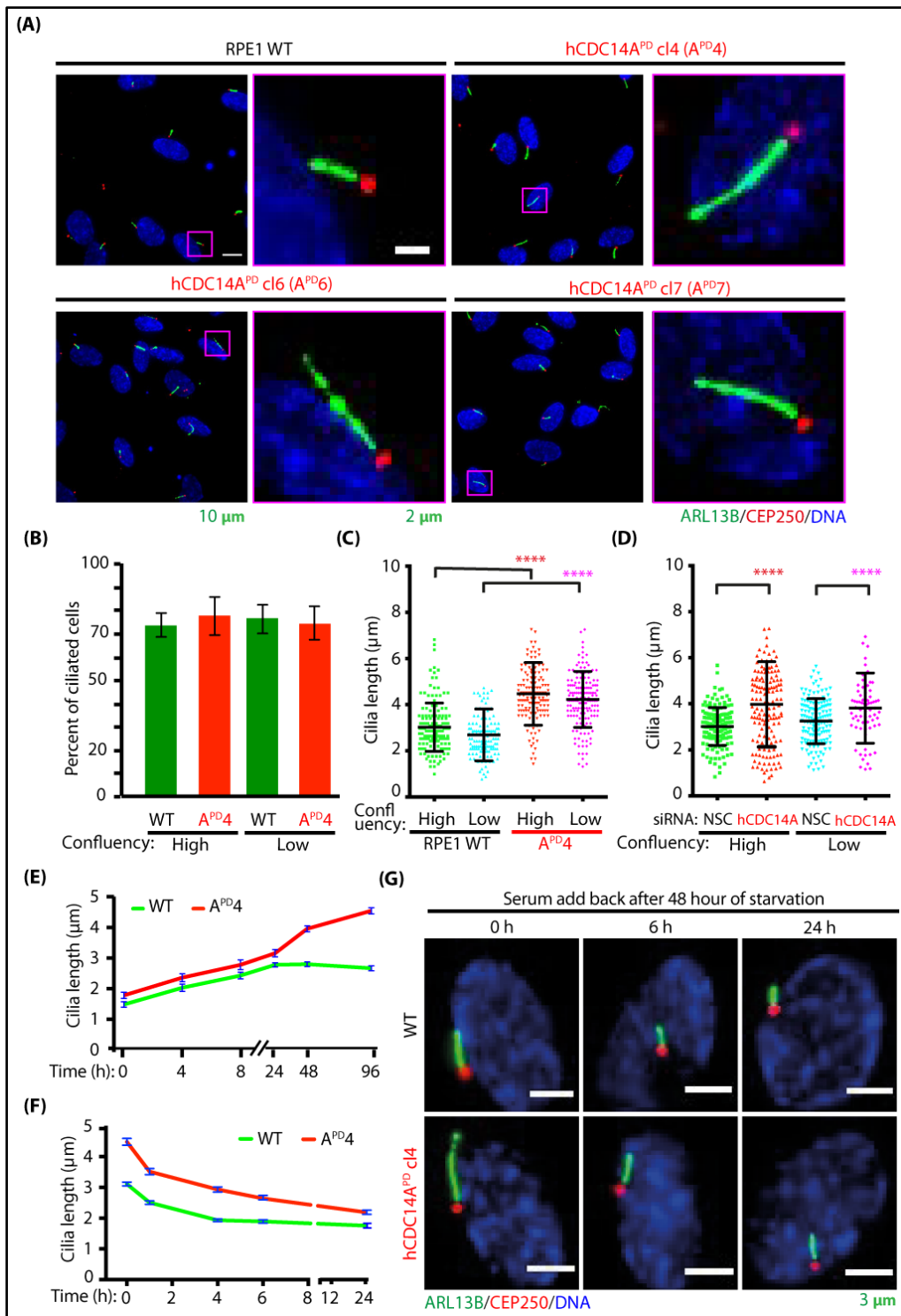


Figure 2.9: Ablation of hCDC14A phosphatase activity in human RPE-1 cells leads to the elongation of primary cilia.

(A) The cells were serum starved for 48 hours for inducing ciliogenesis prior to fixation. Cilia were stained with Arl13B while the basal bodies were marked with CEP250 (C-Nap1). Cilia from the magenta box marked area were enlarged for a clear view. (B, C) Percent of ciliated cells, as well as the length of cilia, was quantified from

A. *hCDC14A* phosphatase dead (*hCDC14A^{PD}*) cells show a similar percentage of cilia compared to wild type (Wt) cells. Cilia length was measured by a semi-automated ImageJ macro as described in methods section. (D) Elongated cilia phenotype was further confirmed by siRNA-mediated knockdown of *hCDC14A*. (E) The dynamics of ciliogenesis was determined by serum starving the Wt and *hCDC14A^{PD}* cells for different time-points (0, 4, 8, 24, 48 and 96 hours). The cilia from *hCDC14A^{PD}* cells continue to grow even after 48 hours of starvation whereas those from Wt cells reach optimum length within 12 to 24 hours. (F, G) In a time course experiment, the cilia disassembly kinetics was measured by first inducing the ciliation through 48 hours of serum starvation prior to incubation with serum containing media for different time points (0, 1, 4, 6, 24 hours). Measurement of cilia length indicated the comparable rates of cilia disassembly in RPE-1 Wt and *hCDC14A^{PD}* cells (**** P<0.0001). Sizes of the scale bars are indicated next to the designated images.

Mutations can affect cilia length because of the impairment of cilia disassembly when cells re-enter the cell cycle upon growth factor addition (Maskey et al., 2015). To evaluate this possibility, we compared cilia formation and cilia disassembly of Wt and *hCDC14A^{PD}* cells. Elongation of cilia in response to serum starvation plateaued in Wt cells after 12 hours with an average cilium length of 2.8 μm (Figure 2.9 E). In contrast, cilia continued to elongate in *hCDC14A^{PD}* cells over 96 hours reaching a length of 4.6 μm . Cilia disassembly was even slightly faster in *hCDC14A^{PD}* cells in comparison to Wt cells (Figure 2.9 F, G). This suggests that it is cilia length control but not cilia formation or disassembly, which is defective in *hCDC14A^{PD}* cells. In addition, *hCDC14^{PD/+}* cells carrying only one Wt *hCDC14A* gene displayed an intermediate cilia length phenotype. Conversely, elongated cilia were not observed in RPE-1 cells lacking the *hCDC14A* paralogue *hCDC14B* (*hCDC14B^{-/-}*) suggesting that the cilia phenotype is specific to *hCDC14A* (Figure 2.10).

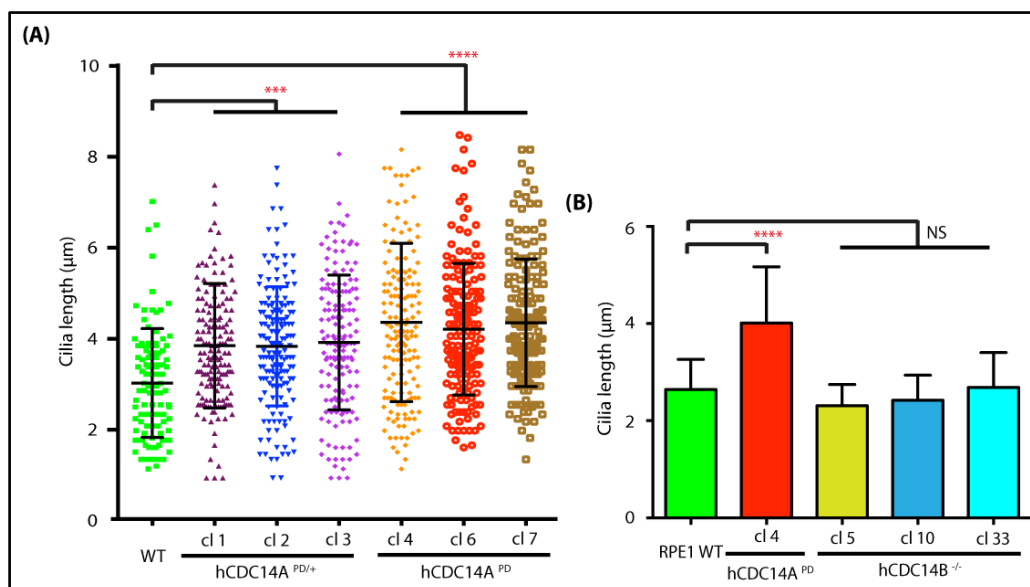


Figure 2.10: Elongated cilia phenotype is specific to $hCDC14A^{PD}$ cells.

(A) One allele targeted $hCDC14^{PD/+}$ cells displayed an intermediate cilia length phenotype compared to Wt and $hCDC14^{PD/PD}$ cells. (B) Elongated cilia were not observed in $hCDC14B^{-/-}$ RPE-1 cells suggesting that the cilia phenotype is specifically due to the lack of hCDC14A phosphatase activity (NS - not significant; *** $P \leq 0.001$; **** $P \leq 0.0001$).

We next characterized the structure of $hCDC14A^{PD}$ cilia in comparison to Wt to exclude structural defects. Electron microscopy did not show obvious defects in the basal body and axoneme organization of $hCDC14A^{PD}$ cilia (Figure 2.11). In addition, the distal appendage protein CEP164, the subdistal appendage proteins CEP170, ODF2, and ninein, the transition zone protein NPHP1, the cilia shaft protein ARL13B, the transport protein IFT88, the linker proteins C-Nap1 and rootletin, and the PCM protein γ -tubulin were similarly associated with cilia in Wt and $hCDC14A^{PD}$ cells (Figure 2.12). Intensity of these important basal body proteins were comparable in RPE-1 Wt and $hCDC14A^{PD}$ cells (Figure 2.13). Thus, continuous elongation of cilia in $hCDC14A^{PD}$ cells is causing the prolonged cilia phenotype without any noticeable structural defects. We next tested whether $hCDC14A$ overexpression has the reverse phenotype of $hCDC14A$ inactivation. Mild overexpression of $hCDC14A$ but not the phosphatase dead version $hCDC14A^{C278S}$ from the inducible TetOn promoter drastically inhibited cilia formation (Figure 2.14 A). Taken together, hCDC14A regulates the assembly and length of cilia.

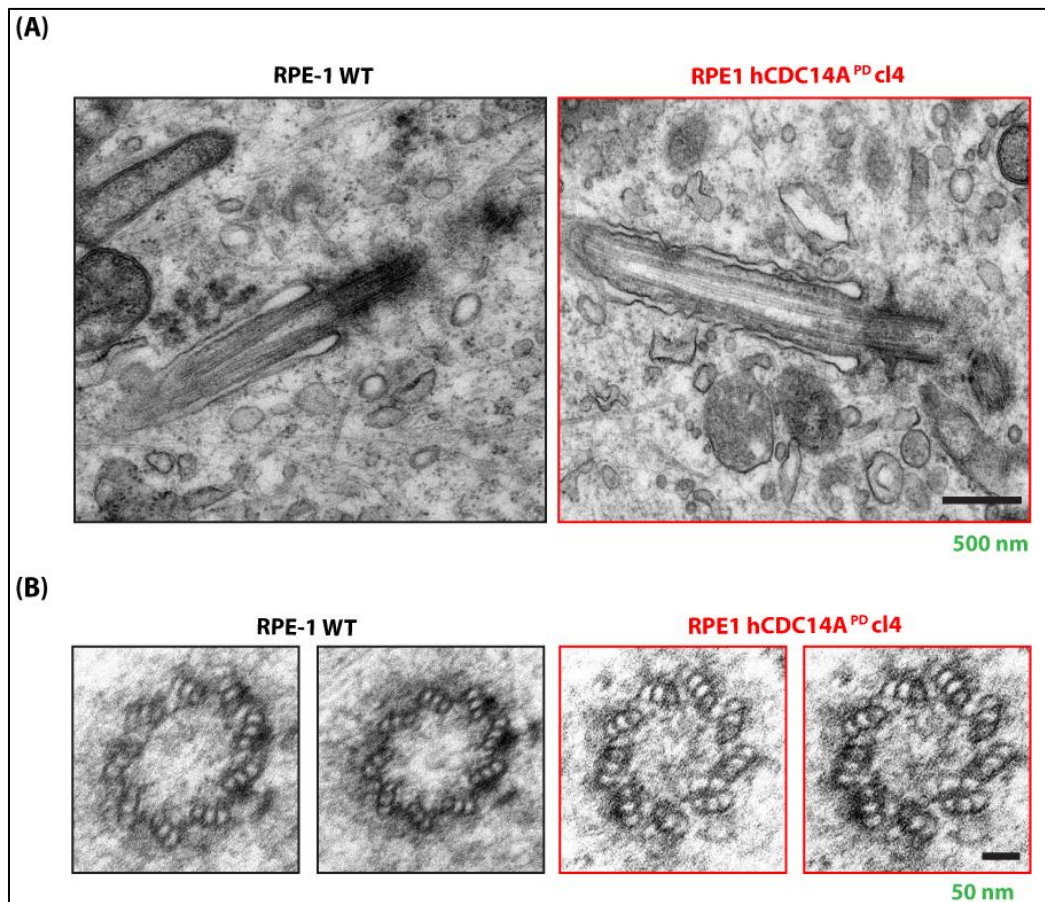


Figure 2.11: Electron micrograph of cilia from Wt and *hCDC14A*^{PD} cells.

- (A) Electron micrograph of cilia from 48 hours serum starved RPE-1 Wt and *hCDC14A*^{PD} cells. Basal body and the ciliary axoneme showed no gross structural defects in the longitudinal ciliary sections from *hCDC14A*^{PD} cells. (B) Similarly, the cross-sections of the basal body from Wt and *hCDC14A*^{PD} cells represented well organized triplet microtubule structure. Sizes of the scale bars are indicated next to the designated images (EM analysis was done in collaboration with Annett Neuner).

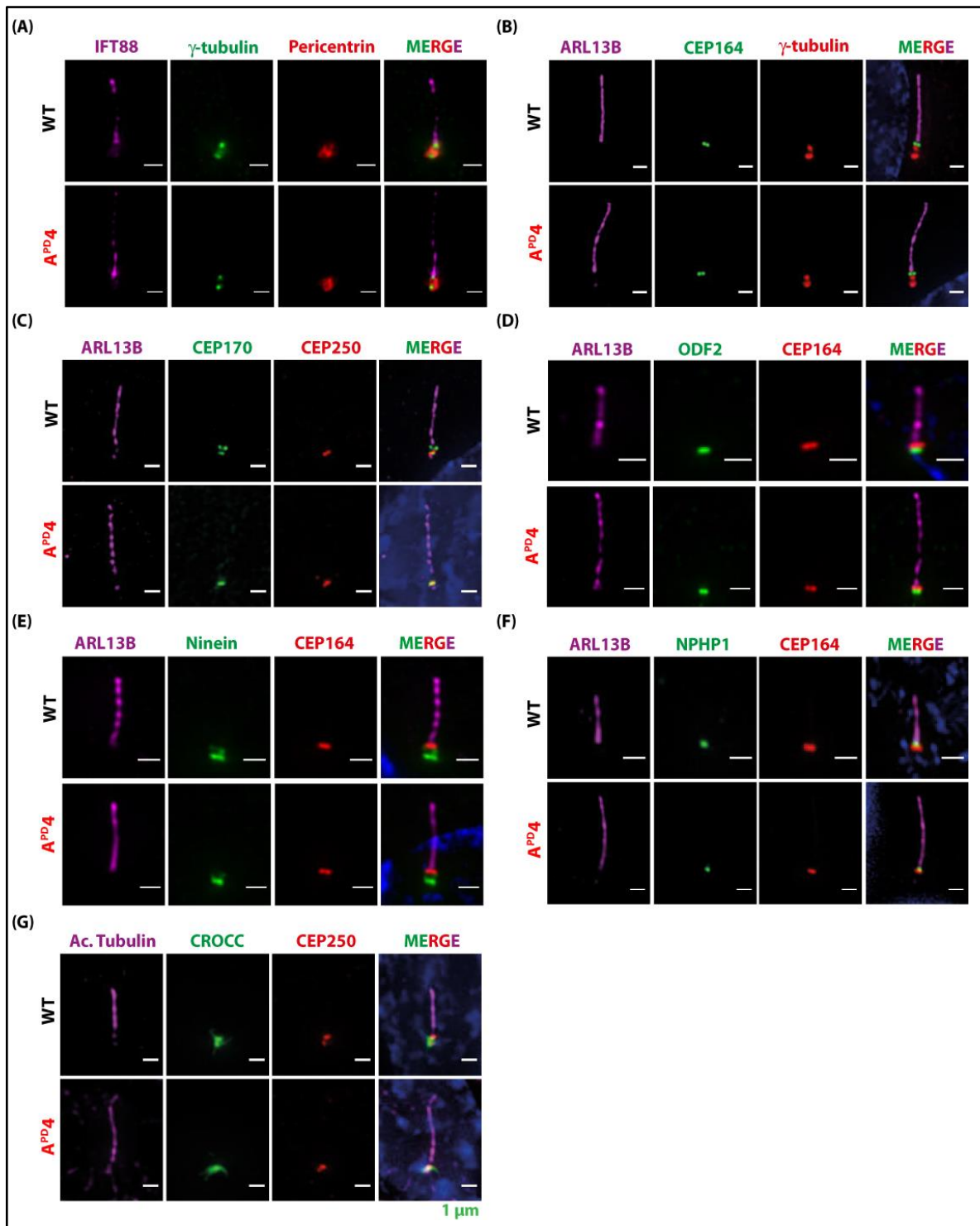


Figure 2.12: Cilia from *hCDC14A^{PD}* cells are structurally similar to those from Wt cells.

Markers representing various basal body localizations showed no obvious localization defects for (A) pericentrin; (B, E and F) the distal appendage protein CEP164; (C, D and E) the subdistal appendage proteins (C) CEP170, (D) ODF2, and (E) Ninein; (C and G) the proximal end protein C-Nap1; (F) the transition zone protein NPHP1 and (G) the ciliary rootlet component rootletin (Scale Bars 1 μ M).

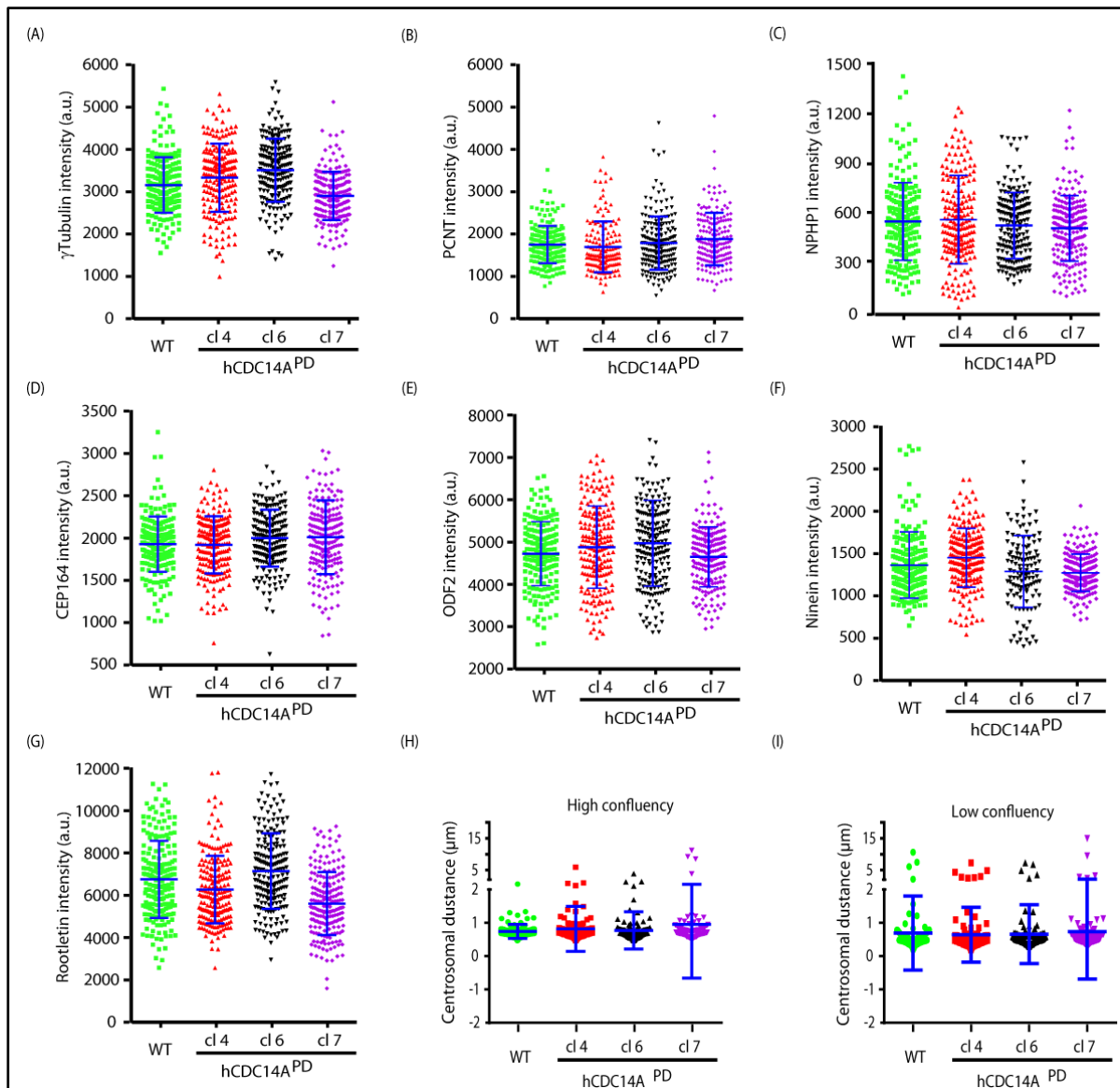


Figure 2.13: Basal body protein intensities and interphase centrosomal distance of $hCDC14A^{PD}$ cells are comparable to Wt cells.

(A-G) Fluorescent intensity of the markers representing various basal body localizations were measured using an ImageJ macro described in method section. In brief, the fluorescent intensities within a 4.5- μm -radius circle surrounding the basal body was measured after background subtraction.

(H-I) Interphase centrosomal distance (from unstarved cycling cells) were measured in Wt and $hCDC14A^{PD}$ cells (clone 4, 6, 7) by manually measuring the linear distance between two centrosomes marked with Tubulin and PCNT.

2.3.2 hCDC14A localizes to the basal body and the actin cytoskeleton of ciliated cells

CDC14A localizes to the axoneme of transient kinocilia of developing cochlear hair cells and the persistent kinocilia of vestibular hair cells (Imtiaz et al., 2018). The localization of hCDC14A in cells with a primary cilium is, however, unclear. Endogenous hCDC14A was detected in the basal body of serum-starved ciliated RPE-1 cells using an established anti-hCDC14A antibody (Chen et al., 2016) (Figure 2.15). Similar localization was observed in RPE-1 cells stably expressing *hCDC14A-GFP* and the phosphatase dead version *hCDC14A^{C278S}-GFP* under TetON promoter control (Figure 2.14 D-G). However, we noticed that *hCDC14A-GFP* expression reduced the number of RPE-1 cells with cilia from 70% to 20%. This reduction was not observed when the phosphatase dead *hCDC14A^{C278S}-GFP* was expressed (Figure 2.14 A). In addition, hCDC14A-GFP was detected along actin cables in ciliated cells (Figure 2.14 B and C) as reported for interphase cycling cells (Chen et al., 2016).

For a more detailed analysis of the hCDC14A localization, we focused on *hCDC14A^{C278S}-GFP* that did not affect ciliogenesis. A closer inspection of the basal body indicated the presence of two pools of *hCDC14A^{C278S}-GFP*. The most intense fraction was enriched at the proximal end of the basal body that contains the linker protein C-Nap1 (encoded by *CEP250*) (Fry et al., 1998; Mayor et al., 2000) (Figure 2.14 D and E). Confirming this localization, hCDC14A-GFP was lost from the basal body's proximal end in *CEP250*^{-/-} RPE-1 cells (Figure 2.14 F and G) (Panic et al., 2015). The second pool, relatively weak in intensity, was at the distal end of the basal body that organizes the cilium (Figure 2.14 D). hCDC14A localized underneath the distal appendage marker CEP164 and overlapped in its localization with the subdistal appendage protein ODF2 (Ishikawa et al., 2005; Mazo et al., 2016). The cartoon in Figure 2.14 E summarizes hCDC14A localization at basal bodies. Thus, in ciliated cells hCDC14A associates with the actin cytoskeleton and basal body.

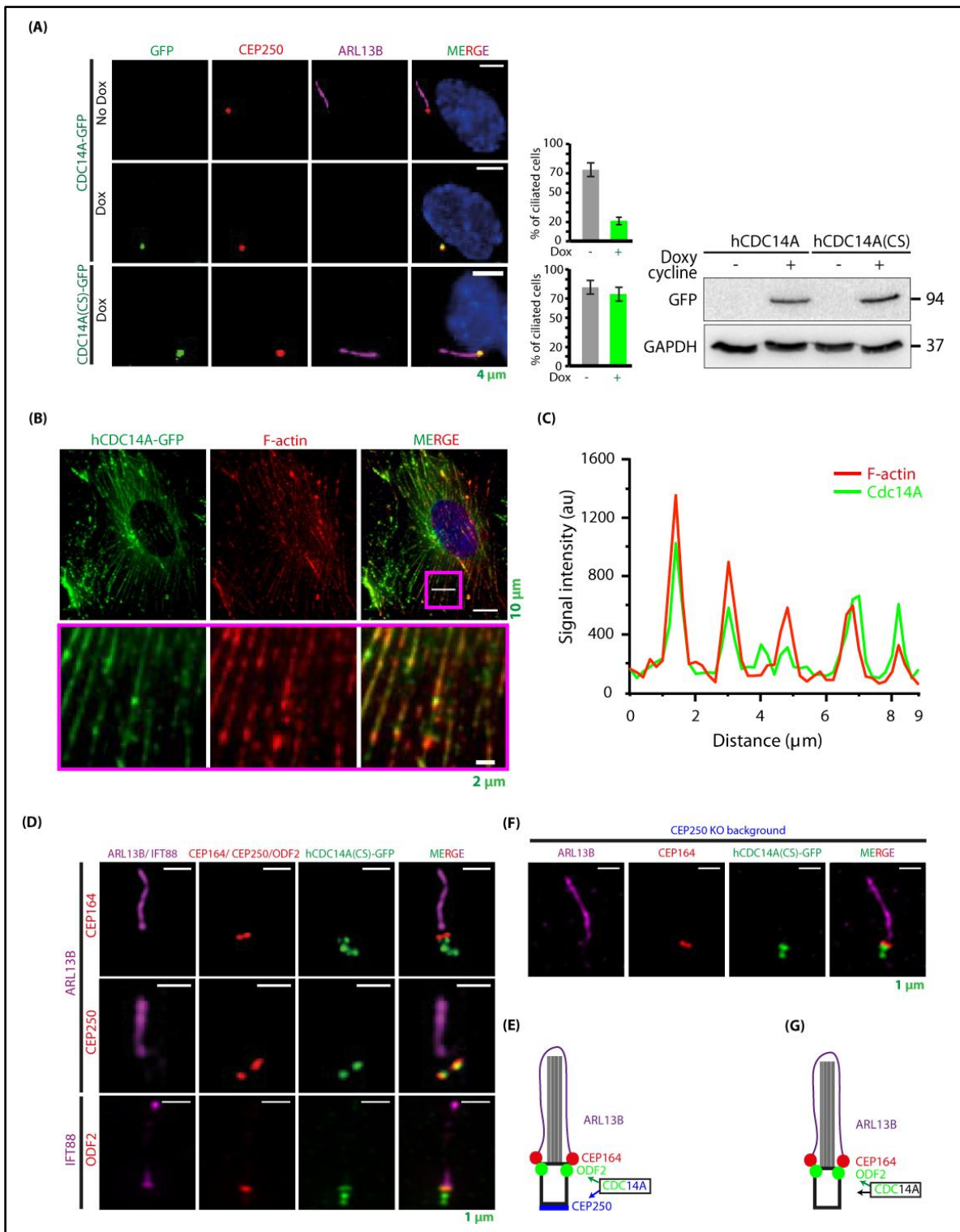


Figure 2.14: hCDC14A negatively regulates ciliogenesis and is localized to actin as well as to the basal body.

(A) *hCDC14A-GFP* and *hCDC14A^{C278S}-GFP* under control of the TetON promoter were stably integrated into RPE-1 cells. *hCDC14A-GFP* and *hCDC14A^{C278S}-GFP* localized to the basal body. In addition, expression of *hCDC14A-GFP* but not the phosphatase dead *hCDC14A^{C278S}-GFP* mutant inhibited cilia formation. Expression of

hCDC14A-GFP and *hCDC14A^{C278S}-GFP* were validated by immunoblot analysis. (B) TetON-*hCDC14A-GFP* RPE-1 cells were serum starved for 48 hours prior to fixation and immunofluorescence microscopy. *hCDC14A-GFP* colocalizes with Phalloidin 555 conjugated dye that marks F-actin fibres. (C) Line scan inside the magenta-coloured box showed in B. The scanned areas were enlarged and displayed below the corresponding images in B. (D) Sub-centrosomal localization of *hCDC14A^{C278S}-GFP* was determined by the correlative positioning of GFP signal with the proteins Arl13B and IFT88 (cilia), C-Nap1 (proximal end), CEP164 (distal appendage) and ODF2 (subdistal appendage). (E) Cartoon of cilia indicating the localization of *hCDC14A*. (F, G) *CEP250^{-/-}* cells showed only the sub-distal and centriolar localizations of *hCDC14A^{C278S}-GFP* indicating the *CEP250* dependence of *hCDC14A* proximal end localization. Sizes of the scale bars are indicated next to the designated images.

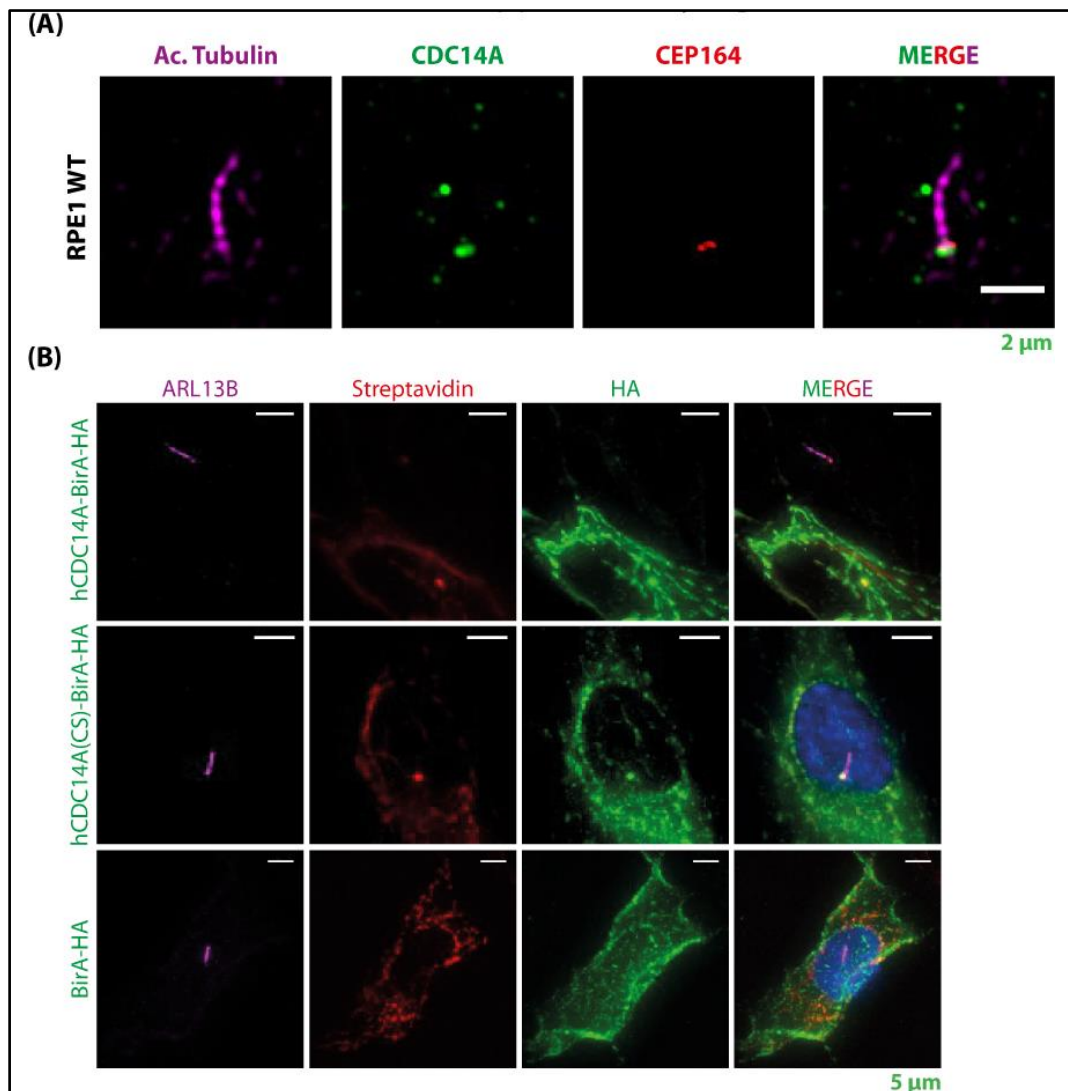


Figure 2.15: Endogenous hCDC14A as well as BirA tagged hCDC14A are localized to basal body.

(A) Endogenous hCDC14A could be detected in the basal body of RPE-1 Wt cells under ciliogenic condition. (B) hCDC14A-BirA or hCDC14A^{C278S}-BirA could also be

detected in the basal body, whereas BirA showed a diffused cellular signal without any basal body enrichment. Sizes of the scale bars are indicated next to the designated images.

2.3.3 hCDC14A dephosphorylates actin associated proteins during ciliogenesis

We have applied global phosphoproteome along with proximity-based interaction proteomics approaches under conditions that favor ciliation to identify substrates and proximity neighbours for hCDC14A. First, stable isotope labelling with amino acids in cell culture (SILAC) (Ong et al., 2002) allowed us to identify proteins that became dephosphorylated upon TetON-induced expression of *hCDC14A-GFP* by doxycycline (Dox) under cilia promoting conditions (Figure 2.16 A-D). Comparison of the phospho-proteomes of non-induced and induced hCDC14A-GFP expressing cells by mass spectrometric analysis identified actin-associated proteins such as DBN1, synaptopodin (SYNPO), and the LIM domain and actin binding 1 (LIMA1). In addition, we identified the microtubule-associated protein MAP4 that functions in cilia length control (Ghossoub et al., 2013) (Figure 2.16 B and C). Interestingly, most of the phosphosites that were dephosphorylated by hCDC14A followed the pSP consensus of CDC14 phosphatases (Figure 2.16 D) (Chen et al., 2017; Eissler et al., 2014; Visintin et al., 1998). However, compared to human cycling cells, in which hCDC14A preferentially dephosphorylates pSPxK/R sites (Chen et al., 2017), the preference for positively charged amino acids at position pS+3 was less pronounced under serum starvation (Figure 2.16 D). The proximity BioID analysis (Roux et al., 2012) was performed with both hCDC14A Wt and the phosphatase dead hCDC14A^{C278S} N-terminally tagged to the promiscuous biotin protein ligase (BirA). The BirA fused hCDC14A also showed actin as well as basal body localization (Figure 2.15). During ciliogenesis, hCDC14A and hCDC14A^{C278S} localized close to actin-associated proteins DBN1 and LIMA1 which is consistent with the phospho-proteome analysis (Figure 2.16 E and F).

phosphorylated proteins in *hCDC14A-GFP* overexpressed cells. Gene network was constructed in Cytoscape using the function prediction GeneMANIA app. Physical interactions are denoted by solid lines (edges) whereas the shared protein domain interactions are represented by broken lines. The extent of interactions (degree) is indicated by the Node size. The query proteins are marked with thick borders and the actin-related proteins are marked with Magenta-coloured nodes. (C) Gene Ontology (GO) analysis of the proteins that are two-fold hypo-phosphorylated in the heavy (*hCDC14A* overexpressed) samples. Values inside the parentheses indicate P values. (D) Substrate motif identified by analysing the sequences of hypo-phosphorylated peptides in Perseus. (E) Molecular network of the neighbours of *hCDC14A* identified by Proximity-dependent biotin identification (BioID) during ciliogenesis. Gene network was constructed in Cytoscape as described in B by considering the physical interactions only. (F) Gene Ontology (GO) analysis of the proteins from which at least five peptides were two-fold enriched in the *hCDC14A-BirA* and *hCDC14A-CS-BirA* samples compared to *BirA* control.

In a secondary screen, we tested proteins that were identified by the phosphoproteome and BioID analyses for their impact on cilia length control. Proteins were depleted by siRNA during ciliogenesis of RPE-1 Wt and *hCDC14A^{PD}* cells (Figure 2.17). Cilia length was subsequently measured by indirect immunofluorescence microscopy. Depletion of several proteins such as the subdistal appendage protein CEP170 had no impact on the cilia length in Wt and *hCDC14A^{PD}* cells (Figure 2.17). *DBN1*, *MTCL1*, and *UBAP2L* depletion significantly increased the length of cilia in Wt cells without affecting those in *hCDC14A^{PD}* cells. On the contrary, siRNA of *KANK2*, *MAP4*, *PDLIM7*, and *RPS2* reduced the length of *hCDC14A^{PD}* cilia without having an impact on Wt cilia. In summary, *hCDC14A* phosphoproteome and BioID analyses identified putative *CDC14A* substrates that affect cilia length.

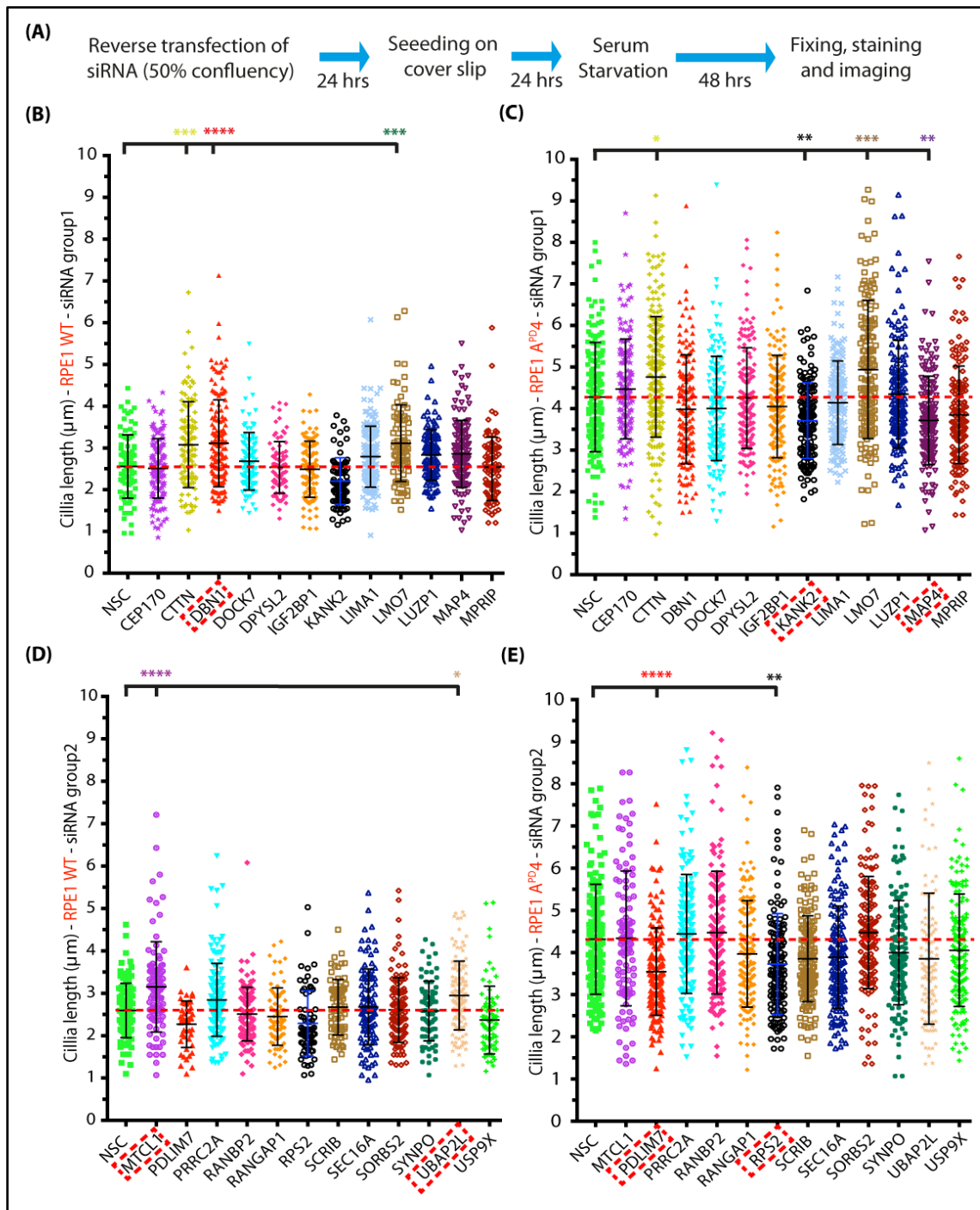


Figure 2.17: siRNA screen to find proteins with critical function in cilia length control.

(A) Experimental scheme for siRNA screen to find hCDC14A substrate(s) essential for cilia length control. (B, C, D and E) Proteins were depleted by siRNA during ciliogenesis of RPE-1 wild type and *hCDC14A^{PD}* cells. Cilia length was subsequently measured by indirect immunofluorescence microscopy. (The experiment was repeated twice, and 70 to 150 cilia were measured for each experiment; * $P \leq 0.05$; ** $P \leq 0.01$; *** $P \leq 0.001$; **** $P \leq 0.0001$).

2.3.4 hCDC14A regulates phosphorylation of DBN1

We focused the further analysis on DBN1, which is a known phosphoprotein with functions in ciliogenesis (Nager et al., 2017; Worth et al., 2013). Mass spec analysis indicated that serine residue 142 of DBN1 became dephosphorylated by hCDC14A in RPE-1 cells during ciliogenesis (Figure 2.18). In cycling cells, this “SP” site is phosphorylated by the proline directed kinase CDK5 (Tanabe et al., 2014; Worth et al., 2013). Analysis of the phosphorylation status of S142 of DBN1 with a phospho-specific antibody confirmed dephosphorylation of this site by Tet induced *hCDC14A-GFP* but not by the inactive *hCDC14A^{C278S}-GFP* or *GFP* (Figure 2.18 A and B). In addition, S142 of DBN1 was hyperphosphorylated in *hCDC14A^{PD}* RPE-1 cell lines during ciliogenesis (clone 4, clone 6, and clone 7) compared to the Wt control (Figure 2.18 C). The identity of the pS142 DBN1 and DBN1 bands was confirmed by their reduction in response to DBN1 siRNA (Figure 2.18 C). Of note, phosphorylation of pS142 of DBN1 was reduced during ciliogenesis relative to cycling cells (Figure 2.22 A). This suggests that DBN1^{pS142} is a substrate of hCDC14A during ciliogenesis. To confirm direct dephosphorylation of DBN1 pS142 by hCDC14A, we incubated immuno-precipitated, phospho DBN1 with recombinant and purified hCDC14A. pS142 was efficiently dephosphorylated by recombinant, purified hCDC14A (Figure 2.18 D) indicating that hCDC14A directly dephosphorylates DBN1.

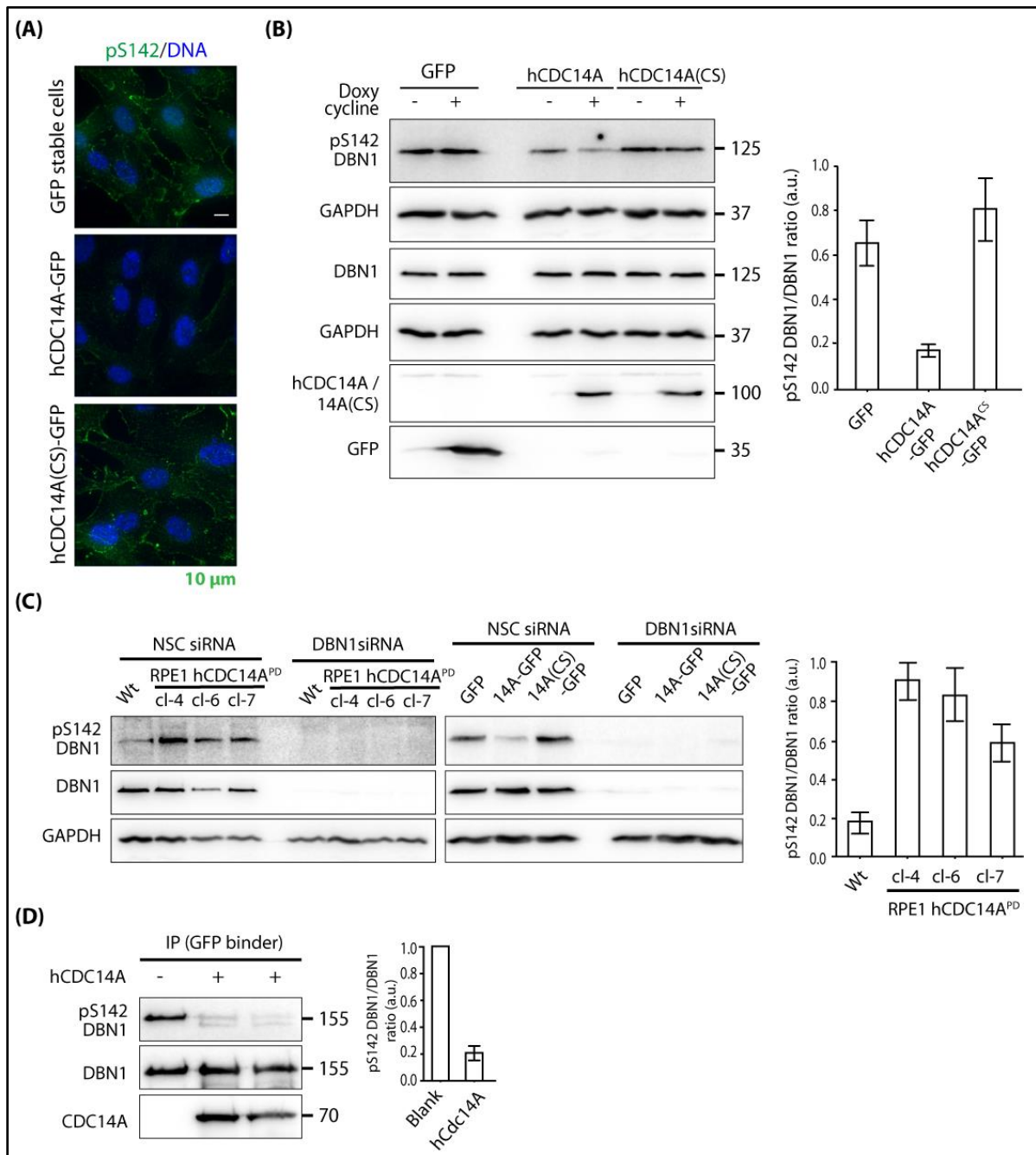


Figure 2.18: The phosphoprotein DBN1 is a substrate for hCDC14A.

(A, B) hCDC14A, not the inactive hCDC14A^{C278S}, dephosphorylates the serine residue 142 of DBN1 *in vivo*. RPE-1 cells expressing GFP, hCDC14A-GFP, and hCDC14A^{C278S}-GFP under TetON promoter were serum starved in presence or absence of Dox for 48 hours prior to fixation for immunofluorescence (A) or lysing for immunoblot analysis (B). (B) The DBN1^{pS142}/DBN1 ratio was densitometrically measured from the Dox treated samples and represented in the graph next to the immunoblot. (C) S142 of DBN1 was hyper-phosphorylated in hCDC14A^{PD} clones during ciliogenesis compared to the wild type control. The specificity of the DBN1^{pS142} antibody was validated by siRNA mediated knock-down of DBN1 in both hCDC14A^{PD} cells and GFP/hCDC14A-

GFP/hCDC14A^{C278S}-GFP stable cells. (D) *In vitro* dephosphorylation of DBN1 by purified hCDC14A enzyme. *DBN1-GFP* was transfected into HEK293T cells and immunoprecipitated with GFP binder after 48 hours of expression. The immunoprecipitated phospho-DBN1 was then incubated with hCDC14A to dephosphorylate *in vitro*.

2.3.5 Phosphoregulation of DBN1 by hCDC14A contributes to cilia length control

To confirm the function of DBN1 in cilia length regulation, we constructed independent *DBN1* RPE-1 knockout cell lines using CRISPR/Cas9 technology (Figure 2.19 A). Three independent gRNAs targeting different exons of *DBN1* were used to construct *DBN1* KO cells (Figure 2.19 A). Analysis of the DNA sequences from several clonal cell lines confirmed the disrupting mutations in the *DBN1* gene (Figure 2.19 B). As expected from gene disruption, DBN1 was no longer detected in *DBN1* KO cell lines by immunoblotting with polyclonal antibodies (Figure 2.19 C). One clone of each gRNA (1.16, 2.18 and 3.3) was used for further ciliogenesis experiment and found to assemble longer cilia than Wt cells (Figure 2.19 D). Clone 2.19 did not affect cilia length as this cell line did not carry a mutation in *DBN1* and DBN1 protein was detected by immunoblotting (Figure 2.19 C). This data further confirms the role of DBN1 in cilia length regulation.

To test the impact of S142 phosphosite in DBN1 on cilia length control, we expressed *DBN1* versions of Wt, phospho-inhibitory (S142A) and phospho-mimetic (S142D) in *DBN1* KO and Wt RPE-1 cells under the control of TetON promoter. Expression of *DBN1* in RPE-1 Wt cells increases cilia length (Figure 2.19 E). Because of this overexpression effect, we did not observe rescue of the cilia length phenotype by TetON-*DBN1* in *DBN1* KO cells (Figure 2.19 F). Interestingly, however, the non-phosphorylated, DBN1^{S142A} (Worth et al., 2013) significantly reduced cilia length in comparison to Wt or phospho-mimetic (S142D) DBN1 (Figure 2.19 F). Similar cilia length in both Wt and phospho-mimetic DBN1^{S142D} has lead us to speculate that the overexpressed *DBN1* might be phosphorylated inside the cells leading to the inactivation of the non-phosphorylated active DBN1. Indeed, immunoblotting of the

cell lysate with phospho-specific antibody confirmed that in TetON-*DBN1* cells, *DBN1* S142 phosphorylation was strongly elevated in comparison to the control without Dox (Figure 2.19 G). No *DBN1*^{pS142} signal was observed in cells expressing the S142A and S142D versions of *DBN1*, confirming the specificity of the *DBN1*^{pS142} antibodies (Figure 2.19 G). Thus phospho-regulation of *DBN1* is a mechanism that contributes to cilia length control.

2.3.6 The kinase CDK5 and hCDC14A phosphatase counteract phosphorylation of *DBN1* during ciliogenesis

CDK5 is a proline directed kinase that in serum starved cells induces degradation of 'nuclear distribution protein nudeE' homolog 1 (NDE1) that promotes cilia disassembly upon re-entry of RPE-1 cells into the division cycle (Maskey et al., 2015). Hence, cells depleted of CDK5 have shorter cilia (Figure 2.19 H). We first asked whether CDK5 counteracts hCDC14A during ciliogenesis. Restoration of cilia length in *hCDC14A*^{PD} cells to Wt by CDK5 depletion supports this model (Figure 2.19 H). However, this length regulation of cilia by hCDC14A/CDK5 was not on the level of NDE1 since protein levels of NDE1 in ciliated *hCDC14A*^{PD} and Wt cells were similar (Figure 2.22 B). We next considered the possibility that S142 of *DBN1* is also phosphorylated by CDK5 in RPE-1 cells during ciliogenesis (Tanabe et al., 2014; Worth et al., 2013). Indeed, depletion of CDK5 in *hCDC14A*^{PD} cells strongly reduced *DBN1*^{pS142} phosphorylation (Figure 2.19 I). To test this further, we expressed S142D phospho-mimetic version of *DBN1*^{S142D} in *hCDC14A*^{PD} RPE-1 cells and subsequently depleted CDK5 by siRNA. Cilia length reduction by CDK5 depletion in *hCDC14A*^{PD} RPE-1 cells was completely inhibited by the expression of *DBN1*^{S142D} (Figure 2.19 J). Thus, opposing phospho-regulation of *DBN1* by CDK5 and hCDC14A affects cilia length.

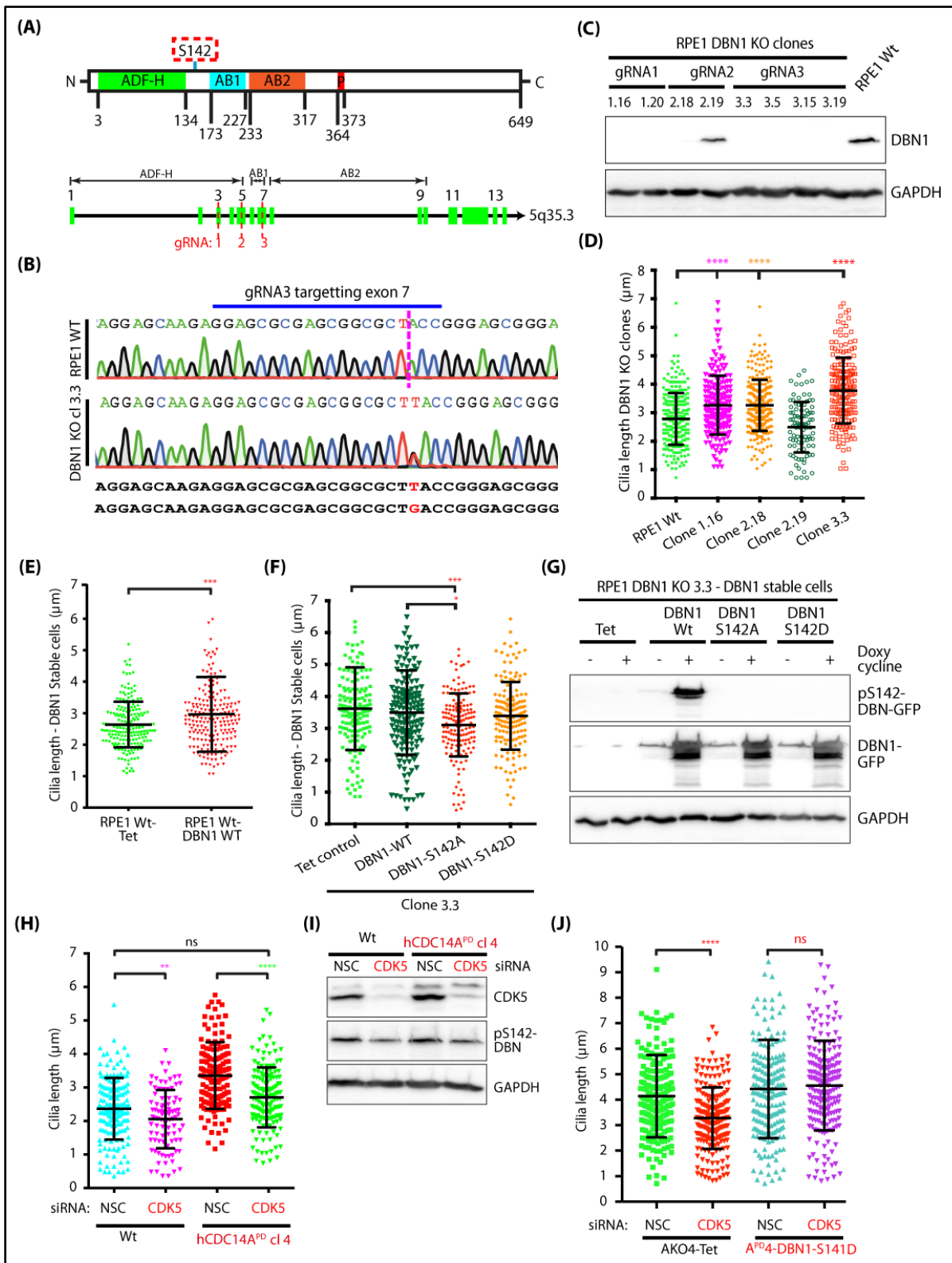


Figure 2.19: Phospho-regulation of DBN1 is critical for cilia length control.

(A) Schematic representation of different domains of drebrin (adapted from Shirao et al., 2017) (here ADF-H: ADF homology domain, AB1: Actin-binding region 1, AB2: Actin-binding region 2, P: Proline-rich region). The numbers represent the amino acid

positions of the denoted domains. Three independent gRNAs targeting three different exons (3,5,7) of *DBN1* were used to generate *DBN1* KO cells. (B) Successful targeting of the locus of interest was confirmed by sequencing the PCR amplicons surrounding the locus. For example, in clone 3.3, there was a single base insertion in both alleles (T/G) to cause disruption of protein expression through introduction of a premature stop codon. (C) The absence of *DBN1* protein in the targeted clones was further verified by immunoblotting of the whole cell lysate. GAPDH is used as loading control. (D) One targeted clone from each gRNA (1.16, 2.18, 3.3) including the nontargeted clone 2.19 and Wt control were serum starved for 48 hours to induce ciliogenesis and measure cilia length. The cilia from *DBN1* KO cells were significantly longer than those from Wt or non-targeted controls. (E) Overexpression of *DBN1-GFP* in RPE-1 Wt cells caused the elongation of primary cilia. (F) The phospho-inhibitory (S142A) version of *DBN1* rescued the elongated cilia of *DBN1* KO cells. (G) The overexpressed Wt *DBN1* was hyper-phosphorylated in cells. The pS142 antibody did not detect the overexpressed *DBN1^{S142A}* or *DBN1^{S142D}*. (H) Depletion of CDK5, the kinase that phosphorylates drebrin S142 (Worth et al., 2013), decreased the cilia length in Wt cells as well as rescued the elongated cilia of *hCDC14A^{PD}* cells. (I) Immunoblot analysis of (H) confirming the successful depletion of CDK5. The decrease in *DBN1^{pS142}* intensity was associated with CDK5 depletion. (J) CDK5 mediated cilia length decrease can be completely blocked by expression of the phospho-mimetic *DBN1^{S142D}* in *hCDC14A^{PD}* cells. (ns = not significant; * P ≤ 0.05; ** P ≤ 0.01; *** P ≤ 0.001; **** P ≤ 0.0001).

2.3.7 *hCDC14A^{PD}* cells show enhanced recycling endosome as well as elevated docking of ciliary vesicles to the basal body

How does phospho-regulation of *DBN1* control cilia length? Previously *DBN1* was described as a member of an actin network that is involved in ectocytosis of ciliary vesicles from the cilia tip of inner medullar collecting duct (IMCD3) kidney cells that have an exposed primary cilium (Nager et al., 2017). In contrast to IMCD3 cells, *DBN1* was not associated with any part of the cilium of RPE-1 cells that assemble cilia via the intracellular pathway (Figure 2.22 C) (Mazo et al., 2016). However, partial actin-*DBN1* colocalization could be confirmed in RPE-1 cells (Figure 2.22 D). Continuous growth of cilia under serum starvation condition (Figure 2.9) raises the possibility that a feedback mechanism restricting cilia length in Wt cells is failing in *hCDC14A^{PD}* cells. Control of endocytic recycling to the pericentrosomal preciliary compartment (PPC) as well as the ciliary vesicle transport from the Golgi to the basal body may be such mechanisms (Joo et al., 2013; Kim et al., 2010; Ye et al., 2014). Interestingly, *DBN1* KO HEK293 cells were reported to display enhanced

endocytosis of dynamin-dependent cargo (Li et al., 2017). Consequently, we first tested the uptake of transferrin as a marker for endocytic recycling during ciliogenesis. Indeed, uptake of transferrin was enhanced in *hCDC14A^{PD}* cells compared to Wt cells (Figure 2.20 A and B). Furthermore, elevated Smoothed (SMO) positive cilia in *hCDC14A^{PD}* cells indicated the enhanced ciliary vesicle docking during ciliogenesis (Figure 2.20 C and D). This elevated Smo signal in *hCDC14A^{PD}* cells also lead to an increase in ratio of Gli3 - full length/Gli3 - repressor form, which indicated that the Sonic Hedgehog signalling was active in these cells (Figure 2.21 C and D). The Hedgehog (Hh) signaling pathway plays pivotal roles in the regulation of embryonic development as well as of the proliferation and differentiation of stem cells. Accumulation of the signalling protein Smoothed (Smo), a 7-pass transmembrane (7TM) protein, in the membrane of primary cilia is a prerequisite for the activation of Hh signalling cascade. In the absence of ligands, the Hh receptor Patched-1 (Ptch) localizes in and around the cilium and inhibits the accumulation of Smo (Milenkovic et al., 2015). However, the cilia length of RPE-1 Wt and *hCDC14A^{PD}* cells could not be altered by inducing (SAG) or inhibiting (cyclopamine) Hedgehog signalling (Figure 2.21 A and B).

Low dose of actin-depolymerizing drug cytochalasin D was reported to promote ciliogenesis by stabilizing the Arp2-associated pericentrosomal actin network (Wu et al., 2018). Similarly, we observed enhanced Arp2 as well as phalloidin intensity surrounding the 1 μm radius of the basal body in *hCDC14A^{PD}* cells (Figure 2.20 E-G). These data denote that *hCDC14A^{PD}* cells have a distinct local actin reorganization surrounding the basal body, which in turn contributes to cilia elongation. The involvement of actin modulation in cilia length control also come from the observation that the ciliogenesis inhibitory effect of hCDC14A over-expression could be reverted by the treatment of low dose of cytochalasin D (Figure 2.22 E).

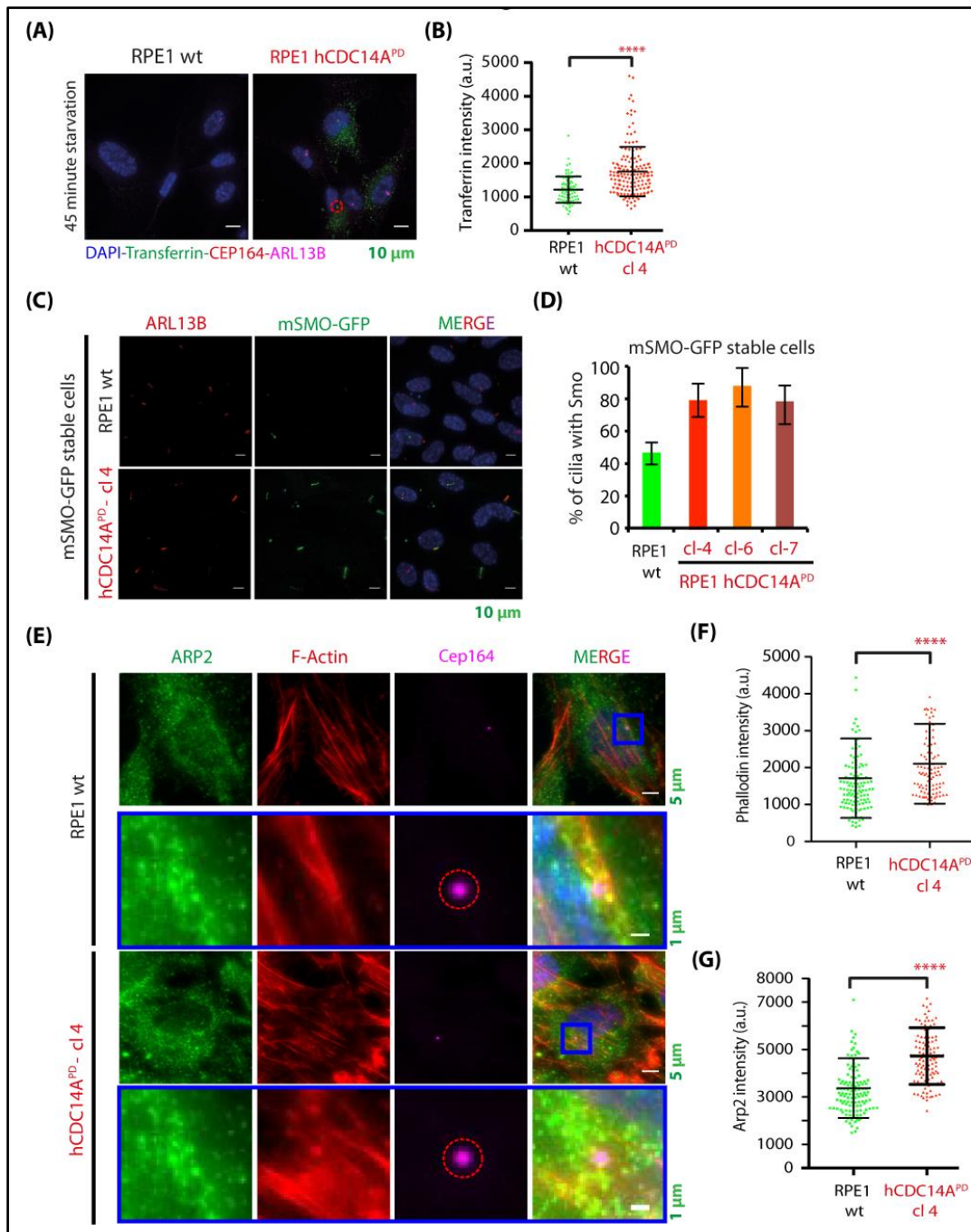


Figure 2.20: $hCDC14A^{PD}$ cells show enhanced recycling endosome as well as elevated docking of ciliary vesicles to the basal body.

(A, B) $hCDC14A^{PD}$ cells take up significantly higher transferrin that marks recycling endosomes. The fluorescence intensities of transferrin within a 2- μ m-radius circle surrounding the CEP164 signal were quantified and presented in B. An ImageJ macro was used to measure the intensity as described in method sections. (C, D) Mouse smoothed C-terminally tagged to GFP was lentivirally integrated into RPE-1 Wt and $hCDC14A^{PD}$ clones under TetON promoter. Cells were starved along with Dox treatment for 48 hours and the percentage of cilia that contain Smo-GFP signal was quantified. All the $hCDC14A^{PD}$ clones contained a higher percentage of Smo-GFP

positive cilia compared to Wt control. (E, F, G) Sub-centrosomal (1- μm -radius) branched actin level was measured by quantifying the intensity of Arp2 and F-actin in Wt and *hCDC14A^{PD}* cells. *hCDC14A^{PD}* cells contain significantly higher branched actin in the pericentrosomal area (1- μm -radius) compared to Wt cells. The blue boxed region are enlarged and represented below the respective channels of both Wt and *hCDC14A^{PD}* cells.

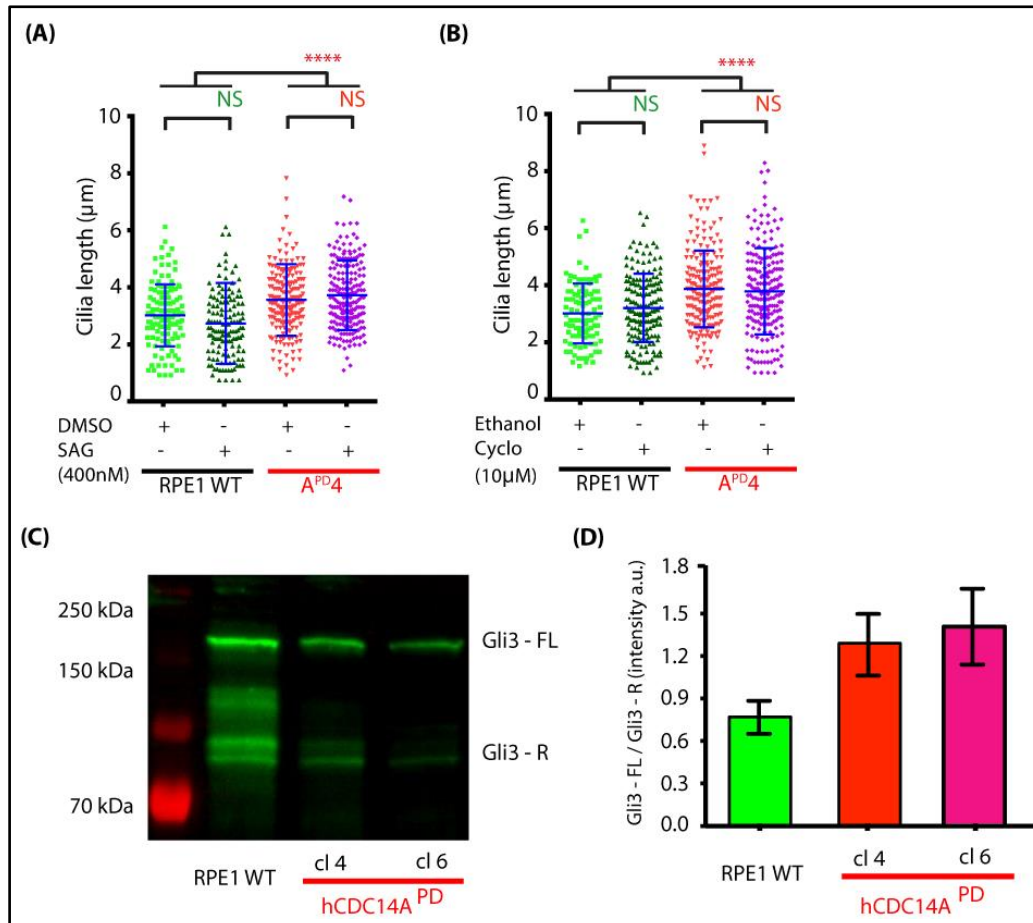


Figure 2.21: Modulation of Hedgehog signalling does not affect cilia length.

(A) RPE-1 Wt and *hCDC14A^{PD}* cells were treated with vehicle control or Hedgehog signal inducing chemical SAG (Smoothened agonist, 0.4 μM). Cells were serum starved for 24 hours prior to SAG treatment along with starvation for 24 hours and fixation for immunofluorescence. (B) The Hedgehog inhibitor cyclopamine was also treated (10 μM) with similar experimental scheme before fixation and immunofluorescence microscopy to measure cilia length. (C) The whole cell lysates from RPE-1 Wt and *hCDC14A^{PD}* cells under ciliogenic condition were analysed for immunoblot detection of Gli3. (D) The ratio Gli3-FL (190KDa)/ Gli3-R (83KDa) was densitometrically determined.

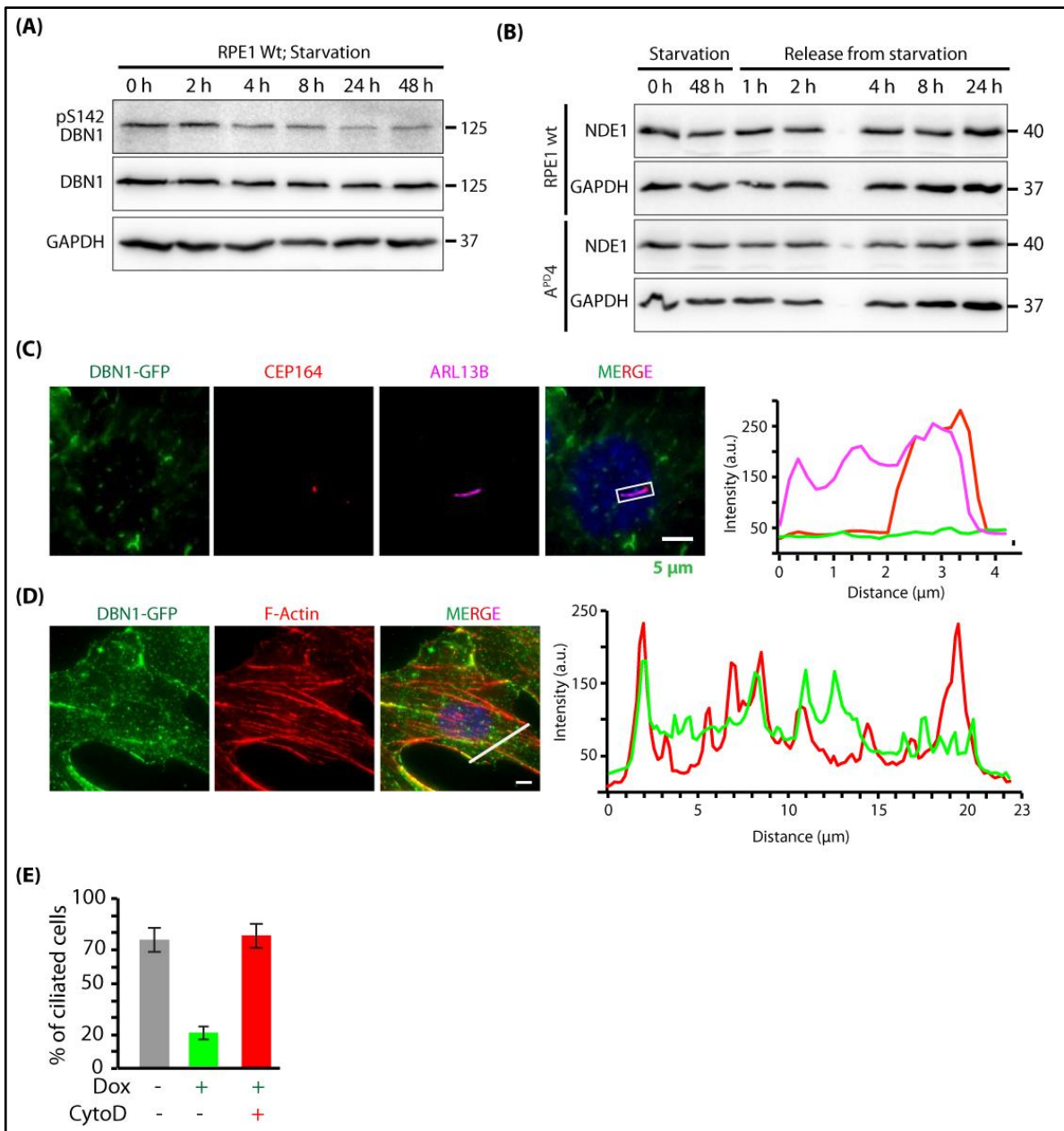


Figure 2.22: DBN1 is dephosphorylated during ciliogenesis.

(A) DBN1^{pS142} level was decreased over time during ciliogenesis. (B) RPE-1 Wt and *hCDC14A^{PD}* cells showed comparable fluctuation of NDE-1 during ciliation and cilia disassembly processes, i.e., the level is decreased upon serum starvation and again elevates gradually upon serum addition. (C) DBN1-GFP could not be detected in cilia. (D) Drebrin and F-actin co-localized in RPE-1 cells during ciliogenesis (scale bar 5 μ m). (E) The ciliogenesis suppressing effect of *hCDC14A-GFP* overexpression could be reversed by treating the cells with actin depolymerizing drug cytochalasin D (200 nM for 16hr in serum- free medium, $n \geq 200$).

3 Discussion

3.1 Genome editing through large insertion leads to the skipping of targeted exon

Genome editing is a robust experimental paradigm to assign cellular function(s) to a molecule. Simplicity of genome editing through engineered nucleases has recently allured the scientific community to generate knockout cellular models. Highly efficient genome editing can be achieved through targeting an endonuclease to specific locus of interest. Engineered zinc-finger nuclease (ZFN) and CRISPR-associated protein-9 nuclease (Cas9) offer such an elegant approach for genome editing in vertebrate cells. In this study, we have utilized ZFN and Cas9-catalyzed double strand break followed by homologous recombination-mediated incorporation of premature stop codon and selection marker to target human cell division cycle 14A (*hCDC14A*) and cell division cycle 14B (*hCDC14B*) genes. Targeting of the *hCDC14A* and *hCDC14B* loci in telomerase immortalized human retinal pigment epithelium (hTERT-RPE-1) and human colon cancer (HCT 116) cells were confirmed by Southern blot hybridization. Nevertheless, DNA sequence analysis of reverse transcription polymerase chain reaction (RT-PCR) products confirmed that in all the single/double allele ablations, the targeted exon was spliced out. The phenomenon of exon skipping was independent of the genome editing approaches exploited, Cas9 or ZFN. Because the exons had a nucleotide number that could be divided by 3, the reading frame of the exon deletion was maintained. This indicates an exon-skipping event possibly due to the insertion of large DNA fragments (1.7 to 2.5 Kb) within the targeted exons. As a proof-of-principle, we have used gene disruption followed by non-homologous end joining (NHEJ) approach. Small alterations in the exon (one to fifteen bases) were transcribed to mRNA without exon skipping. Furthermore, loxP site-mediated removal of selection markers left a 45 bp scar within the targeted exon that can be traced in mRNA without exon skipping.

Thus, insertion of a large DNA fragment into an exon by genome editing has the potential to annihilate secondary pre-mRNA structure and impede cellular mRNA processing leading to exon skipping. Hence, more cautious approach needs to be taken while designing target sites in such that the possible skipping of targeted exon causes a frame-shift mediated incorporation of pre-mature stop codon. An alternative strategy could be the introduction of double strand break in an intronic sequence to incorporate homologous recombination mediated subtle changes in the adjacent exon. These exon modifications could be introduced in the donor along with the selection marker. Of note, such skipping mechanisms can be useful to engineer proteins with small deletions or for the analysis of acute knockouts in response to Cre induced selection marker removal.

3.2 *hCDC14A* and *hCDC14B* double knockout cells show no obvious growth defects

Expression analysis of Wt as well as *hCDC14A* and *hCDC14B* double knockout cells showed that *hCDC14C* was not expressed in RPE-1 and HCT 116 cells. This ruled out the possible functional complementation of *hCDC14A* and *hCDC14B* loss by *hCDC14C*. The generated knockout cells were also subjected to general growth analysis by MTT and cell cycle distribution analysis by FACS. Absence of any obvious growth defects in the knockout cells have indicated that *hCDC14A* and *hCDC14B* are dispensable for cell cycle progression in RPE-1 and HCT 116 cells. Thus, the mitotic exit function of ScCDC14 is not conserved in higher eukaryotes like human and is considered to be taken over by PP1 and PP2A (De Wulf et al., 2009).

3.3 The phosphatase *hCDC14A* regulates cilia length

CDC14 phosphatases regulate ciliogenesis in several organisms including Zebrafish, mouse and human cells. *CDC14A* mutations in humans and mice that affect the activity of the phosphatase impair formation of the transient kinocilia of developing

cochlear hair cells and the persistent kinocilia of vestibular hair cells in the organ of Corti (Imtiaz et al., 2018). Kinocilia in the organ of Corti are motile 9+2 cilia with a special function in the organization of actin-based stereocilia. Data presented in this study now indicate that hCDC14A plays a role in cilia length control of 9+0, non-motile primary cilia. However, in contrast to Zebrafish that showed shorter cilia in response to CDC14A or CDC14B depletion (Clément et al., 2011, 2012), expression of a phosphatase dead version or hCDC14A depletion resulted in longer cilia. This length phenotype was specific to hCDC14A and was not observed in cells lacking the paralogue hCDC14B. Presently, it is unclear why inactivation of CDC14A in Zebrafish and human cells impact cilia length in opposite ways. However, variations in cilia phenotypes between organisms upon inactivation of orthologous have been reported before (Hamel et al., 2017).

Phospho-proteome and BioID analysis revealed several hCDC14A substrates during ciliogenesis, which were mostly dephosphorylated on pSP sites. This is the signature of CDC14A phosphatases from yeast to human cells (Chen et al., 2017; Eissler et al., 2014). However, in contrast to cycling cells, in which hCDC14A prefers pSPxK/R sites (Chen et al., 2017) the preference for the positively charged amino acid in +3 position was less pronounced under serum starvation conditions that promoted cilia formation. The reason for this difference in substrate specificity may be the regulation of hCDC14A during ciliogenesis. Here we focused our analysis on the actin bundling protein DBN1 because of its reported role in ciliogenesis (Nager et al., 2017). Analysis of DBN1^{pS142} with a phospho-specific antibody confirmed that DBN1 was hyper-phosphorylated in *hCDC14^{PD}* RPE-1 cells in comparison to Wt cells, while overexpression of *hCDC14A* reduced pS142 phosphorylation. Purified, recombinant hCDC14A dephosphorylated DBN1 at S142 indicating direct regulation by hCDC14A. Our data suggest that S142 of DBN1 is phosphorylated by the proline directed kinase CDK5 during ciliogenesis. This is in line with reports on the phosphorylation of DBN1 by CDK5 in filopodia formation (Tanabe et al., 2014; Worth et al., 2013). Analysis of ciliogenesis in RPE-1 cells expressing the phospho-mimetic *DBN1^{S142D}* suggests that the hCDC14A/CDK5 phospho-regulation of S142

contributes to cilia length control. Phosphorylation of DBN1^{S142} by CDK5 relieves an intra-molecular interaction within DBN1 and promotes its actin bundling activity (Worth et al., 2013). Thus, bundling of actin probably promotes ciliogenesis. Presently, it is unclear why *DBN1* KO has the same impact on cilia length as *DBN1*^{S142D}. Further studies are required to compare the actin cytoskeleton of *DBN1* KO and *DBN1*^{S142} cells and whether cilia elongation in both mutant cell types has the same molecular cause.

CDK5 has been implicated in cilia length regulation since this kinase phosphorylates the cilia disassembly factor NDE1 promoting its ubiquitination by the E3 ligase FBW7 and the subsequent degradation by the proteasome (Maskey et al., 2015). However, Maskey et al. indicated that the CDK5-FBW7-NDE1 branch is only one of several possible modes of action of CDK5 in cilia length control. NDE1 levels were not affected in *hCDC14A*^{PD/PD} cells during ciliogenesis and *hCDC14A*^{PD} cells disassembled cilia even slightly faster than Wt cells in response to serum addition. Furthermore, NDE1 was not identified in the *hCDC14A* phospho-proteome or BioID screens. This together suggests that NDE1 is not a substrate of *hCDC14A*. Rather, CDK5 affects cilia length in at least two ways: via NDE1 and DBN1 (Maskey et al., 2015). While NDE1 regulation reflects the untimely activation of a cilia disassembly factor during ciliogenesis, phospho-regulation of DBN1 may contribute to cilia length control that is seen between tissues. Additional experiments are needed to test this model.

How does phospho-regulation of DBN1 affect cilia length? DBN1 was reported to function in ectosome release from the tip of the exposed cilia (Nager et al., 2017). Ectocytosis is a selective process that removes activated signalling molecules from cilia. However, in RPE-1 cells that assemble cilia via the intracellular pathway, DBN1 was not detected at the tip of the cilia. This suggests that DBN1 functions differently in RPE-1 cells. DBN1 negatively regulates endocytosis in HEK292 cells (Li et al., 2017). Endocytosis promotes ciliogenesis by delivering preciliary vesicles to the basal body (Kim et al., 2010). Interestingly, we observed an

increase uptake to transferrin in *hCDC14A^{PD}* RPE-1 cells. We therefore suggest that hCDC14A and CDK5 regulate cilia length, at least in part, through phosphoregulation of DBN1 that then controls the delivery of preciliary vesicles to the basal body through endocytosis (Figure 3.1).

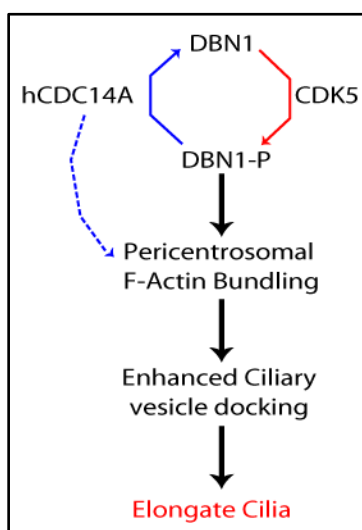


Figure 3.1: Proposed model for the elongation of primary cilia in RPE-1 *hCDC14A^{PD}* cells.

Apart from DBN1, several other proteins such as CEP170, DPYSL2, LIMA1 and MAP4 were identified as substrates for hCDC14A. Centrosomal protein of 170 kDa (CEP170) is a sub-distal appendage protein which is important for the maturation of mother centriole and microtubule anchoring at centrosomes (Huang et al., 2017). However, loss of CEP170 affects neither the length of primary cilia nor the percentage of ciliated cells, but alters the spatial configuration of cilia (Mazo et al., 2016). Dihydropyrimidinase-related protein 2 (DPYSL2), which is also known as Collapsin response mediator protein 2 (CRMP2), is a substrate for CDK5 and was reported to be involved in affecting cilia length by altering microtubule dynamics (Husson et al., 2016). In cystic kidney disease, both total CRMP2 and pCRMP2 (Ser522) are increased, whereas, inhibition of CDK5 activity leads to the reduction of CRMP2 and pCRMP2. Microtubule-associated protein 4 (MAP4) was reported to be localized to the axoneme where it negatively regulated ciliogenesis (Ghossoub et al., 2013). Thus hCDC14A has the potential to affect cilia length by modulating

axonemal microtubule dynamics through DPYSL2 and MAP4. The actin bundler protein LIMA1 might also regulate local pericentrosomal as well as cellular actin cytoskeletal status.

In general, enrichment of actin related proteins in both global phospho-proteome and BioID analyses indicates a close connection between hCDC14A function and cellular actin regulation. Such cytoskeletal regulation might lead to the alteration of a plethora of cellular processes including ciliogenesis, hearing, and fertility. For hearing, the epidermal growth factor receptor pathway substrate 8 (EPS8), an actin filament remodelling protein that interact with Rab5 GTPase-activator RNTre, was proposed to be a substrate for hCDC14A (Imtiaz et al., 2018; Lanzetti et al., 2007). However, a precise molecular understanding of the mechanism(s) that govern hearing loss in *hCDC14A* mutants is missing. Another key question that remain unresolved is that how hCDC14A is regulated during cell cycle or ciliogenesis. One possible mode could be the cell cycle dependent distinct localizations of hCDC14A. In such case, the non-conserved variable C-terminal sequence of hCDC14A may be involved in determining its localization to exact intracellular compartments (Imtiaz et al., 2018). However, post-translational modification dependent regulation could also be critical for both localization and function of hCDC14A.

4 Concluding Remarks

In this study, we have employed state-of-the-art gene editing techniques to generate hCDC14A and/or hCDC14B knockout cell lines to decode molecular mechanisms of their functions. The phenotypic analysis of these generated cells was aided by various imaging, biochemical and mass-spectrometry techniques. Taking all the findings of this study into consideration, we can conclude that -

- hCDC14A and hCDC14B phosphatases are dispensable for cell cycle progression in RPE-1 and HCT 116 cells.
- hCDC14A is localized to the proximal end (C-NAP1-dependent) and the sub-distal appendage regions of mother centriole (basal body).
- Lack of hCDC14A phosphatase activity in RPE-1 cells causes the elongation of primary cilia.
- The elongated cilia in *hCDC14A^{PD}* cells are structurally comparable to those from Wt cells.
- Regulated expression of hCDC14A but not its phosphatase dead version suppresses cilia formation.
- S142 of DBN1 is a substrate for hCDC14A.
- CDK5 kinase and CDC14A phosphatase regulated phospho-status of DBN1 pS142 is crucial for cilia length control.
- *hCDC14A^{PD}* cells show enhanced recycling endosomes (transferrin) as well as increased ciliary vesicle docking (smoothened) in the pericentrosomal areas.

5 Materials and Methods

5.1 Cell culture and transfection

RPE-1, HEK293T (human embryonic kidney) and HEK293-GP (GP2-293, Clontech) cells were cultured in Gibco DMEM/F-12 (ThermoFisher) media containing 10% FBS, 1% L-glutamine and 1% penicillin/streptomycin. HCT116 cells were cultured in McCoy's 5A (Gibco) medium supplemented with 10% FBS, 1% L-glutamine and 1% penicillin/streptomycin. All cell lines were cultured at 37 °C with 5% CO₂. For HCT116 cells, fibronectin (Santa Cruz, sc-29011) coatings were made by incubating glass coverslips with 5 µg/cm² of fibronectin in PBS for 30 min at 37 °C. Plasmid DNA transfections were made according to manufacturer's protocol using Lipofectamine 2000 or Lipofectamine LTX (RPE-1 cells). Lipofectamine RNAiMAX transfection reagent (ThermoFisher) was used according to the manufacturer's instructions with a final concentration of 20 nM siRNA (please see Table 1 and Table 2 for details of used siRNA).

Table 1: List of ON-TARGET_{plus} SMARTpool siRNA Reagents - Human (Dharmacon)

Catalog Number	Gene Symbol	siRNA Sequence (5'-3')
LU-003469-00	CDC14A	GGACAUUGAUAGCCUGUUA
LU-003469-00	CDC14A	CUUGUGAGUUCAUGAAAGA
LU-003469-00	CDC14A	GCACAGUAAAUAACCCACUA
LU-003469-00	CDC14A	GAACAUUAUGAGCGAGUUG
L-003239-00	CDK5	UAUAAGCCCUAUCCGAUGU
L-003239-00	CDK5	CCGGGAGACUCAUGAGAUC
L-003239-00	CDK5	GGCUGGGGAUUCUGUCAUA
L-003239-00	CDK5	GGAUUCCCGUCCGCUGUUA
L-010508-00	CTTN	CCACGAAUAUCAGUCGAAA
L-010508-00	CTTN	GAACAAGACCGAAUGGAUA
L-010508-00	CTTN	GAGCAUAUCAACAUCACA
L-010508-00	CTTN	CAAGUAACAUCAGAGCUAA
L-011841-00	DBN1	GGAGGAGGCAGCAGCUAAU
L-011841-00	DBN1	GGAUUAACCGAGAGCAGUU
L-011841-00	DBN1	CCUCAAGCUUGCAGCAUCA
L-011841-00	DBN1	GGAGUUUGCCCAAUCGGAA
L-031725-00	DOCK7	GAUCGAAGUUGUAAUCGUA
L-031725-00	DOCK7	UCUCGAAGCCUAGUAAUA

Catalog Number	Gene Symbol	siRNA Sequence (5'-3')
L-031725-00	DOCK7	CGACUCUGCUUUAAGAUU
L-031725-00	DOCK7	UAACCAAACUUGCAGAGAU
L-009519-01	DPYSL2	CCGGGAUUAUUGGCGCCAUA
L-009519-01	DPYSL2	GGUCAAAACCUAAAACACCGA
L-009519-01	DPYSL2	GAACUGUGGUGUAUGGCGA
L-009519-01	DPYSL2	AGUUA AAAACCUGACGAUUU
L-003977-00	IGF2BP1	CGAAACACCUGACUCCAAA
L-003977-00	IGF2BP1	UGAAGGCCAUCGAAACUUU
L-003977-00	IGF2BP1	GAAAGUAGAAUACAAGGA
L-003977-00	IGF2BP1	GCUUAGAGAUUGAACAUUC
L-027345-00	KANK2	CGUGCGAUCUAUCAUGAAA
L-027345-00	KANK2	CAGCUCACAGUACAACUUA
L-027345-00	KANK2	GACGAGAGCCCUACAUCAU
L-027345-00	KANK2	GAACGGGACUUGGGCAUGC
L-019252-00	LMO7	GAUGAUUACUCCACAAAUA
L-019252-00	LMO7	GAAAGCUUGUGAACAGAUU
L-019252-00	LMO7	AGAGAGAGAAUCCAAGUA
L-019252-00	LMO7	UAGCAGGAUUGGAUAAUUAU
L-013027-01	LUZP1	AAGAAAUAGACCUACGGAUU
L-013027-01	LUZP1	GAAGACAACACGAACGUUU
L-013027-01	LUZP1	GAGUUUAGCGUCAGAGUUA
L-013027-01	LUZP1	AUAACGACCUUCAGGAUAA
L-011724-01	MAP4	GGAGUAGAAGGGAGCGAUA
L-011724-01	MAP4	GGAGAGAUAAAGCGGGACU
L-011724-01	MAP4	GAUGAUGUUGUGGGAGAAA
L-011724-01	MAP4	GAGUCAAGAAGAAACCGU
L-014102-01	MPRIP	CGGGACAAGAAGUACGCAA
L-014102-01	MPRIP	GUGCCACGGUGUCCGGAUA
L-014102-01	MPRIP	GUGCACCGGUCUCGGAAAU
L-014102-01	MPRIP	CGGGUAAAGGAAUCGGAAA
L-023376-01	MTCL1	GCAGUACCGUCUUCGGAAA
L-023376-01	MTCL1	CCGAGAGUGAUGCGGGCAA
L-023376-01	MTCL1	GGAUGAGCGUGCCCGACUA
L-023376-01	MTCL1	CAGCAAUAUGCCAGCGACA
L-013081-00	PDLIM7	GCACCGAGUUCAUGCAAGA
L-013081-00	PDLIM7	UCACACACAUCGAAGCUCA
L-013081-00	PDLIM7	GAGCAUCGAUGGCGAGAAU
L-013081-00	PDLIM7	CGGAUGAGGAGCACCUGAA
L-013299-01	PRRC2A	CCAAAUAUCAGAAGUCGUU
L-013299-01	PRRC2A	GGACUCAGACUUACGCCUA
L-013299-01	PRRC2A	CCUGCAGAGUCUCGGGAAA
L-013299-01	PRRC2A	GGAAAGGGAGUCUGCCGAA
L-004746-00	RANBP2	GCGAAGUGAUGAU AUGUUU
L-004746-00	RANBP2	CAAACCACGUUAUUAUCAA
L-004746-00	RANBP2	CAGAACAACUUGCUAUUAG
L-004746-00	RANBP2	GAAGGAAUGUUCAUCAGGA

Catalog Number	Gene Symbol	siRNA Sequence (5'-3')
L-006846-00	RANGAP1	GACCGAAUGUCACCGGAAA
L-006846-00	RANGAP1	UGUACAAGGUCUAGACUCA
L-006846-00	RANGAP1	GAAACCGUCUGGAGAAUGA
L-006846-00	RANGAP1	GCAAGAGCCUCAAACUCAA
L-013690-00	RPS2	UUAAGGAAUCAGAGAUCAU
L-013690-00	RPS2	CGUCAAGACCCACACCAGA
L-013690-00	RPS2	CAUGAUGGCUGGUAUCGAU
L-013690-00	RPS2	AGUGGAUGCCCGUCACCAA
L-010500-00	SCRIB	GACCGCGUCCUCUCUAUUA
L-010500-00	SCRIB	GGACGACGAGGGCAUAUUC
L-010500-00	SCRIB	CGACAGAGCUGCACGUGCU
L-010500-00	SCRIB	ACAACGAGAUCCAGCGGUU
L-026032-01	SEC16A	GGACGGAAGCCUAUGAGUA
L-026032-01	SEC16A	CCUACAGGAGACGGGCUA
L-026032-01	SEC16A	AAGCGGACUUUGACGAUUU
L-026032-01	SEC16A	CCUCAGUCCUCUAGCGUGU
L-010657-01	SND1	GGAAGUCUGUUUCACGAUA
L-010657-01	SND1	UGAUGGAGAACAUGCGCAA
L-010657-01	SND1	CGAGAGUUCUUCGAAAGA
L-010657-01	SND1	UCAUGGUGGAGGUGCGCAA
L-011479-01	SORBS2	AGCAAGAGGAGGCGAGUUA
L-011479-01	SORBS2	GGUAAAAGAAACAUCGUUGA
L-011479-01	SORBS2	AAAUAAAAGCCUUCGGUAA
L-011479-01	SORBS2	UUGUAAAGUUGCAUCGCUA
L-021390-01	SYNPO	AAUCAGAACCCACCGGCAA
L-021390-01	SYNPO	CCAGAGAAGCUACGCUCAU
L-021390-01	SYNPO	CCACCAAGCAGCCGCCAUA
L-021390-01	SYNPO	GAGAAUAUGUCAUCGAGU
L-021220-01	UBAP2L	CAACACAGCAGCACGUUAU
L-021220-01	UBAP2L	GUGUGGAGAGUGAGGCGAA
L-021220-01	UBAP2L	CAACAGAACCAGACGCAGA
L-021220-01	UBAP2L	CCUGGGAGAUGGUCGGGAA
L-006099-00	USP9X	AGAAAUCGCUGGUAUAAAU
L-006099-00	USP9X	ACACGAUGCUUUAGAAUUU
L-006099-00	USP9X	GUACGACGAUGUAUUCUCA
L-006099-00	USP9X	GAAAUAAUCUCCUACCGAA

In all the siRNA experiments, ON-TARGETplus Non-Targeting Control siRNA (Dharmacon D-001810-01-20; 5'-UGUUUACAUGUCGACUAA-3') was used as control.

Table 2: List of Silencer® Select siRNAs from Ambion®.

Gene Symbol	siRNA Sequence (5'-3')
CEP170	GCAUGAGAAGUUUACCAU
LIMA1	UUAUAGAGGUUUCUGAGAGGCGUGG

5.2 Generation of ZFN-mediated knockout cells

Human *CDC14A* and *CDC14B* specific CompoZr™ knockout Zinc Finger Nucleases (ZFN) were designed and evaluated by Sigma Advanced Genetic Engineering Labs. The ZFN for *hCDC14A* (product Number: CKOZFND2170-1KT) targets the sequence 5'-AGCACACCCAGTGACAcaatCGTGCGAAGGTTCCCTGAA-3' in the 9th exon (cutting site in lower cases). Target sequence for ZFN against *hCDC14B* is in the 4th exon 5'-TGCTGCCTTCCTTGTtggatGCTACATGGTAAGTATTTG-3' (product Number: CKOZFND5769-1KT). The donor vector was constructed by PCR amplification of the genomic locus as described in the previous publications from our group (Chen et al., 2016; Panic et al., 2015). In short, the genomic locus 800 bp upstream and downstream of the ZFN cut site was amplified and sub-cloned into pJet 1.2 vector. The insertion cassette including STOP codon in every frame and neomycin/ puromycin resistance was inserted at the cut site of donor vector.

10⁶ cells were co-transfected with the ZFN mRNAs (2.5 µg of each) and donor vector (7 µg) by electroporation (Invitrogen, Neon transfection system). After electroporation, cells were cultured for 24 hours at 37 °C (recovery) followed by 48 hours at 30 °C (enhancing ZFN efficiency (Doyon et al., 2010)). Cells were further cultured at 37 °C for 72 hours prior to single cell dilution (limiting) in 96 well plates (500 µg/ml neomycin). Two weeks later, the emerging clones were screened by genomic PCR and positive clones were further confirmed by RT-PCR as well as Southern blot hybridization. Junction PCR with one primer in donor construct and the other in the genome outside homology arm confirmed successful targeting and insertion of the selection markers. The following primers were used for junction PCR - ***hCDC14A***: forward 5'-CGGCTATGACTGGGCACAAC-3'; reverse 5'-GCCTCCTCGAAGTCAAACAAG -3'; ***hCDC14B*** (for NeoR insertion): forward 5'-CGGCTATGACTGGGCACAAC-3'; reverse 5'-CGATCTCCGCTCACTG-3'; ***hCDC14B*** (for PuroR insertion): forward 5'-CGGGGCGAAGGCAAC-3'; reverse 5'-CGATCTCCGCTCACTG-3'. Similar approach without the donor construct was taken in case of NHEJ-facilitated disruption of *hCDC14B* gene. The resultant

insertion/deletion-mediated mutagenesis was detected by sequencing of the amplified (Q5® High-Fidelity DNA Polymerase - NEB) genomic locus surrounding the ZFN cut site (primers used - forward 5'-TGAATGGTTATGGGATTTGGA-3'; reverse 5'-GCACAGCTTCCTTGAATTGG-3').

5.3 Generation of Cas9-mediated *hCDC14A* knockout cells

Guide RNAs (gRNAs) targeting the exon 9 of *hCDC14A* was designed using the web tool (<http://crispr.mit.edu/>) (Hsu et al., 2013). gRNA1 (5'-CCAGTGACAACATCGTGCGA-3'), gRNA2 (5'-CCTTCGCACGATGTTGTTCAC-3') and gRNA5 (5'-CTTCGCACGATGTTGTCACT-3') with scores 96, 91 and 86, respectively, were selected as they were exactly targeting the ZFN binding site (5'-AGCACACCCAGTGACAacatCGTGCGAAGGTTCCCTGAA-3'). 'Churh gRNA insert' containing the U6 promoter and gRNA scaffold (Mali et al., 2013) was first synthesized as gBlock from IDT (<http://www.idtdna.com/pages/products/genes/gblocks-gene-fragments>) and cloned into pJet1.2 vector. The intended gRNAs were then ordered as PCR primers with overhangs from U6 promoter and gRNA-scaffold and inserted between U6 promoter and gRNA scaffold through PCR mutagenesis.

Different strategies were used to generate Cas9-mediated *hCDC14A*-KO HCT116 and RPE1 cells. For HCT116, hCas9 plasmid (a gift from George Church (Addgene # 41815, (Mali et al., 2013))) was transiently transfected with gRNA and donor plasmids. Whereas for RPE1 cells, pCW-Cas9 plasmid (a gift from Eric Lander & David Sabatini (Addgene # 50661 (Wang et al., 2014))) containing doxycycline (Dox) inducible spCas9 was lentivirally integrated into RPE1 FRT/T-Rex cells. Successful expression and nuclear localization of Cas9 was confirmed by indirect immunofluorescence and western blot analysis. The cells were then electroporated with the plasmids containing gRNA and donor vector. Junction PCR with forward primer in NeoR cassette (5'-CGGCTATGACTGGGCACAAC-3') and reverse primer

in the genome outside homology arms (5'-GCCTCCTCGAAGTCAAACAAG-3') confirmed successful targeting and insertion of the selection marker.

5.4 Southern blot hybridization to confirm knockouts

Genome editing in both RPE1 and HCT116 cells was verified by Southern blot hybridization (Southern, 2006). Genomic DNA was isolated using MasterPure DNA purification kit (Epicentre, Cat MCD85201) following manufacturer's instructions. 20 µg of DNA were digested overnight with FastDigest Hind III-HF (Thermo Scientific) and run overnight onto a long (18 cm) 0.8% agarose gel at 30-35 V. The gel was subsequently stained and photographed (fluorescent ruler of gel-casting tray was used to track the distance of migration of DNA bands). The gel was then washed in double distilled water (ddH₂O) and DNA was denatured in 0.5 M NaOH, 1.5 M NaCl (twice for 20 min with gentle shaking). After rinsing once with ddH₂O, DNA was neutralized by washing thrice for 15 min with 1.5 M NaCl, 0.5 M Tris-HCl (pH 7.0) and transferred onto a GeneScreen Plus® Hybridization Transfer Membrane (PerkinElmer) by overnight capillary transfer in 10xSSC buffer (1.5 M NaCl, 0.15 M trisodium citrate). After rinsing the membrane with 2XSSC buffer, DNA was UV-crosslinked with a Stratalinker 1800 (Stratagene).

The membrane was hybridized overnight in DIG Easy Hyb buffer (Roche, cat#11603558001) with DIG labeled probe generated by PCR DIG probe Synthesis kit (Roche, cat#11636090910). Primers used to generate DIG probes for *hCDC14A*: forward 5'-CATCGCCGTTCACTGC-3', reverse 5'-ACGTGGGCCTGGAAAG-3'; and *hCDC14B*: forward 5'-GCCCAACTACTTTGGCAAAG-3', reverse 5'-CCAATGATCCAAATGGAGCAC-3'.

5.5 RNA preparation and expression analysis

Total RNA was isolated from cells using the RNeasy Mini Kit (Qiagen, Hilden, Germany) following manufacturer's instructions. RT-PCR analysis confirming

expression of wild type and exon-skipped *hCDC14A/B* transcripts were carried out using SuperScript® III One-Step RT-PCR System with Platinum® Taq DNA Polymerase (Invitrogen). Forward primer binding to 8th exon (5'-ATGGTGA CT TCAACTGGA-3') and reverse primer binding to 10th exon (5'-CTCCAGGAAGTGCTGC-3') were used for RT-PCR of *hCDC14A* coding sequence (CDS). In case of *hCDC14B*, the forward primer was designed in the 2nd exon (5'-GCCATTCTCTACAGCAG-3') while reverse primer in 6th exon (5'-GCAACTTCCATAGGCAGC-3'). Bands corresponding to wild type and exon-skipped clones were excised from the gel and sequenced to verify the presence of the splice junctions (*hCDC14A*: exon 8-10; *hCDC14B*: exon 3-5). Human *GAPDH* was amplified with the primers described by Zhang et al (2007): forward 5'-ATCCCATCACCATCTTCCAG-3' and reverse 5'-CCATCACGCCACAGTTTCC-3'. For semi-quantitative RT-PCR, 40 ng of total RNA was used as template and the relative amount of mRNA in different samples was calculated by measuring the band intensity (normalized to *GAPDH*) using NIH ImageJ software (Carbery et al., 2010).

5.6 Generation of RPE-1 stable cell lines

RPE-1 cells with inducible expression of proteins of interest were constructed using retroviral-mediated integration as previously described (Vlijm et al., 2018). RPE-1 tetR cell line with the tetON system was generated according to the manufacturer's instructions (Retro-X Tet-On 3G, Clontech). The virus particles were first generated by co-transfecting the pRetroX-TRE3G vector carrying the gene of interest and the envelope vector pCMV-VSV-G (a gift from Bob Weinberg; Addgene plasmid # 8454; (Stewart et al., 2003)) to a HEK293-based retroviral packaging cell line (GP2-293, Clontech). Then, the RPE-1-tetR cells were infected by adding the virus-containing media and 72 hours later, the positively transduced cells were enriched either by puromycin selection or FACS sorting.

5.7 Generation of Cas9-mediated DBN1 knockout cells

CRISPR/Cas9-Mediated drebrin knockout was generated by targeting three different exons with three guide RNAs (gRNA1: GTACGGCTTCTGCAGTGTCA for exon 3; gRNA2: GCAGCGGCTCTCTAACGGGC for exon 5; and gRNA3: GGAGCGCGAGCGGCGCTACC for exon 7). The gRNAs were designed using the web tool (crispr.mit.edu/), ordered as primers and inserted next to the U6 promoter in the scaffold vector pSpCas9(BB)-2A-GFP(PX458) (a gift from Feng Zhang, Broad Institute of MIT and Harvard, Cambridge, MA; Addgene plasmid #48138) (Hsu et al., 2013; Ran et al., 2013). The plasmid pX458 with gRNA were electroporated into RPE-1 cells (Neon transfection system, Invitrogen; pulse voltage 1,050 V, pulse width 30 ms, and pulse number 2) and 48 hours later, the transfected cells were selected for GFP expression through FACS sorting. The sorted cells were then subjected to clonal propagation through limiting dilution on 96-well plate. The emerging clones were harvested and screened via sequencing the genomic PCR amplicons (please see the Table 3 for primer list). The successfully targeted clones were further confirmed by immunoblot analysis.

Table 3: Primer list for amplifying the gRNA targeted loci in *DBN1* gene.

Primer Name	Sequence (5'-3')
Dbn1_Exon3_gRNA1_fw_1	AGACCTGACACTCTCCTGATTA
Dbn1_Exon3_gRNA1_rev_1	CTACACGATAGGGTGCATCTTC
Dbn1_Exon5_gRNA2_fw_1	CCCTCTTTGCTGGTACTTT
Dbn1_Exon5_gRNA2_rev_1	CCAGAACTGCTCTCGGTAAAT
Dbn1_Exon7_gRNA3_fw_2	GGCACCACCTACCAGAAGAC
Dbn1_Exon7_gRNA3_rev_2	GCTGTTTCCTCCTGGAACGA

5.8 Immunofluorescence and Microscopy

Cells were seeded on coverslips ~24 hours before the treatments (starvation +/- and/or doxycycline +/- depending on the experimental set up) and washed once with PBS prior to fixation. The fixation condition was decided depending on the primary antibody used (please see Table 4 for the detailed list of antibodies and fixation conditions). 4% paraformaldehyde was used for 10 min at room temperature

whereas methanol fixation was carried out at -20 °C for 5 min with ice cold methanol. Then the cells were permeabilized with 0.1% Triton-X100 in PBS (10 min at room temperature (RT)), incubated with 10% FBS to block unspecific binding and incubated with primary antibodies inside a wet chamber for 1 hour. Upon three times washing with PBS, the cells were incubated with fluorescently labeled secondary antibodies for 30 min at RT, washed thrice and mounted with Mowiol (company ?) and dried overnight at RT. DNA was counterstained by adding DAPI (4',6-diamidino-2-phenylindole) with the secondary antibody solutions. A DeltaVision RT system (Applied Precision) equipped with an Olympus IX71 microscope was used to image immunofluorescence samples using Softworx software (Applied Precision). Comparable samples were always imaged with same exposures and intensities as well as the background subtracted images were displayed with ImageJ using same Minimum and Maximum brightness.

Table 4: List for commonly used antibodies in immunofluorescence.

Name	Species	Dilution	Fixation	Source
Acetylated Tubulin	Mouse	1:200	Both	Invitrogen (32-2700)
Arl13B	Rabbit	1:200	Both	17711-1-AP
Cep164	Guinea Pig	1:500	Both	Gislene Pereira
Cep170	Mouse	1:500	Methanol	Thermo Fisher (72-413-1)
Cep250	Goat	1:200	Methanol	(Panic et al., 2015)
Cortactin	Rabbit	1:100	PFA	CST 3503
DBN1-pS142	Mouse	1:50	PFA	Millipore (MABN833)
DBN1	Mouse	1:10	PFA	Progen (MX823)
Gamma tubulin	Mouse	1:1000	Methanol	Abchem (ab27074)
GFP	Mouse	1:200	Both	Roche (11814460001)
IFT88	Guinea Pig	1:500	Both	Gislene Pereira
Ninein	Rabbit	1:300	Methanol	Michel Bornens
ODF2	Rabbit	1:100	Methanol	Gislene Pereira
Pericentrin	Rabbit	1:1000	Methanol	Abchem (ab4448)
Phalloidin		1:500	PFA	Invitrogen A34055
Rootletin-C	Rabbit	1:200	Methanol	(Panic et al., 2015)
Smoothened	Rabbit	1:200	Methanol	Abchem (ab38686)
Alexa Fluor 488/555/647 (Anti-Mouse/ Rabbit/ Goat/ Guinea Pig)		1:500	Both	Invitrogen

5.9 Immunoblot analysis

Cells were seeded on 6 or 12 well plate and lysed directly with Laemmli Buffer supplemented with protease inhibitor (Roche; 11 873 580 001), phosphatase inhibitor (Roche; 04 906 845 001), phenylmethylsulfonyl fluoride (PMSF) and Benzodase (Merck, 101656; 1:500). The lysates were heated at 95 °C for 5 min and centrifuged at 14,000 rpm for 5 min. Sodium dodecyl sulfate - polyacrylamide gel electrophoresis (SDS-PAGE) was performed as previously described (Laemmli, 1970). The membranes were blocked in 5% nonfat milk in TBS-T and incubated with appropriate primary and secondary antibodies (Table 5).

Table 5: List for commonly used antibodies in immunoblot.

Name	Species	Dilution	Source
acetylated α -Tubulin	Mouse	1:500	Invitrogen (32-2700)
Cdc14A	Rabbit	1:1000	Zymed (34-8100)
CDK5	Rabbit	1:1000	CST (2506)
Cep170	Mouse	1:1000	Thermo Fisher (72-413-1)
Cortactin	Rabbit	1:1000	CST (3503)
Drebrin	Mouse	1:300	Progen (MX823)
GAPDH	Rabbit	1:2000	CST (2118)
GFP	Mouse	1:1000	Roche (11814460001)
pS142-DBN1	Mouse	1:1000	Millipore (MABN833)

5.10 Measuring Cilia length and protein intensity within a defined region of interest (ROI)

Cilia lengths of the background subtracted images were measured by a semi-automated ImageJ macro developed and optimized by ZMBH imaging facility. In short, the macro finds the best line fit for the channel that represent cilia. The line is then skeletonized and inflated to measure the length. Upon mouse click, the macro visualizes the processing steps with 400X zoom allowing the poorly processed cilia measurements to be discarded. Another macro that allows to select the size of region of interest (ROI) as well as to define channels to be measured were used for intensity

measurements of signals e.g., transferrin, Arp2, Phalloidin surrounding the centrosomes in a 1 to 2 μm radius. If not otherwise mentioned, at least 150 cilia or centrosomes were quantified for each experiment and the findings were confirmed by at least two independent experiments. The results were expressed as mean \pm SD (Standard deviation). Prism 7 software (GraphPad) was used for statistical analyses. Mean between two groups were compared by t tests whereas multiple inter-group differences were analysed by one-way ANOVA (analysis of variance) followed by Tukey's multiple comparison test for post hoc comparisons.

5.11 *In Vitro* Phosphatase Assay

DBN1-eGFP construct was transfected into HEK293T cells using polyethylenimine (PEI). The cells were harvested by scrapping after 48 hours of transfection and lysed with RIPA buffer supplemented with protease inhibitor (Roche; 11 873 580 001), phenylmethylsulfonyl fluoride (PMSF) and Benzonase (Merck, 101656; 1:500). The DBN1-GFP was immunoprecipitated by GFP-Trap[®]_A beads (Chromotek) following manufacturer's protocol. Equal amount of bead-captured DBN1 protein was incubated with purified hCDC14A in phosphatase assay buffer (30 mM imidazole, 1 mM DTT, 1 mM EDTA, 150 mM KCl, 1 mM MgCl₂, and 25 mM K-Hepes) for 2 hours at 30 °C. The products were analyzed on immunoblots following SDS/PAGE. A buffer control was used to determine the extent of dephosphorylation by quantifying pS142-DBN1/ DBN1 ratio.

5.12 Electron microscopy (in collaboration with Annett Neuner)

RPE-1 cells were seeded on coverslips and cultured at 37°C and 5% CO₂ till they reached a confluency of 70% to 80%. Cells were rinsed in 100 mM phosphate buffer (PBS) three times and then fixed with 2.5% glutaraldehyde (GA) in 50 mM cacodylate buffer and 2% sucrose for 30 min at RT. After 5 times washing for 5 minutes with 50 mM cacodylate buffer, cells were incubated for 40 min in 2%

osmium/cacodylate buffer on ice in darkness. Followed by 4 times rinsing with dH₂O and staining overnight at 4 °C in 0.5% uranyl acetate (in H₂O). On the following day coverslips were rinsed again 4 times with dH₂O and via dehydration row (40, 50, 70, 80, 90, 95, 100% ethanol). Water was removed by ethanol within the cells. Coverslips were immediately placed on capsules filled with Spurr-resin and polymerized at 60 °C for 24 to 48 hours. Embedded cells were sectioned using a Reichert Ultracut S Microtome (Leica Instruments, Vienna, Austria) to a thickness of 70 nm. Post-staining with 3% uranyl acetate and lead citrate was performed. Sections were imaged at a Jeol JE-1400 (Jeol Ltd., Tokyo, Japan), operating at 80 kV, equipped with a 4k x 4k digital camera (F416, TVIPS, Gauting, Germany). Micrographs were adjusted in brightness and contrast using ImageJ.

5.13 Quantitative phosphoproteome and BioID mass-spectrometry analyses

The quantitative phosphoproteome and BioID mass-spectrometry analyses were conducted as described before (Chen et al., 2017). For global phosphoproteome analysis, RPE-1 cells with inducible expression of hCDC14A-YFP were cultured in light (Arg¹²C¹⁴N Lys¹²C¹⁴N) and heavy (Arg¹³C¹⁵N Lys¹³C¹⁵N) SILAC medium (Silantes) in separate flasks. After seven passages, cells were expanded to four T175 flasks for each condition and starved for 48 hours. Doxycycline (10ng/mL) was added only to the heavy samples along with starvation for inducing hCDC14A-YFP expression. Proteins were extracted and mixed at a ratio of 1:1. Strong cation exchange chromatography/immobilized metal affinity chromatography (SCX/IMAC) technique was used to enrich phospho-peptides (Villen et al., 2008). The resulted 48 fractions (24 phospho-enriched and 24 phospho-depleted) were analysed by LC-MS using a Dionex UltiMate 3000RSLC nano HPLC system (Thermo Scientific) coupled to a LTQ Orbitrap Elite mass spectrometer (Thermo Scientific). Peptide identification and quantification was achieved using the MaxQuant software package (1.5.3.8) with its built-in Andromeda search algorithm (Cox and Mann, 2008). The results of the database search were analysed using Perseus (Tyanova et

al., 2016). Two replicates of the experiment were run, and a short list of the results are represented in the Table 7 in Appendix section.

For BioID mass-spectrometry analysis, RPE-1 hCDC14A-BirA-HA, hCDC14A^{C278S}-BirA-HA, and BirA-HA cells were cultured in medium containing 50 μ M biotin. Protein expression was induced by adding Doxycycline (10 ng/mL) during 48 hours of starvation. The cells were harvested and lysed using RIPA buffer [10 mM Tris-Cl, 150 mM NaCl, 1% Triton X-100, 0.1% SDS] supplemented with protease inhibitor (Roche; 11 873 580 001), phenylmethylsulfonyl fluoride (PMSF) and Benzonase (Merck, 101656; 1:500). The lysate was clarified by centrifuging for 15 min at 20,000 \times g and the supernatant was incubated with streptavidin Sepharose beads (GE 17-5113-01) at 4 °C for 3 hours. Then the beads were washed thrice with RIPA buffer and the bound proteins were eluted by heating at 95 °C for 10 min with 2X Laemmli buffer containing 2 mM biotin. The samples were dimethyl labelled (Heavy - BirA control; Medium - hCDC14A^{CS}BirA and Light - hCDC14A-BirA prior to mass spectrometry analysis (Boersema et al., 2009) (Table 8 in the Appendix section).

5.14 Flow cytometry

Cells were trypsinized and washed twice with PBS, followed by fixation using 70% ethanol at -20°C for 3 hours before permeabilization with 0.25% Triton X-100 on ice (15 min). Cells were subsequently treated with 250 μ g/mL RNase for 30 min at 37 °C before adding 25 μ g/ml propidium iodide to stain the DNA for analysis with a BD FACS Canto II flow cytometer. For analysing any proteins by FACS, the primary antibody solutions in 1% BSA in PBS are added after permeabilization and incubated for 90 min at RT. The cells were washed once with 1 ml PBS + 1%BSA and appropriate secondary antibodies (1/250 in 1% BSA in PBS) are added and incubated for 30 min at RT in dark. After a single wash in PBS, the cells were subjected to RNase treatment and DNA staining.

5.15 Transformation of *E. coli*

50 µl of CaCl₂- competent DH5alpha *E. coli* cells were mixed with 0.5 µl of plasmid DNA or 10 µl from ligation reaction on ice for 30 min and heat shock at 42 °C for 1 min. Cells were incubated in 1 ml LB-medium at 37 °C for 1 hour by shaking if Kanamycin selection was applied afterwards. Cells were spun down and resuspended in 200 µl LB medium before bead spreading on antibiotic containing LB plates.

5.16 List of plasmids

During this study different plasmids were generated and details (maps and sequences) of all the plasmids can be found in the collection of the Schiebel group (Table 6).

Table 6: List of plasmids

Name	Used for
pRetroX-TRE3G_hCdc14A-YFP	Stable cells
pRetroX-TRE3G_hCdc14A ^{C278S} -YFP	Stable cells
pRetroX-TRE3G_GFP	Stable cells
pRetroX-TRE3G_mSmo-GFP	Stable cells
pRetroX-TRE3G_hCdc14A-BirA-HA	Stable cells
pRetroX-TRE3G_hCdc14A ^{C278S} -BirA-HA	Stable cells
pRetroX-TRE3G_BirA-HA	Stable cells
pRetroX-TRE3G_DBN1-GFP	Stable cells
pRetroX-TRE3G_DBN1S142A-GFP	Stable cells
pRetroX-TRE3G_DBN1S142D-GFP	Stable cells
pRetroX-TRE3G_DBN1S141A-S142A-GFP	Stable cells
pRetroX-TRE3G_DBN1S141D-S142D-GFP	Stable cells
pRetroX-TRE3G_IFT20-GFP	Stable cells
pRetroX-TRE3G_mRuby2-Rab8a	Stable cells

6 References

- Agircan, F.G., Schiebel, E., and Mardin, B.R. (2014). Separate to operate: control of centrosome positioning and separation. *Philos Trans R Soc L. B Biol Sci* 369.
- Ah-Fong, A.M.V., and Judelson, H.S. (2011). New role for Cdc14 phosphatase: Localization to basal bodies in the oomycete *Phytophthora* and its evolutionary coinheritance with eukaryotic flagella. *PLoS One* 6.
- Amon, A. (2008). A decade of Cdc14--a personal perspective. Delivered on 9 July 2007 at the 32nd FEBS Congress in Vienna, Austria. *FEBS J.* 275, 5774–5784.
- Arif, A. (2012). Extraneuronal activities and regulatory mechanisms of the atypical cyclin-dependent kinase Cdk5. *Biochem. Pharmacol.* 84, 985–993.
- Aubusson-Fleury, A., Lemullois, M., de Loubresse, N.G., Laligné, C., Cohen, J., Rosnet, O., Jerka-Dziadosz, M., Beisson, J., and Koll, F. (2012). The conserved centrosomal protein FOR20 is required for assembly of the transition zone and basal body docking at the cell surface. *J. Cell Sci.* 125, 4395 LP-4404.
- Avasthi, P., and Marshall, W.F. (2012). Stages of ciliogenesis and regulation of ciliary length. *Differentiation* 83, S30–S42.
- Axton, J.M., Dombrádi, V., Cohen, P.T., and Glover, D.M. (1990). One of the protein phosphatase 1 isoenzymes in *Drosophila* is essential for mitosis. *Cell* 63, 33–46.
- Barr, F.A., Elliott, P.R., and Gruneberg, U. (2011). Protein phosphatases and the regulation of mitosis. *J. Cell Sci.* 124, 2323–2334.
- Baserga, R. (1968). Biochemistry of the cell cycle: A review. *Cell Prolif.* 1, 167–191.
- Bassermann, F., Frescas, D., Guardavaccaro, D., Busino, L., Peschiaroli, A., and Pagano, M. (2008). The Cdc14B-Cdh1-Plk1 axis controls the G2 DNA-damage-response checkpoint. *Cell* 134, 256–267.
- Berdougo, E., Nachury, M. V, Jackson, P.K., and Jallepalli, P. V (2008). The nucleolar phosphatase Cdc14B is dispensable for chromosome segregation and mitotic exit in human cells. *Cell Cycle* 7, 1184–1190.

- Bettencourt-Dias, M., and Glover, D.M. (2007). Centrosome biogenesis and function: centrosomics brings new understanding. *Nat. Rev. Mol Cell Biol* 8, 451–463.
- Boersema, P.J., Raijmakers, R., Lemeer, S., Mohammed, S., and Heck, A.J.R. (2009). Multiplex peptide stable isotope dimethyl labeling for quantitative proteomics. *Nat. Protoc.* 4, 484–494.
- Brawand, D., Soumillon, M., Necsulea, A., Julien, P., Csárdi, G., Harrigan, P., Weier, M., Liechti, A., Aximu-Petri, A., Kircher, M., et al. (2011). The evolution of gene expression levels in mammalian organs. *Nature* 478, 343–348.
- Bremmer, S.C., Hall, H., Martinez, J.S., Eissler, C.L., Hinrichsen, T.H., Rossie, S., Parker, L.L., Hall, M.C., and Charbonneau, H. (2012). Cdc14 phosphatases preferentially dephosphorylate a subset of cyclin-dependent kinase (Cdk) sites containing phosphoserine. *J. Biol. Chem.* 287, 1662–1669.
- Broekhuis, J.R., Verhey, K.J., and Jansen, G. (2014). Regulation of cilium length and intraflagellar transport by the RCK-kinases ICK and MOK in renal epithelial cells. *PLoS One* 9.
- Carbery, I.D., Ji, D., Harrington, A., Brown, V., Weinstein, E.J., Liaw, L., and Cui, X. (2010). Targeted genome modification in mice using zinc-finger nucleases. *Genetics* 186, 451–459.
- Chen, C.T., Peli-Gulli, M.P., Simanis, V., and McCollum, D. (2006). *S. pombe* FEAR protein orthologs are not required for release of Clp1/Flp1 phosphatase from the nucleolus during mitosis. *J Cell Sci* 119, 4462–4466.
- Chen, N.-P., Uddin, B., Hardt, R., Ding, W., Panic, M., Lucibello, I., Kammerer, P., Ruppert, T., and Schiebel, E. (2017). Human phosphatase CDC14A regulates actin organization through dephosphorylation of epithelial protein lost in neoplasm. *Proc. Natl. Acad. Sci.* 201619356.
- Chen, N., Uddin, B., Voit, R., Schiebel, E., Materials, S.I., Frt, H., Frt, H., Rpe, T., Rpe, F., Hct, F., et al. (2016). Human phosphatase CDC14A is recruited to the cell leading edge to regulate cell migration and adhesion. *Proc. Natl. Acad. Sci.* 113, 990–995.

- Cheung, Z.H., and Ip, N.Y. (2012). Cdk5: a multifaceted kinase in neurodegenerative diseases. *Trends Cell Biol.* 22, 169–175.
- Cho, H.P., Liu, Y., Gomez, M., Dunlap, J., Wang, Y., Tyers, M., and Wang, Y. (2005). The Dual-Specificity Phosphatase CDC14B Bundles and Stabilizes Microtubules. *Mol. Cell. Biol.* 25, 4541–4551.
- Clément, A., Solnica-Krezel, L., Gould, K.L., Clément, A., Solnica-Krezel, L., and Gould, K.L. (2011). The Cdc14B phosphatase contributes to ciliogenesis in zebrafish. *Development* 138, 291–302.
- Clément, A., Solnica-Krezel, L., and Gould, K.L. (2012). Functional redundancy between Cdc14 phosphatases in zebrafish ciliogenesis. *Dev. Dyn.* 241, 1911–1921.
- Clifford, D.M., Chen, C.T., Roberts, R.H., Feoktistova, A., Wolfe, B.A., Chen, J.S., McCollum, D., and Gould, K.L. (2008). The role of Cdc14 phosphatases in the control of cell division. *Biochem. Soc. Trans.* 36, 436–438.
- Conduit, P.T., Wainman, A., and Raff, J.W. (2015). Centrosome function and assembly in animal cells. *Nat. Rev. Mol. Cell Biol.*
- Cox, J., and Mann, M. (2008). MaxQuant enables high peptide identification rates, individualized p.p.b.-range mass accuracies and proteome-wide protein quantification. *Nat Biotechnol* 26, 1367–1372.
- Cueille, N., Salimova, E., Esteban, V., Blanco, M., Moreno, S., Bueno, A., and Simanis, V. (2001). Flp1, a fission yeast orthologue of the *S. cerevisiae* CDC14 gene, is not required for cyclin degradation or rum1p stabilisation at the end of mitosis. *J Cell Sci* 114, 2649–2664.
- Delmaghani, S., Aghaie, A., Bouyacoub, Y., El Hachmi, H., Bonnet, C., Riahi, Z., Chardenoux, S., Perfettini, I., Hardelin, J.-P., Houmeida, A., et al. (2016). Mutations in CDC14A, Encoding a Protein Phosphatase Involved in Hair Cell Ciliogenesis, Cause Autosomal-Recessive Severe to Profound Deafness. *Am. J. Hum. Genet.* 98, 1266–1270.
- Doyon, Y., Choi, V.M., Xia, D.F., Vo, T.D., Gregory, P.D., and Holmes, M.C. (2010).

Transient cold shock enhances zinc-finger nuclease-mediated gene disruption. *Nat. Methods* 7, 459–460.

Eissler, C.L., Mazon, G., Powers, B.L., Savinov, S.N., Symington, L.S., Hall, M.C., Mazón, G., Powers, B.L., Savinov, S.N., Symington, L.S., et al. (2014). The Cdk/cDc14 module controls activation of the Yen1 holliday junction resolvase to promote genome stability. *Mol. Cell* 54, 80–93.

Feldman, R.M.R., Correll, C.C., Kaplan, K.B., and Deshaies, R.J. (1997). A Complex of Cdc4p, Skp1p, and Cdc53p/Cullin Catalyzes Ubiquitination of the Phosphorylated CDK Inhibitor Sic1p. *Cell* 91, 221–230.

Fry, A.M., Mayor, T., Meraldi, P., Stierhof, Y.D., Tanaka, K., and Nigg, E.A. (1998). C-Nap1, a novel centrosomal coiled-coil protein and candidate substrate of the cell cycle-regulated protein kinase Nek2. *J Cell Biol* 141, 1563–1574.

Fry, A.M., Leaper, M.J., and Bayliss, R. (2014). The primary cilium: Guardian of organ development and homeostasis. *Organogenesis* 10, 62–68.

Ghossoub, R., Hu, Q., Failler, M., Rouyez, M.-C.M.-C., Spitzbarth, B., Mostowy, S., Wolfrum, U., Saunier, S., Cossart, P., Jamesnelson, W., et al. (2013). Septins 2, 7 and 9 and MAP4 colocalize along the axoneme in the primary cilium and control ciliary length. *J. Cell Sci.* 126, 2583–2594.

Gluezn, E., Höög, J.L., Smith, A.E., Dawe, H.R., Shaw, M.K., and Gull, K. (2010). Beyond 9+0: noncanonical axoneme structures characterize sensory cilia from protists to humans. *FASEB J.* 24, 3117–3121.

Gray, C.H., Good, V.M., Tonks, N.K., and Barford, D. (2003). The structure of the cell cycle protein Cdc14 reveals a proline-directed protein phosphatase. *EMBO J.* 22, 3524–3535.

Guen, V.J., Gamble, C., Perez, D.E., Bourassa, S., Zappel, H., Gärtner, J., Lees, J.A., and Colas, P. (2016). STAR syndrome-associated CDK10/Cyclin M regulates actin network architecture and ciliogenesis. *Cell Cycle* 15, 678–688.

Guen, V.J., Edvardson, S., Fraenkel, N.D., Fattal-Valevski, A., Jalas, C., Anteby, I.,

- Shaag, A., Dor, T., Gillis, D., Kerem, E., et al. (2018). A homozygous deleterious CDK10 mutation in a patient with agenesis of corpus callosum, retinopathy, and deafness. *Am. J. Med. Genet. Part A* 176, 92–98.
- Guillamot, M., Manchado, E., Chiesa, M., Gpmez-López, G., Pisano, D.G., Sacristán, M.P., Malumbres, M., Gómez-López, G., Pisano, D.G., Sacristán, M.P., et al. (2011). Cdc14b regulates mammalian RNA polymerase II and represses cell cycle transcription. *Sci. Rep.* 1, 189.
- Hall, M.C., Jeong, D.E., Henderson, J.T., Choi, E., Bremmer, S.C., Iliuk, A.B., and Charbonneau, H. (2008). Cdc28 and Cdc14 control stability of the anaphase-promoting complex inhibitor Acm1. *J Biol Chem* 283, 10396–10407.
- Hamel, V., Steib, E., Hamelin, R., Armand, F., Borgers, S., Flückiger, I., Busso, C., Olieric, N., Sorzano, C.O.S., Steinmetz, M.O., et al. (2017). Identification of Chlamydomonas Central Core Centriolar Proteins Reveals a Role for Human WDR90 in Ciliogenesis. *Curr. Biol.* 27, 2486–2498.e6.
- Hartwell, L.H., and Weinert, T.A. (1989). Checkpoints: controls that ensure the order of cell cycle events. *Science* 246, 629–634.
- Hartwell, L.H., Mortimer, R.K., Culotti, J., and Culotti, M. (1973). Genetic control of the cell division cycle in yeast: V. Genetic analysis of cdc mutants. *Genetics* 74, 267–286.
- Heinrich, R., Neel, B.G., and Rapoport, T.A. (2002). Mathematical models of protein kinase signal transduction. *Mol. Cell* 9, 957–970.
- Hoerner, C., and Stearns, T. (2013). Remembrance of cilia past. *Cell* 155, 271–273.
- Hsu, P.D., Scott, D. a, Weinstein, J. a, Ran, F.A., Konermann, S., Agarwala, V., Li, Y., Fine, E.J., Wu, X., Shalem, O., et al. (2013). DNA targeting specificity of RNA-guided Cas9 nucleases. *Nat. Biotechnol.* 31, 827–832.
- Huang, J., and Moazed, D. (2003). Association of the RENT complex with nontranscribed and coding regions of rDNA and a regional requirement for the replication fork block protein Fob1 in rDNA silencing. *Genes Dev.* 17, 2162–2176.

- Huang, N., Xia, Y., Zhang, D., Wang, S., Bao, Y., He, R., Teng, J., and Chen, J. (2017). Hierarchical assembly of centriole subdistal appendages via centrosome binding proteins CCDC120 and CCDC68. *Nat. Commun.* 8, 15057.
- Husson, H., Moreno, S., Smith, L.A., Smith, M.M., Russo, R.J., Pitstick, R., Sergeev, M., Ledbetter, S.R., Bukanov, N.O., Lane, M., et al. (2016). Reduction of ciliary length through pharmacologic or genetic inhibition of CDK5 attenuates polycystic kidney disease in a model of nephronophthisis. *Hum. Mol. Genet.* 25, 2245–2255.
- Imtiaz, A., Belyantseva, I.A., Beirl, A.J., Fenollar-Ferrer, C., Bashir, R., Bukhari, I., Bouzid, A., Shaukat, U., Azaiez, H., Booth, K.T., et al. (2018). CDC14A phosphatase is essential for hearing and male fertility in mouse and human. *Hum. Mol. Genet.* 27, 780–798.
- Inoko, A., Matsuyama, M., Goto, H., Ohmuro-Matsuyama, Y., Hayashi, Y., Enomoto, M., Ibi, M., Urano, T., Yonemura, S., Kiyono, T., et al. (2012). Trichoplein and Aurora A block aberrant primary cilia assembly in proliferating cells. *J. Cell Biol.* 197, 391–405.
- Ishikawa, H., and Marshall, W.F. (2017). Intraflagellar Transport and Ciliary Dynamics. *Cold Spring Harb. Perspect. Biol.* 9, a021998.
- Ishikawa, H., Kubo, A., Tsukita, S., and Tsukita, S. (2005). Odf2-deficient mother centrioles lack distal/subdistal appendages and the ability to generate primary cilia. *Nat. Cell Biol.* 7, 517–524.
- Jaspersen, S.L., Charles, J.F., and Morgan, D.O. (1999). Inhibitory phosphorylation of the APC regulator Hct1 is controlled by the kinase Cdc28 and the phosphatase Cdc14. *Curr Biol* 9, 227–236.
- Joo, K., Kim, C.G., Lee, M.-S., Moon, H.-Y., Lee, S.-H., Kim, M.J., Kweon, H.-S., Park, W.-Y., Kim, C.-H., Gleeson, J.G., et al. (2013). CCDC41 is required for ciliary vesicle docking to the mother centriole. *Proc. Natl. Acad. Sci.* 110, 5987–5992.
- Ke, Y.N., and Yang, W.X. (2014). Primary cilium: An elaborate structure that blocks cell division? *Gene* 547, 175–185.

- Keeling, J., Tsiokas, L., and Maskey, D. (2016). Cellular Mechanisms of Ciliary Length Control. *Cells* 5, 6.
- Khmelniskii, A., Roostalu, J., Roque, H., Antony, C., and Schiebel, E. (2009). Phosphorylation-dependent protein interactions at the spindle midzone mediate cell cycle regulation of spindle elongation. *Dev Cell* 17, 244–256.
- Kim, J., Lee, J.E., Heynen-Genel, S., Suyama, E., Ono, K., Lee, K., Ideker, T., Aza-Blanc, P., and Gleeson, J.G. (2010). Functional genomic screen for modulators of ciliogenesis and cilium length. *Nature* 464, 1048–1051.
- Kim, J.J.J.M.J., Jo, H., Hong, H., Kim, M.H., Kim, J.J.J.M.J., Lee, J.-K., Heo, W. Do, and Kim, J.J.J.M.J. (2015). Actin remodelling factors control ciliogenesis by regulating YAP/TAZ activity and vesicle trafficking (Supplementary). *Nat Commun* 6, 6781.
- Kinzel, D., Boldt, K., Davis, E.E., Burtscher, I., Trümbach, D., Diplas, B., Attié-Bitach, T., Wurst, W., Katsanis, N., Ueffing, M., et al. (2010). Pitchfork regulates primary cilia disassembly and left-right asymmetry. *Dev. Cell* 19, 66–77.
- Knapp, D., Bhoite, L., Stillman, D.J., and Nasmyth, K. (1996). The transcription factor Swi5 regulates expression of the cyclin kinase inhibitor p40SIC1. *Mol. Cell Biol.* 16, 5701–5707.
- Kumagai, A., and Dunphy, W.G. (1991). The cdc25 protein controls tyrosine dephosphorylation of the cdc2 protein in a cell-free system. *Cell* 64, 903–914.
- Laemmli, U.K. (1970). Cleavage of structural proteins during the assembly of the head of bacteriophage T4. *Nature* 227, 680–685.
- Lanzetti, L., Margaria, V., Melander, F., Virgili, L., Lee, M.H., Bartek, J., and Jensen, S. (2007). Regulation of the Rab5 GTPase-activating protein RN-tre by the dual specificity phosphatase Cdc14A in human cells. *J Biol Chem* 282, 15258–15270.
- Li, B., Ding, S., Feng, N., Mooney, N., Ooi, Y.S., Ren, L., Diep, J., Kelly, M.R., Yasukawa, L.L., Patton, J.T., et al. (2017). Drebrin restricts rotavirus entry by inhibiting dynamin-mediated endocytosis. *Proc. Natl. Acad. Sci.* 114, E3642–E3651.

- Li, L., Ernsting, B.E., Wishart, M.J., Lohse, D.L., and Dixon, J.E. (1997). A family of putative tumor suppressors is structurally and functionally conserved in humans and yeast. *J. Biol. Chem.* 272, 29403–29406.
- Li, L., Ljungman, M., Dixon, J.E., Ljungmann, M., and Dixon, J.E. (2000). The Human Cdc14 Phosphatases Interact with and Dephosphorylate the Tumor Suppressor Protein p53. *J. Biol. Chem.* 275, 2410–2414.
- Lim, S., and Kaldis, P. (2013). Cdks, cyclins and CKIs: roles beyond cell cycle regulation. *Development* 140, 3079–3093.
- Lin, H., Ha, K., Lu, G., Fang, X., Cheng, R., Zuo, Q., and Zhang, P. (2015). Cdc14A and Cdc14B Redundantly Regulate DNA Double-Strand Break Repair. *Mol. Cell Biol.* 35, 3657–3668.
- Lucocq, J., Warren, G., and Pryde, J. (1991). Okadaic acid induces Golgi apparatus fragmentation and arrest of intracellular transport. *J. Cell Sci.* 100 (Pt 4), 753–759.
- Mailand, N., Falck, J., Lukas, C., Syljuåsen, R.G., Welcker, M., Bartek, J., and Lukas, J. (2000). Rapid Destruction of Human Cdc25A in Response to DNA Damage. *Science* (80-). 288, 1425–1429.
- Mailand, N., Lukas, C., Kaiser, B.K., Jackson, P.K., Bartek, J., and Lukas, J. (2002). Deregulated human Cdc14A phosphatase disrupts centrosome separation and chromosome segregation. *Nat Cell Biol* 4, 317–322.
- Mali, P., Yang, L., Esvelt, K.M., Aach, J., Guell, M., DiCarlo, J.E., Norville, J.E., and Church, G.M. (2013). RNA-guided human genome engineering via Cas9. *Science* 339, 823–826.
- Malicki, J.J., Johnson, C.A., Hildebrandt, F., al., et, Valente, E.M., al., et, Ishikawa, H., Marshall, W.F., Nigg, E.A., Stearns, T., et al. (2017). The Cilium: Cellular Antenna and Central Processing Unit. *Trends Cell Biol.* 27, 126–140.
- Malumbres, M. (2014). Cyclin-dependent kinases. *Genome Biol.* 15, 122.
- Mardin, B.R., and Schiebel, E. (2012). Breaking the ties that bind: New advances in

- centrosome biology. *J Cell Biol* 197, 11–18.
- Maskey, D., Marlin, M.C., Kim, S.S., Kim, S.S., Ong, E.-C., Li, G., and Tsiokas, L. (2015). Cell cycle-dependent ubiquitylation and destruction of NDE1 by CDK5-FBW7 regulates ciliary length. *EMBO J.* 34, 2424–2440.
- Mayor, T., Stierhof, Y.D., Tanaka, K., Fry, A.M., and Nigg, E.A. (2000). The centrosomal protein C-Nap1 is required for cell cycle-regulated centrosome cohesion. *J Cell Biol* 151, 837–846.
- Mazo, G., Soplop, N., Wang, W., Uryu, K., and Tsou, M.B. (2016). Spatial Control of Primary Ciliogenesis by Subdistal Appendages Alters Sensation-Associated Properties of Cilia. *Dev. Cell* 1–14.
- Milenkovic, L., Weiss, L.E., Yoon, J., Roth, T.L., Su, Y.S., Sahl, S.J., Scott, M.P., and Moerner, W.E. (2015). Single-molecule imaging of Hedgehog pathway protein Smoothed in primary cilia reveals binding events regulated by Patched1. *Proc. Natl. Acad. Sci.* 112, 1510094112-.
- Mocciaro, A., and Schiebel, E. (2010). Cdc14: a highly conserved family of phosphatases with non-conserved functions? *J. Cell Sci.* 123, 2867–2876.
- Mocciaro, A., Berdough, E., Zeng, K., Black, E., Vagnarelli, P., Earnshaw, W., Gillespie, D., Jallepalli, P., and Schiebel, E. (2010). Vertebrate cells genetically deficient for Cdc14A or Cdc14B retain DNA damage checkpoint proficiency but are impaired in DNA repair. *J. Cell Biol.* 189, 631–639.
- Morgan, D.O. (1997). Cyclin-dependent kinases: engines, clocks, and microprocessors. *Annu. Rev. Cell Dev. Biol.* 13, 261–291.
- Nager, A.R., Goldstein, J.S., Herranz-Pérez, V., Portran, D., Ye, F., Garcia-Verdugo, J.M., and Nachury, M. V. (2017). An Actin Network Dispatches Ciliary GPCRs into Extracellular Vesicles to Modulate Signaling. *Cell* 168, 252–263.
- Ong, S.E., Blagoev, B., Kratchmarova, I., Kristensen, D.B., Steen, H., Pandey, A., and Mann, M. (2002). Stable isotope labeling by amino acids in cell culture, SILAC, as a simple and accurate approach to expression proteomics. *Mol Cell Proteomics* 1, 376–

386.

Ovejero, S., Ayala, P., Bueno, A., and Sacristán, M.P. (2012). Human Cdc14A regulates Wee1 stability by counteracting CDK-mediated phosphorylation. *Mol. Biol. Cell* 23, 4515–4525.

Panic, M., Hata, S., Neuner, A., and Schiebel, E. (2015). The Centrosomal Linker and Microtubules Provide Dual Levels of Spatial Coordination of Centrosomes. *PLOS Genet.* 11, e1005243.

Pardee, A.B. (1974). A restriction point for control of normal animal cell proliferation. *Proc. Natl. Acad. Sci. U. S. A.* 71, 1286–1290.

Pereira, G., Manson, C., Grindlay, J., and Schiebel, E. (2002). Regulation of the Bfa1p-Bub2p complex at spindle pole bodies by the cell cycle phosphatase Cdc14p. *J Cell Biol* 157, 367–379.

Picard, A., Capony, J.P., Brautigan, D.L., and Dorée, M. (1989). Involvement of protein phosphatases 1 and 2A in the control of M phase-promoting factor activity in starfish. *J. Cell Biol.* 109, 3347–3354.

Plotnikova, O. V., Nikonova, A.S., Loskutov, Y. V., Kozyulina, P.Y., Pugacheva, E.N., and Golemis, E.A. (2012). Calmodulin activation of Aurora-A kinase (AURKA) is required during ciliary disassembly and in mitosis. *Mol. Biol. Cell* 23, 2658–2670.

Pringle, J.R., and Hartwell, L.H. (1981). The *Saccharomyces cerevisiae* cell cycle. In *The Molecular Biology of the Yeast Saccharomyces: Life Cycle and Inheritance*, J.N. Strathern, E.W. Jones, and J.R. Broach, eds. (New York: Cold Spring Harbor Laboratory Press), p.

Queralt, E., and Uhlmann, F. (2008). Cdk-counteracting phosphatases unlock mitotic exit. *Curr Opin Cell Biol* 20, 661–668.

Ran, F.A.F.A., Hsu, P.D.P.P.D., Wright, J., Agarwala, V., Scott, D.A., and Zhang, F. (2013). Genome engineering using the CRISPR-Cas9 system. *Nat. Protoc.* 8, 2281–2308.

- Ran, J., Yang, Y., Li, D., Liu, M., and Zhou, J. (2015). Deacetylation of α -tubulin and cortactin is required for HDAC6 to trigger ciliary disassembly. *Sci. Rep.* 5, 12917.
- Reiter, J.F., and Leroux, M.R. (2017). Genes and molecular pathways underpinning ciliopathies. *Nat. Rev. Mol. Cell Biol.* 18, 533–547.
- Rosso, L., Marques, A.C., Weier, M., Lambert, N., Lambot, M.-A.A., Vanderhaeghen, P., and Kaessmann, H. (2008). Birth and rapid subcellular adaptation of a hominoid-specific CDC14 protein. *PLoS Biol.* 6, e140.
- Roux, K.J., Kim, D.I., Raida, M., and Burke, B. (2012). A promiscuous biotin ligase fusion protein identifies proximal and interacting proteins in mammalian cells. *J. Cell Biol.* 196, 801–810.
- Sánchez, I., and Dynlacht, B.D. (2016). Cilium assembly and disassembly. *Nat. Cell Biol.* 18, 711–717.
- Satir, P., and Christensen, S.T. (2007). Overview of Structure and Function of Mammalian Cilia. *Annu. Rev. Physiol.* 69, 377–400.
- Satir, P., Mitchell, D.R., and Jékely, G. (2008). *How Did the Cilium Evolve?* (Elsevier Inc.).
- Shirao, T., Hanamura, K., Koganezawa, N., Ishizuka, Y., Yamazaki, H., and Sekino, Y. (2017). The role of drebrin in neurons. *J. Neurochem.* 1–16.
- Shou, W., Seol, J.H., Shevchenko, A., Baskerville, C., Moazed, D., Chen, W.S., Jang, J., Shevchenko, A., Charbonneau, H., and Deshaies, R. (1999). Exit from mitosis is triggered by Tem1-dependent release of the protein phosphatase Cdc14 from nucleolar RENT complex. *Cell* 97, 233–244.
- Simanis, V. (2003). Events at the end of mitosis in the budding and fission yeasts. *J. Cell Sci.* 116, 4263–4275.
- Southern, E. (2006). Southern blotting. *Nat. Protoc.* 1, 518–525.
- Stegmeier, F., and Amon, A. (2004). Closing mitosis: the functions of the Cdc14 phosphatase and its regulation. *Annu. Rev. Genet.* 38, 203–232.

- Stewart, S.A., Dykxhoorn, D.M., Palliser, D., Mizuno, H., Yu, E.Y., An, D.S., Sabatini, D.M., Chen, I.S.Y., Hahn, W.C., Sharp, P.A., et al. (2003). Lentivirus-delivered stable gene silencing by RNAi in primary cells. *RNA* 9, 493–501.
- Straight, A.F., Shou, W., Dowd, G.J., Turck, C.W., Deshaies, R.J., Johnson, A.D., and Moazed, D. (1999). Net1, a Sir2-associated nucleolar protein required for rDNA silencing and nucleolar integrity. *Cell* 97, 245–256.
- Takeda, S., and Narita, K. (2012). Structure and function of vertebrate cilia, towards a new taxonomy. *Differentiation* 83, S4–S11.
- Tanabe, K., Yamazaki, H., Inaguma, Y., Asada, A., Kimura, T., Takahashi, J., Taoka, M., Ohshima, T., Furuichi, T., Isobe, T., et al. (2014). Phosphorylation of Drebrin by Cyclin-dependent Kinase 5 and Its role in neuronal migration. *PLoS One* 9.
- Temin, H.M. (1971). Stimulation by serum of multiplication of stationary chicken cells. *J. Cell. Physiol.* 78, 161–170.
- Tonks, N.K. (2006). Protein tyrosine phosphatases: from genes, to function, to disease. *Nat. Rev. Mol. Cell Biol.* 7, 833–846.
- Trautmann, S., Wolfe, B.A., Jorgensen, P., Tyers, M., Gould, K.L., and McCullum, D. (2001). Fission yeast Clp1p phosphatase regulates G2/M transition and coordination of cytokinesis with cell cycle progression. *Curr Biol* 11, 931–940.
- Trinkle-Mulcahy, L., and Lamond, A.I. (2006). Mitotic phosphatases: no longer silent partners. *Curr. Opin. Cell Biol.* 18, 623–631.
- Tumurbaatar, I., Cizmecioglu, O., Hoffmann, I., Grummt, I., and Voit, R. (2011). Human Cdc14B promotes progression through mitosis by dephosphorylating Cdc25 and regulating Cdk1/cyclin B activity. *PLoS One* 6, e14711.
- Tyanova, S., Temu, T., Sinitcyn, P., Carlson, A., Hein, M.Y., Geiger, T., Mann, M., and Cox, J. (2016). The Perseus computational platform for comprehensive analysis of (prote)omics data. *Nat. Methods* 13, 731–740.
- Uddin, B., Chen, N.-P., Panic, M., and Schiebel, E. (2015). Genome editing through

- large insertion leads to the skipping of targeted exon. *BMC Genomics* 16, 1082.
- Valentine, C.R. (1998). The association of nonsense codons with exon skipping. *Mutat. Res. - Rev. Mutat. Res.* 411, 87-117.
- Villen, J., Gygi, S.P., Villén, J., and Gygi, S.P. (2008). The SCX/IMAC enrichment approach for global phosphorylation analysis by mass spectrometry. *Nat. Protoc.* 3, 1630-1638.
- Visintin, R., Craig, K., Hwang, E.S., Prinz, S., Tyers, M., and Amon, A. (1998). The phosphatase Cdc14 triggers mitotic exit by reversal of Cdk-dependent phosphorylation. *Mol Cell* 2, 709-718.
- Vlijm, R., Li, X., Panic, M., Rüttnick, D., Hata, S., Herrmannsdörfer, F., Kuner, T., Heilemann, M., Engelhardt, J., Hell, S.W., et al. (2018). STED nanoscopy of the centrosome linker reveals a CEP68-organized, periodic rootletin network anchored to a C-Nap1 ring at centrioles. *Proc. Natl. Acad. Sci. U. S. A.* 201716840.
- Wang, T., Wei, J.J., Sabatini, D.M., and Lander, E.S. (2014). Genetic screens in human cells using the CRISPR-Cas9 system. *Science* 343, 80-84.
- Wei, Z., Peddibhotla, S., Lin, H., Fang, X., Li, M., Rosen, J.M., and Zhang, P. (2011). Early-onset aging and defective DNA damage response in Cdc14b-deficient mice. *Mol. Cell. Biol.* 31, 1470-1477.
- Worth, D.C., Daly, C.N., Geraldo, S., Oozeer, F., and Gordon-Weeks, P.R. (2013). Drebrin contains a cryptic F-actin-bundling activity regulated by Cdk5 phosphorylation. *J. Cell Biol.* 202, 793-806.
- Wu, C.-T., Chen, H.-Y., and Tang, T.K. (2018). Myosin-Va is required for preciliary vesicle transportation to the mother centriole during ciliogenesis. *Nat. Cell Biol.*
- De Wulf, P., Montani, F., and Visintin, R. (2009). Protein phosphatases take the mitotic stage. *Curr. Opin. Cell Biol.* 21, 806-815.
- Wurzenberger, C., and Gerlich, D.W. (2011). Phosphatases: Providing safe passage through mitotic exit. *Nat. Rev. Mol. Cell Biol.* 12, 469-482.

Yamashita, K., Yasuda, H., Pines, J., Yasumoto, K., Nishitani, H., Ohtsubo, M., Hunter, T., Sugimura, T., and Nishimoto, T. (1990). Okadaic acid, a potent inhibitor of type 1 and type 2A protein phosphatases, activates cdc2/H1 kinase and transiently induces a premature mitosis-like state in BHK21 cells. *EMBO J.* 9, 4331–4338.

Ye, X., Zeng, H., Ning, G., Reiter, J.F., and Liu, A. (2014). C2cd3 is critical for centriolar distal appendage assembly and ciliary vesicle docking in mammals. *Proc. Natl. Acad. Sci.* 111, 2164–2169.

Zhang, Y., Ba, Y., Liu, C., Sun, G., Ding, L., Gao, S., Hao, J., Yu, Z., Zhang, J., Zen, K., et al. (2007). PGC-1alpha induces apoptosis in human epithelial ovarian cancer cells through a PPARgamma-dependent pathway. *Cell Res.* 17, 363–373.

7 Publications during PhD

1. **Uddin, B.**, Chen, N.P., Panic, M., and Schiebel, E. (2015). Genome editing through large insertion leads to the skipping of targeted exon. *BMC Genomics* 16, 1082.
2. Chen, N.P., **Uddin, B.**, Voit, R., Schiebel, E., Materials, S.I., Frt, H., Frt, H., Rpe, T., Rpe, F., Hct, F., et al. (2016). Human phosphatase CDC14A is recruited to the cell leading edge to regulate cell migration and adhesion. *Proc. Natl. Acad. Sci.* 113, 990–995.
3. Chen, N.P., **Uddin, B.**, Hardt, R., Ding, W., Panic, M., Lucibello, I., Kammerer, P., Ruppert, T., and Schiebel, E. (2017). Human phosphatase CDC14A regulates actin organization through dephosphorylation of epithelial protein lost in neoplasm. *Proc. Natl. Acad. Sci.* 201619356.

8 Appendix

Table 7: List of hypophosphorylated peptides upon hCDC14A-YFP expression.

Gene.names	Protein.names	Positions	Amino Acid	Ratio.H.L. normalized
ABI2	Abl interactor 2	224	S	0.43155
ABI2	Abl interactor 2	227	S	0.54756
AKAP10	A-kinase anchor protein 10, mitochondrial	281	S	0.57212
CARHSP1	Calcium-regulated heat stable protein 1	17	S	0.54136
DBN1	Drebrin	142	S	0.53107
DPYSL2	Dihydropyrimidinase-related protein 2	514	T	0.55474
DPYSL2	Dihydropyrimidinase-related protein 2	521	T	0.46302
DPYSL2	Dihydropyrimidinase-related protein 2	517	S	0.47602
DPYSL2	Dihydropyrimidinase-related protein 2	522	S	0.50275
DPYSL2	Dihydropyrimidinase-related protein 2	518	S	0.47058
EEF1D	Elongation factor 1-delta	133	S	0.39367
EIF2A	Eukaryotic translation initiation factor 2A;Eukaryotic translation initiation factor 2A, N-terminally processed	501	S	0.54618
HEATR5B	HEAT repeat-containing protein 5B	1737	S	0.47532
IGF2BP1	Insulin-like growth factor 2 mRNA-binding protein 1	181	S	0.44091
KCNMA1	Calcium-activated potassium channel subunit alpha-1	543	S	0.48962
LARP1B	La-related protein 1B	574	S	0.3842
LIMA1	LIM domain and actin-binding protein 1	610	S	0.45948
LMO7	LIM domain only protein 7	591	S	0.3737
MAP4	Microtubule-associated protein;Microtubule-associated protein 4	297	S	0.5814
MAPRE3	Microtubule-associated protein RP/EB family member 3	162	S	0.46471
MAPRE3	Microtubule-associated protein RP/EB family member 3	161	T	0.51671
MPRIP	Myosin phosphatase Rho-interacting protein	365	S	0.57032
NUF2	Kinetochore protein Nuf2	247	S	0.55403

Gene.names	Protein.names	Positions	Amino Acid	Ratio.H.L. normalized
NUP160	Nuclear pore complex protein Nup160	1122	S	0.54839
PDLIM7	PDZ and LIM domain protein 7	217	S	0.563
PPP1R18	Phostensin	530	S	0.55116
PTDSS1	Phosphatidylserine synthase 1	296	S	0.41335
PURB	Transcriptional activator protein Pur-beta	101	S	0.36843
RANBP2	E3 SUMO-protein ligase RanBP2	2276	S	0.34595
RANGAP1	Ran GTPase-activating protein 1	442	S	0.30462
RPRD2	Regulation of nuclear pre-mRNA domain-containing protein 2	923	S	0.17653
RPS2	40S ribosomal protein S2	264	S	0.54946
SCRIB	Protein scribble homolog	1348	S	0.54901
SEC16A	Protein transport protein Sec16A	1069	S	0.4981
STUB1	E3 ubiquitin-protein ligase CHIP	19	S	0.49963
SYNPO	Synaptopodin	784	S	0.37795
SYNPO	Synaptopodin	589	S	0.56312
SZRD1	SUZ domain-containing protein 1	19	S	0.54282
UBAP2L	Ubiquitin-associated protein 2- like	609	S	0.51679
USP9X	Probable ubiquitin carboxyl- terminal hydrolase FAF-X	2443	S	0.51447

Table 8: List of proteins identified in hCDC14A BioID proximity assay.

Gene names	Protein names	Unique peptides	Ratio H/L normalized	Ratio H/M normalized
AAK1	AP2-associated protein kinase 1	12	-232.634	-208.767
AASS	Alpha-aminoadipic semialdehyde synthase, mitochondrial;Lysine ketoglutarate reductase;Saccharopine dehydrogenase	13	-174.463	-162.313
ABLIM1	Actin-binding LIM protein 1	10	-255.741	-188.422
ACAD9	Acyl-CoA dehydrogenase family member 9, mitochondrial	27	-278.448	-263.173
ACADVL	Very long-chain specific acyl-CoA dehydrogenase, mitochondrial	28	-231.933	-17.731
ACAT1	Acetyl-CoA acetyltransferase, mitochondrial	12	-151.231	-110.392
ACOT2;ACOT1	Acyl-coenzyme A thioesterase 2, mitochondrial;Acyl-coenzyme A thioesterase 1	28	-352.017	-338.737
ACOT9	Acyl-coenzyme A thioesterase 9, mitochondrial	13	-18.039	-170.167
ACTN1	Alpha-actinin-1	35	-178.513	-38.895
ACTN4	Alpha-actinin-4	32	-152.745	-147.369
ADD1	Alpha-adducin	19	-13.105	-198.604
AFG3L2	AFG3-like protein 2	31	-189.604	-155.733
AHNAK	Neuroblast differentiation-associated protein AHNAK	417	-548.597	-645.748
AHNAK2	Protein AHNAK2	105	-213.651	-188.763
AKAP2	A-kinase anchor protein 2	13	-200.144	-158.571
ALDH18A1	Delta-1-pyrroline-5-carboxylate synthase;Glutamate 5-kinase;Gamma-glutamyl phosphate reductase	28	-145.233	-222.176
ALMS1	Alstrom syndrome protein 1	18	-133.657	-177.685
ANAPC1	Anaphase-promoting complex subunit 1	25	-246.212	-192.134
ANAPC5	Anaphase-promoting complex subunit 5	11	-244.733	-182.495
ANKRD17	Ankyrin repeat domain-containing protein 17	12	-210.011	-127.953
AP2A1	AP-2 complex subunit alpha-1	12	-14.346	-127.495
AP3B1	AP-3 complex subunit beta-1	17	-166.827	-199.447
ARCN1	Coatomer subunit delta	14	-135.424	-156.009
ARHGAP21	Rho GTPase-activating protein 21	19	-266.722	-215.991

Gene names	Protein names	Unique peptides	Ratio H/L normalized	Ratio H/M normalized
ARHGAP29	Rho GTPase-activating protein 29	17	-233.964	-213.581
ASCC3	Activating signal cointegrator 1 complex subunit 3	38	-178.126	-160.117
ATAD3A	ATPase family AAA domain-containing protein 3A	15	-120.929	-137.759
ATP5A1	ATP synthase subunit alpha, mitochondrial	33	-217.573	-204.139
ATP5B	ATP synthase subunit beta, mitochondrial;ATP synthase subunit beta	22	-302.362	-327.914
ATXN2L	Ataxin-2-like protein	19	-199.062	-146.454
BCR	Breakpoint cluster region protein	10	-158.766	-168.971
BCS1L	Mitochondrial chaperone BCS1	11	-148.965	-127.233
C17orf80	Uncharacterized protein C17orf80	14	-160.283	-194.886
CAD	CAD protein;Glutamine-dependent carbamoyl-phosphate synthase;Aspartate carbamoyltransferase;Dihydroorotase	12	-215.862	-205.685
CALD1	Caldesmon	38	-216.495	-282.941
CAMSAP2	Calmodulin-regulated spectrin-associated protein 2	11	-309.863	-33.823
CAND1	Cullin-associated NEDD8-dissociated protein 1	24	-176.538	-183.126
CAPZB	F-actin-capping protein subunit beta	10	-106.196	-104.552
CCT2	T-complex protein 1 subunit beta	24	-197.778	-206.407
CCT3	T-complex protein 1 subunit gamma	23	-167.397	-214.248
CCT4	T-complex protein 1 subunit delta	21	-282.021	-301.648
CCT5	T-complex protein 1 subunit epsilon	25	-109.062	-180.738
CCT6A	T-complex protein 1 subunit zeta	16	-114.283	-172.953
CCT7	T-complex protein 1 subunit eta	24	-115.418	-201.363
CCT8	T-complex protein 1 subunit theta	38	-360.679	-473.989
CD2AP	CD2-associated protein	33	-294.109	-283.013
CDC14A	Dual specificity protein phosphatase CDC14A	48	-318.744	-339.358
CDC23	Cell division cycle protein 23 homolog	17	-131.646	-170.844
CEP131	Centrosomal protein of 131 kDa	35	-302.868	-191.855
CKAP4	Cytoskeleton-associated protein 4	11	-121.508	-165.018
CLINT1	Clathrin interactor 1	12	-135.045	-145.954
CLPX	ATP-dependent Clp protease ATP-binding subunit clpX-like, mitochondrial	19	-256.482	-178.876

Gene names	Protein names	Unique peptides	Ratio H/L normalized	Ratio H/M normalized
CLTC	Clathrin heavy chain;Clathrin heavy chain 1	16	-205.968	-205.859
CNOT1	CCR4-NOT transcription complex subunit 1	32	-16.748	-158.273
COPA	Coatomer subunit alpha;Xenin;Proxenin	34	-182.715	-190.498
COPB1	Coatomer subunit beta	28	-127.879	-153.249
COPB2	Coatomer subunit beta	16	-161.989	-165.717
COPG2	Coatomer subunit gamma-2	30	-265.145	-291.191
CORO1B	Coronin-1B	25	-342.762	-30.418
CORO1C	Coronin-1C;Coronin	23	-32.033	-416.385
CRK	Adapter molecule crk	12	-255.334	-262.691
CSDE1	Cold shock domain-containing protein E1	34	-234.938	-236.848
CTNND1	Catenin delta-1	24	-201.188	-302.315
CTPS1	CTP synthase 1	13	-177.226	-178.463
CYFIP1	Cytoplasmic FMR1-interacting protein 1	11	-167.738	-159.579
DAP3	28S ribosomal protein S29, mitochondrial	21	-3.423	-322.351
DARS	Aspartate--tRNA ligase, cytoplasmic	15	-211.223	-229.414
DBN1	Drebrin	11	-132.775	-134.626
DBT	Lipoamide acyltransferase component of branched-chain alpha-keto acid dehydrogenase complex, mitochondrial	26	-43.166	-417.132
DCTN1;DKF Zp686E0752	Dynactin subunit 1	34	-175.326	-232.388
DCTN2	Dynactin subunit 2	10	-14.032	-116.188
DDX1	ATP-dependent RNA helicase DDX1	12	-189.475	-129.846
DDX21	Nucleolar RNA helicase 2	15	-165.045	-142.341
DDX3X;DDX3Y	ATP-dependent RNA helicase DDX3X;ATP-dependent RNA helicase DDX3Y	32	-145.795	-134.979
DENND4C	DENN domain-containing protein 4C	17	-230.979	-195.428
DHX9	ATP-dependent RNA helicase A	32	-11.151	-112.249

Gene names	Protein names	Unique peptides	Ratio H/L normalized	Ratio H/M normalized
DLAT	Dihydrolipoyllysine-residue acetyltransferase component of pyruvate dehydrogenase complex, mitochondrial;Acetyltransferase component of pyruvate dehydrogenase complex	18	-291.159	-270.566
DLD	Dihydrolipoyl dehydrogenase, mitochondrial;Dihydrolipoyl dehydrogenase	22	-244.568	-451.655
DLG5	Disks large homolog 5	86	-272.557	-251.928
DLST	Dihydrolipoyllysine-residue succinyltransferase component of 2-oxoglutarate dehydrogenase complex, mitochondrial	18	-344.941	-335.842
DNAJC13	DnaJ homolog subfamily C member 13	47	-17.134	-153.629
DNMBP	Dynamin-binding protein	45	-227.739	-19.703
DOCK7	Dedicator of cytokinesis protein 7	35	-177.932	-176.695
DPYSL2	Dihydropyrimidinase-related protein 2	28	-174.087	-2.044
DPYSL3	Dihydropyrimidinase-related protein 3	18	-222.075	-23.879
DYNC1H1	Cytoplasmic dynein 1 heavy chain 1	30	-179.411	-10.858
EDC4	Enhancer of mRNA-decapping protein 4	23	-187.758	-161.741
EEF1G	Elongation factor 1-gamma	16	-199.522	-242.391
EFTUD1	Elongation factor Tu GTP-binding domain-containing protein 1	12	-182.808	-183.501
EIF3A	Eukaryotic translation initiation factor 3 subunit A	42	-239.373	-207.686
EIF3B	Eukaryotic translation initiation factor 3 subunit B	15	-175.901	-145.728
EIF3C;EIF3CL	Eukaryotic translation initiation factor 3 subunit C;Eukaryotic translation initiation factor 3 subunit C-like protein	19	-315.804	-251.854
EIF3E	Eukaryotic translation initiation factor 3 subunit E	11	-25.154	-18.594
EIF3L	Eukaryotic translation initiation factor 3 subunit L	15	-243.355	-250.504
EIF4B	Eukaryotic translation initiation factor 4B	15	-328.729	-272.537
EIF4G1	Eukaryotic translation initiation factor 4 gamma 1	35	-19.443	-181.604

Gene names	Protein names	Unique peptides	Ratio H/L normalized	Ratio H/M normalized
EIF4G3	Eukaryotic translation initiation factor 4 gamma 3	22	-20.077	-193.335
EIF5	Eukaryotic translation initiation factor 5	15	-235.675	-207.467
EML4	Echinoderm microtubule-associated protein-like 4	14	-213.062	-213.087
EPB41L2	Band 4.1-like protein 2	18	-188.801	-158.005
EPB41L3	Band 4.1-like protein 3;Band 4.1-like protein 3, N-terminally processed	15	-175.916	-174.812
EPHA2	Ephrin type-A receptor 2	15	-167.683	-138.481
EPRS	Bifunctional glutamate/proline--tRNA ligase;Glutamate--tRNA ligase;Proline--tRNA ligase	38	-162.411	-220.178
EPS15L1	Epidermal growth factor receptor substrate 15-like 1	26	-164.268	-141.323
ERBB2IP	Protein LAP2	40	-234.652	-195.054
ERC1	ELKS/Rab6-interacting/CAST family member 1	68	-258.779	-241.596
ESYT1	Extended synaptotagmin-1	21	-2.124	-160.073
ESYT2	Extended synaptotagmin-2	10	-184.166	-167.696
EXOC4	Exocyst complex component 4	19	-206.401	-199.344
EZR	Ezrin	13	-165.845	-325.925
FAM120A	Constitutive coactivator of PPAR-gamma-like protein 1	27	-146.678	-219.008
FAM129B	Niban-like protein 1	17	-104.068	-19.771
FASN	Fatty acid synthase;[Acyl-carrier-protein] S-acetyltransferase;[Acyl-carrier-protein] S-malonyltransferase;3-oxoacyl-[acyl-carrier-protein] synthase;3-oxoacyl-[acyl-carrier-protein] reductase;3-hydroxyacyl-[acyl-carrier-protein] dehydratase;Enoyl-[acyl-carrier-protein] reductase;Oleoyle-[acyl-carrier-protein] hydrolase	94	-199.183	-227.593
FLNB	Filamin-B	110	-266.731	-284.415
FLNC	Filamin-C	118	-3.769	-393.514
FXR1	Fragile X mental retardation syndrome-related protein 1	10	-127.355	-175.502
GAPVD1	GTPase-activating protein and VPS9 domain-containing protein 1	22	-179.626	-174.933
GBF1	Golgi-specific brefeldin A-resistance guanine nucleotide exchange factor 1	10	-220.583	-199.798

Gene names	Protein names	Unique peptides	Ratio H/L normalized	Ratio H/M normalized
GCN1L1	Translational activator GCN1	65	-253.525	-227.991
GEMIN5	Gem-associated protein 5	36	-158.005	-172.571
GIGYF2	PERQ amino acid-rich with GYF domain-containing protein 2	35	-247.161	-260.489
GLUD1;GLU D2	Glutamate dehydrogenase 1, mitochondrial;Glutamate dehydrogenase 2, mitochondrial	30	-232.735	-213.068
GOLGA3	Golgin subfamily A member 3	14	-133.308	-146.705
HAUS3	HAUS augmin-like complex subunit 3	14	-162.118	-164.543
HAUS5	HAUS augmin-like complex subunit 5	15	-127.932	-143.319
HDLBP	Vigilin	45	-269.825	-414.242
HSD17B10	3-hydroxyacyl-CoA dehydrogenase type-2	11	-231.854	-213.334
HSDL2	Hydroxysteroid dehydrogenase-like protein 2	13	-262.665	-277.873
HSPA1B;HSPA1A	Heat shock 70 kDa protein 1B;Heat shock 70 kDa protein 1A	23	-176.975	-197.551
HSPA5	78 kDa glucose-regulated protein	38	-231.545	-251.474
HSPA8	Heat shock cognate 71 kDa protein	23	-242.291	-242.577
HSPA9	Stress-70 protein, mitochondrial	33	-158.437	-19.463
IARS	Isoleucine--tRNA ligase, cytoplasmic	25	-105.544	-142.717
IARS2	Isoleucine--tRNA ligase, mitochondrial	34	-372.994	-392.148
IGF2BP1	Insulin-like growth factor 2 mRNA-binding protein 1	11	-171.558	-161.251
IGF2BP2	Insulin-like growth factor 2 mRNA-binding protein 2	16	-266.749	-258.519
IPO7	Importin-7	11	-144.721	-123.708
IQGAP1	Ras GTPase-activating-like protein IQGAP1	40	-115.053	-17.092
KIAA0196	WASH complex subunit strumpellin	13	-302.315	-312.469
KIAA1033	WASH complex subunit 7	12	-144.501	-214.318
KIAA1217	Sickle tail protein homolog	15	-261.493	-18.558
KIAA1671	Uncharacterized protein KIAA1671	50	-244.175	-158.268
KIF5B	Kinesin-1 heavy chain	37	-179.771	-145.724
KPNB1	Importin subunit beta-1	37	-273.034	-277.932
KRT18	Keratin, type I cytoskeletal 18	18	-345.263	-313.062
KTN1	Kinectin	30	-157.734	-139.236
LARS	Leucine--tRNA ligase, cytoplasmic	20	-152.787	-110.045

Gene names	Protein names	Unique peptides	Ratio H/L normalized	Ratio H/M normalized
LETM1	LETM1 and EF-hand domain-containing protein 1, mitochondrial	30	-237.079	-18.984
LIMCH1	LIM and calponin homology domains-containing protein 1	50	-341.018	-19.686
LPP	Lipoma-preferred partner	18	-202.862	-186.533
LRPPRC	Leucine-rich PPR motif-containing protein, mitochondrial	75	-294.053	-257.596
LUZP1	Leucine zipper protein 1	65	-217.332	-208.724
MACF1	Microtubule-actin cross-linking factor 1, isoforms 1/2/3/5	36	-201.829	-144.878
MAP1B	Microtubule-associated protein 1B;MAP1B heavy chain;MAP1 light chain LC1	46	-154.785	-123.396
MAP4	Microtubule-associated protein;Microtubule-associated protein 4	28	-408.792	-43.687
MAP7D3	MAP7 domain-containing protein 3	13	-184.715	-151.083
MAPRE2	Microtubule-associated protein RP/EB family member 2	10	-270.134	-219.383
MAST4	Microtubule-associated serine/threonine-protein kinase 4	14	-283.054	-185.679
MCM7	DNA replication licensing factor MCM7	18	-120.128	-122.769
MDH2	Malate dehydrogenase, mitochondrial;Malate dehydrogenase	12	-162.238	-101.762
MKL2	MKL/myocardin-like protein 2	28	-285.194	-238.037
MPRIIP	Myosin phosphatase Rho-interacting protein	50	-250.038	-233.337
MRPL1	39S ribosomal protein L1, mitochondrial	12	-157.785	-126.382
MRPL15	39S ribosomal protein L15, mitochondrial	16	-24.661	-21.334
MRPL19	39S ribosomal protein L19, mitochondrial	10	-341.648	-310.495
MRPL28	39S ribosomal protein L28, mitochondrial	10	-162.482	-137.565
MRPL37	39S ribosomal protein L37, mitochondrial	20	-253.349	-209.302
MRPL38	39S ribosomal protein L38, mitochondrial	14	-22.477	-185.872
MRPL39	39S ribosomal protein L39, mitochondrial	13	-247.361	-217.821
MRPL4	39S ribosomal protein L4, mitochondrial	10	-298.188	-226.708

Gene names	Protein names	Unique peptides	Ratio H/L normalized	Ratio H/M normalized
MRPL44	39S ribosomal protein L44, mitochondrial	12	-174.676	-181.188
MRPL9	39S ribosomal protein L9, mitochondrial	11	-350.476	-306.106
MRPS18B	28S ribosomal protein S18b, mitochondrial	12	-349.761	-341.551
MRPS2	28S ribosomal protein S2, mitochondrial	10	-233.439	-262.531
MRPS22	28S ribosomal protein S22, mitochondrial	18	-334.511	-278.677
MRPS27	28S ribosomal protein S27, mitochondrial	20	-344.758	-31.428
MRPS30	28S ribosomal protein S30, mitochondrial	10	-170.139	-168.427
MRPS31	28S ribosomal protein S31, mitochondrial	18	-230.287	-204.311
MRPS34	28S ribosomal protein S34, mitochondrial	13	-332.516	-273.178
MRPS35	28S ribosomal protein S35, mitochondrial	15	-261.476	-210.774
MRPS5	28S ribosomal protein S5, mitochondrial	17	-217.338	-216.527
MRPS7	28S ribosomal protein S7, mitochondrial	14	-259.396	-225.498
MRPS9	28S ribosomal protein S9, mitochondrial	22	-258.753	-249.834
MSN	Moesin	11	-237.527	-205.439
MTCL1	Microtubule cross-linking factor 1	19	-279.927	-248.149
MTHFD1L	Monofunctional C1-tetrahydrofolate synthase, mitochondrial	13	-206.631	-186.292
MYH10	Myosin-10	43	-211.466	-16.291
MYH9	Myosin-9	178	-494.484	-599.806
MYO18A	Unconventional myosin-XVIIIa	17	-192.517	-110.058
MYO1B	Unconventional myosin-Ib	22	-140.446	-156.854
MYO1C	Unconventional myosin-Ic	28	-166.594	-161.228
MYO5A	Unconventional myosin-Va	15	-164.562	-125.384
MYO6	Unconventional myosin-VI	11	-15.014	-124.274
MYOF	Myoferlin	39	-184.773	-193.633
NAP1L4	Nucleosome assembly protein 1-like 4	10	-196.162	-189.293
NCKAP1	Nck-associated protein 1	13	-115.817	-146.973
NCL	Nucleolin	14	-105.218	-112.759

Gene names	Protein names	Unique peptides	Ratio H/L normalized	Ratio H/M normalized
NDUFA9	NADH dehydrogenase [ubiquinone] 1 alpha subcomplex subunit 9, mitochondrial	14	-347.881	-256.619
NDUFS1	NADH-ubiquinone oxidoreductase 75 kDa subunit, mitochondrial	42	-330.031	-300.243
NDUFS2	NADH dehydrogenase [ubiquinone] iron-sulfur protein 2, mitochondrial	22	-2.662	-241.974
NDUFS3	NADH dehydrogenase [ubiquinone] iron-sulfur protein 3, mitochondrial	17	-314.051	-257.021
NDUFV1	NADH dehydrogenase [ubiquinone] flavoprotein 1, mitochondrial	23	-267.586	-236.223
NDUFV2	NADH dehydrogenase [ubiquinone] flavoprotein 2, mitochondrial	10	-236.312	-206.148
NDUFV3	NADH dehydrogenase [ubiquinone] flavoprotein 3, mitochondrial	24	-377.391	-304.228
NEK1	Serine/threonine-protein kinase Nek1	17	-159.118	-173.154
NEXN	Nexilin	14	-355.543	-226.951
NNT	NAD(P) transhydrogenase, mitochondrial	19	-193.501	-203.074
NT5DC2	5-nucleotidase domain-containing protein 2	14	-159.244	-175.867
NUP214	Nuclear pore complex protein Nup214	42	-135.038	-179.436
NUP88	Nuclear pore complex protein Nup88	15	-154.422	-176.601
OFD1	Oral-facial-digital syndrome 1 protein	19	-241.442	-162.919
OGDH	2-oxoglutarate dehydrogenase, mitochondrial	55	-278.886	-275.419
OTUD4	OTU domain-containing protein 4	12	-234.373	-205.475
PABPC1;PABPC3	Polyadenylate-binding protein;Polyadenylate-binding protein 1;Polyadenylate-binding protein 3	12	-204.311	-190.574
PACS1	Phosphofurin acidic cluster sorting protein 1	10	-156.162	-120.806

Gene names	Protein names	Unique peptides	Ratio H/L normalized	Ratio H/M normalized
PAICS	Multifunctional protein ADE2;Phosphoribosylaminoimidazole-succinocarboxamide synthase;Phosphoribosylaminoimidazole carboxylase	14	-16.218	-128.026
PALLD	Palladin	37	-143.195	-163.249
PARP4	Poly [ADP-ribose] polymerase 4	55	-256.602	-222.735
PDLIM1	PDZ and LIM domain protein 1	17	-143.327	-121.307
PDLIM4	PDZ and LIM domain protein 4	13	-213.214	-230.251
PDLIM5	PDZ and LIM domain protein 5	28	-333.625	-323.555
PDLIM7	PDZ and LIM domain protein 7	14	-228.694	-189.223
PDPR	Pyruvate dehydrogenase phosphatase regulatory subunit, mitochondrial	16	-15.655	-14.323
PEAK1	Pseudopodium-enriched atypical kinase 1	21	-122.597	-179.786
PHB	Prohibitin	18	-289.604	-270.237
PHB2	Prohibitin-2	18	-36.678	-330.173
PLEC	Plectin	40	-20.095	-188.892
PLEKHA5	Pleckstrin homology domain-containing family A member 5	32	-269.947	-23.734
PNPLA8	Calcium-independent phospholipase A2-gamma	13	-274.923	-182.434
PPFIA1	Liprin-alpha-1	16	-161.295	-189.502
PPFIBP1	Liprin-beta-1	29	-204.204	-133.555
PPP1R9B	Neurabin-2	22	-308.277	-313.302
PPP6C	Serine/threonine-protein phosphatase 6 catalytic subunit;Serine/threonine-protein phosphatase 6 catalytic subunit, N-terminally processed	12	-126.979	-198.879
PPP6R1	Serine/threonine-protein phosphatase 6 regulatory subunit 1	17	-193.545	-174.758
PPP6R2	Serine/threonine-protein phosphatase 6 regulatory subunit 2	26	-184.752	-177.655
PPP6R3	Serine/threonine-protein phosphatase 6 regulatory subunit 3	12	-171.781	-146.391
PRKDC	DNA-dependent protein kinase catalytic subunit	42	-159.166	-147.823
PRRC2A	Protein PRRC2A	31	-223.175	-166.392
PRRC2C	Protein PRRC2C	32	-236.045	-146.857
PSMC2	26S protease regulatory subunit 7	11	-165.513	-140.095

Gene names	Protein names	Unique peptides	Ratio H/L normalized	Ratio H/M normalized
PSMD2	26S proteasome non-ATPase regulatory subunit 2	11	-201.293	-156.303
PSMD3	26S proteasome non-ATPase regulatory subunit 3	17	-148.362	-143.269
PTCD3	Pentatricopeptide repeat domain-containing protein 3, mitochondrial	27	-314.893	-318.968
PTK2	Focal adhesion kinase 1	10	-121.488	-173.078
PTRF	Polymerase I and transcript release factor	10	-254.532	-241.411
PYCR1	Pyrroline-5-carboxylate reductase 1, mitochondrial;Pyrroline-5-carboxylate reductase	14	-269.862	-266.347
PYCR2	Pyrroline-5-carboxylate reductase 2;Pyrroline-5-carboxylate reductase	12	-297.562	-249.867
QARS	Glutamine--tRNA ligase	14	-128.891	-169.469
RAI14	Ankycorbin	70	-305.445	-285.716
RAN	GTP-binding nuclear protein Ran	13	-214.778	-244.191
RANBP2	E3 SUMO-protein ligase RanBP2	93	-175.156	-186.675
RANGAP1	Ran GTPase-activating protein 1	32	-227.872	-254.439
RAPH1	Ras-associated and pleckstrin homology domains-containing protein 1	15	-202.573	-137.699
RARS	Arginine--tRNA ligase, cytoplasmic	28	-190.644	-204.841
REPS1	RalBP1-associated Eps domain-containing protein 1	11	-271.302	-149.924
RPL3	60S ribosomal protein L3	19	-132.016	-187.118
RPL6	60S ribosomal protein L6	13	-16.827	-243.831
RPL7	60S ribosomal protein L7	15	-191.001	-191.615
RPL7A	60S ribosomal protein L7a	12	-153.604	-140.148
RPN1	Dolichyl-diphosphooligosaccharide-protein glycosyltransferase subunit 1	14	-134.168	-143.952
RPS2	40S ribosomal protein S2	14	-163.075	-179.206
RPS3	40S ribosomal protein S3	20	-118.161	-155.881
RRBP1	Ribosome-binding protein 1	32	-110.061	-173.399
RUVBL1	RuvB-like 1	21	-349.214	-323.868
RUVBL2	RuvB-like 2	18	-192.895	-251.548
SCRIB	Protein scribble homolog	19	-189.164	-151.742
SEC16A	Protein transport protein Sec16A	40	-188.646	-188.449
SEC23A	Protein transport protein Sec23A	11	-152.966	-119.044
SEPT11	Septin-11	15	-226.333	-229.612
SEPT2	Septin-2	15	-366.345	-37.665

Gene names	Protein names	Unique peptides	Ratio H/L normalized	Ratio H/M normalized
SERBP1	Plasminogen activator inhibitor 1 RNA-binding protein	16	-110.377	-187.049
SH3D19	SH3 domain-containing protein 19	14	-230.814	-162.937
SHMT2	Serine hydroxymethyltransferase, mitochondrial; Serine hydroxymethyltransferase	30	-422.523	-383.894
SIPA1L1	Signal-induced proliferation-associated 1-like protein 1	33	-14.058	-153.374
SIPA1L3	Signal-induced proliferation-associated 1-like protein 3	10	-117.325	-114.922
SLC30A9	Zinc transporter 9	20	-239.775	-210.135
SMC2	Structural maintenance of chromosomes protein 2	10	-14.097	-110.076
SMC3	Structural maintenance of chromosomes protein 3	14	-119.067	-101.063
SND1	Staphylococcal nuclease domain-containing protein 1	10	-142.082	-157.209
SNX1	Sorting nexin-1	13	-152.301	-160.147
SNX6	Sorting nexin-6; Sorting nexin-6, N-terminally processed	18	-231.452	-255.716
SORBS2	Sorbin and SH3 domain-containing protein 2	18	-188.119	-209.943
SPAG9	C-Jun-amino-terminal kinase-interacting protein 4	15	-169.619	-128.525
SPECC1	Cytospin-B	11	-250.635	-193.644
SPECC1L; SPECC1L-ADORA2A	Cytospin-A	14	-188.854	-24.323
SPTAN1	Spectrin alpha chain, non-erythrocytic 1	59	-20.235	-183.624
SRP68	Signal recognition particle subunit SRP68	15	-136.145	-112.098
SSFA2	Sperm-specific antigen 2	16	-175.545	-160.274
STAT1	Signal transducer and activator of transcription 1-alpha/beta; Signal transducer and activator of transcription	22	-224.154	-22.623
STRAP	Serine-threonine kinase receptor-associated protein	19	-201.403	-188.646
SUCLA2	Succinyl-CoA ligase [ADP-forming] subunit beta, mitochondrial	10	-224.811	-163.873
SVIL	Supervillin	77	-199.752	-168.121
SYNJ2	Synaptojanin-2	26	-136.863	-126.309
SYNPO	Synaptopodin	31	-305.565	-226.029

Gene names	Protein names	Unique peptides	Ratio H/L normalized	Ratio H/M normalized
TANC1	Protein TANC1	26	-226.868	-300.671
TCP1	T-complex protein 1 subunit alpha	33	-183.506	-204.216
TDRD3	Tudor domain-containing protein 3	14	-193.998	-112.743
TLN1	Talin-1	104	-330.315	-287.229
TLN2	Talin-2	17	-168.316	-101.861
TNKS1BP1	182 kDa tankyrase-1-binding protein	26	-163.859	-105.718
TNS3	Tensin-3	36	-384.765	-381.464
TP53BP2	Apoptosis-stimulating of p53 protein 2	11	-177.863	-136.264
TRAP1	Heat shock protein 75 kDa, mitochondrial	16	-169.106	-143.098
TRIM25	E3 ubiquitin/ISG15 ligase TRIM25	12	-176.322	-176.068
TRIOBP	TRIO and F-actin-binding protein	32	-20.373	-226.444
TRMT10C	Mitochondrial ribonuclease P protein 1	14	-164.783	-145.166
TTC28	Tetratricopeptide repeat protein 28	26	-259.423	-208.884
UACA	Uveal autoantigen with coiled-coil domains and ankyrin repeats	41	-222.465	-252.209
UBAP2	Ubiquitin-associated protein 2	14	-181.522	-182.383
UBAP2L	Ubiquitin-associated protein 2-like	22	-254.937	-204.979
UGDH	UDP-glucose 6-dehydrogenase	11	-134.806	-102.163
UNC45A	Protein unc-45 homolog A	15	-177.374	-184.467
UPF1	Regulator of nonsense transcripts 1	14	-20.916	-213.258
UQCRC2	Cytochrome b-c1 complex subunit 2, mitochondrial	13	-141.939	-153.751
USP10	Ubiquitin carboxyl-terminal hydrolase 10	12	-145.712	-166.841
USP15	Ubiquitin carboxyl-terminal hydrolase 15	11	-213.885	-150.422
USP9X	Probable ubiquitin carboxyl-terminal hydrolase FAF-X	19	-160.999	-193.159
UTRN	Utrophin	78	-183.743	-15.804
VAR5	Valine--tRNA ligase	14	-160.863	-187.086
VCL	Vinculin	36	-154.743	-170.162
VCPIP1	Deubiquitinating protein VCIP135	18	-205.367	-22.587
VDAC2	Voltage-dependent anion-selective channel protein 2	11	-153.291	-160.025
VIM	Vimentin	51	-271.615	-273.015
VWA8	von Willebrand factor A domain-containing protein 8	47	-18.039	-160.463
WDR11	WD repeat-containing protein 11	19	-190.942	-175.176
XPO1	Exportin-1	13	-14.286	-178.121

Gene names	Protein names	Unique peptides	Ratio H/L normalized	Ratio H/M normalized
XRN1	5-3 exoribonuclease 1	53	-233.105	-234.593
ZC3HAV1	Zinc finger CCCH-type antiviral protein 1	17	-138.387	-152.957
ZYX	Zyxin	16	-232.265	-179.156

9 Acknowledgements

I am grateful to Professor Dr. Elmar Schiebel for providing me with this precious opportunity to conduct PhD thesis in his group. His constructive criticism and thoughtful discussion were the driving force to build the project and achieve plausible outcomes in limited time-frame. I would like to thank Professor Dr. Gislene Pereira and Professor Dr. Sylvia Erhardt for their suggestions during my TAC meetings. My project was heavily benefitted by the expertise of Dr. Gislene Pereira as well as by the innumerable chemicals from her lab. Her innovative thoughts metamorphosed the project to its present shape.

I would like to express sincere thanks to Nan-Peng Chen and Patrick Partscht for their vital supports throughout the project. I happily remember the helpful suggestions of all my generous lab mates specially Shoji Hata, Ana Pastor Peidro, Berati Cerikan, Diana Ruethnick, Wanlu Zheng and Xue Li. Thanks Annette for nice EM images. I would also like to appreciate the support and technical expertise of Ursula Jaekle throughout this study. Special thanks to Sibylle Heller for her administrative supports.

Finally, I would like to appreciate my wife Taslima and daughters Lubaba and Tasifa for their absolute supports. I shared the frustrations and joy of lab life with them to survive my PhD!!

